

**PALLADIUM SUPPORTED GRAPHENE OXIDE BASED METAL ORGANIC  
FRAMEWORK COMPOSITE FOR HYDROGEN TECHNOLOGY**

By

MOGWASHA DAPHNEY MAKHAFOLA

DISSERTATION

Submitted in fulfilment of the requirements for the degree of

MASTER OF SCIENCE

In

CHEMISTRY

In the

FACULTY OF SCIENCE AND AGRICULTURE

(School of Physical and Mineral Sciences)

At the

UNIVERSITY OF LIMPOPO

SUPERVISOR: DR K.D. MODIBANE

CO-SUPERVISORS: PROF M.J. HATO

PROF L. KATATA-SERU (NWU)

2019

## DEDICATION

---

### TO MY FAMILY

Lucy, Alpheus, Elizabeth, Angie, Ronny Makhafola.  
My Beautiful Daughter Mashilo Palesa Makhafola and My Husband Matlou Moses  
Seapela

## DECLARATION BY CANDIDATE

---

I declare that PALLADIUM SUPPORTED GRAPHENE OXIDE BASED METAL ORGANIC FRAMEWORK COMPOSITE FOR HYDROGEN TECHNOLOGY is my own work and that all the sources that I have used or quoted have been indicated and acknowledged by means of complete references and that this work has not been submitted before for any other degree at any other institution.

.....

Full Names

.....

Date

## ACKNOWLEDGEMENTS

---

Completion of this dissertation would not have been possible without the guidance and help of several individuals who in one way or another contributed and extended their valuable assistance throughout the study.

First and foremost, all thanks to the **CREATOR OF ALL THINGS**, for the life, strength and ability given to me throughout my existence on this planet.

My greatest gratitude goes to my supervisor Dr K.D. Modibane for his utmost assistance from the start of the research to date and for all the support he gave me throughout the study. For the critical role you played in my academic life, you introduced me to research and made me fall in love with it from my Honours level. Not only were you my supervisor in research, but also in social life. You listened whenever I needed you to, and your motivational words kept me going because you believed so much in me.

I would like further extend my gratitude to my co-supervisors, Prof. M.J. Hato and Prof. L. Katata-Seru for the work and effort they added in making sure that the work is a success. The guidance and valuable advices they showed throughout this MSc journey. To Dr K.M. Molapo, thanks for the efforts you took in helping me understand the electrochemistry section of this research work.

Special thanks to all my colleagues and friends in the department of chemistry at University of Limpopo, especially the Nanotechnology Research Group at UL (NanoRG@UL 2018) Monama G.R, Maponya T.C, Ramohlola K.E, Pasha T, Mulaudzi K.P, Somo T.R, Ramaripa P.S, Teffo D, Malatji N and Mashao G for the knowledge we shared amongst each other and for making the laboratory room work-friendly and productive.

From University of the Western Cape, thanks to Prof. El Iwuoha (Father of Electrochemistry), Dr. M Masikini and Mr. SB Mdluli, for accommodating me during my one-month at the Chemical Science Department, Sensor Laboratory and for allowing and assisting me to use their instruments for electrochemical characterisations and hydrogen studies.

To my wonderful family, thanks for the continuous love and support. My mother and father, Lucy and Alpheus Makhafola, thanks for the financial and emotional support you provided from the time I enrolled at the university to date. Special thanks to my loving sisters Lisbeth and Angie Makhafola, for moral support and friendship you showed me throughout my entire life. Not forgetting my one and only brother, for the love and respect he showed me. I would like to send my gratitude to my husband and smile keeper, Matlou Moses Seapela, for the love and support he gave me in good and bad times. Thanks for being with me academically (accompanying me to the laboratory and reading my work), trying to understand my work, even though we are not in the same field of research. You did all these in support of the work that I was doing because you believed so much in me. To my very beautiful daughter, Mashilo Palesa Makhafola, thank you for being part of my life. To my friends, my stress relievers, Mogale Mahlomola and Sekokotla Silas, thanks for the emotional support. I will always cherish the great moments we shared together.

Thank You All.

## ABSTRACT

---

The concept of sustainable energy development is one of the crucial topics of the 21<sup>st</sup> century. It has evolved into a guiding principle for a liveable future world where human needs are met while maintaining balance with the environment. In this regard, hydrogen technology is a promising alternative energy source since it does not produce undesirable greenhouse gas (CO<sub>2</sub>). In order to place hydrogen energy into practical applications, there are certain problems that need to be addressed, these include the efficient production and storage of hydrogen. Currently, hydrogen is mostly produced from conventional processes such as steam reforming of fossil fuels, gasification and water splitting (photo/electrochemical and thermochemical). Among these methods, electrochemical water splitting is identified as a noble process to produce clean hydrogen gas and monitor all processes through hydrogen evolution reactions (HER). The entire HER processes are sluggish in nature and cathodic electrocatalysts are utilised to accelerate the process. Hence, in this work, we present highly active graphene oxide/metal organic framework (GO/MOF) and palladium (Pd) supported GO/MOF electrocatalysts for HER. GO/MOF was prepared through impregnation method of MOF and GO, whereas Pd@GO/MOF composite was synthesised using electroless Pd deposition on GO and followed by impregnation method of direct mixing of Pd@GO and MOF. The structural, morphological and electrochemical properties of the synthesised materials (GO/MOF and Pd@GO/MOF) were characterised by X-ray diffraction (XRD), Fourier transform infrared (FTIR), simultaneous thermogravimetric analysis (STA), scanning electron microscopy/energy dispersive spectroscopy (SEM/EDS), high resolution transmission electron microscopy/Energy dispersive x-ray spectroscopy/selected area electron diffraction (HRTEM/EDX/SAED) and cyclic voltammetry (CV). XRD, FTIR, TGA and DSC results revealed the presence of GO on MOF confirming the formation of composites. The SEM/EDS and HRTEM/EDX/SAED results confirmed the presence of octahedral structure of MOF in the Pd@GO sheet-like structure, elemental composition and crystallinity of the synthesised materials. Furthermore, the

electrocatalytic efficiency of GO/MOF and Pd@GO/MOF composites on HER was studied using three important parameters (exchange current density, Tafel slope and charge transfer coefficient) calculated from Tafel analysis. The GO/MOF and Pd@GO/MOF composites showed excellent HER activity at 0.45 mol.L<sup>-1</sup> H<sub>2</sub>SO<sub>4</sub> with exchange current densities of 25.12 A.m<sup>-2</sup> and 24.5 A.m<sup>-2</sup>, Tafel slopes of 116 mV/dec and 123 mV/dec, and transfer coefficients of 0.49 and 0.52, respectively. These observed results are consistent with theory, thus suggesting the Volmer reaction as the limiting mechanism at high concentration. However, at low concentration both composites showed an increase in the Tafel slope and transfer coefficient, suggesting the reaction order of Volmer reaction coupled with either Heyrovsky or Tafel reaction. The proposed reaction order was further supported by slope of logarithm of current as a function of pH and Pourbaix diagram. The composites demonstrated the enhancement turnover frequency (TOF) values in this order MOF < GO/MOF < Pd@GO/MOF. The large TOF value of 7.81 mol H<sub>2</sub>.s<sup>-1</sup> in the case of Pd@GO/MOF was due the H<sub>2</sub> spillover effect as a result of the presence of Pd nanoparticles. The fabricated composites displayed high activity, good stability and excellent tolerance to the crossover effect, which may be used as a promising catalyst in electrochemical hydrogen production and storage technology via hydrogen evolution reaction.

## RESEARCH OUTPUTS

---

### PUBLICATIONS

- (i) **Mogwasha D. Makhafola**, Mpitloane J. Hato\*, Thabiso C. Maponya, Gobeng R. Monama, Kabelo E. Ramohlola, Phuti S. Ramaripa, Kerileng M. Molapo, Emmanuel I. Iwuoha, L. Katata-Seru, Kwena D. Modibane\*, “Synergetic Effect of Graphene Oxide and Metal Organic Framework Nanocomposites as Electrocatalysts for Hydrogen Evolution Reaction: A Review”. *Pending Submission as a Book Chapter for possible publication to Springer.*
- (ii) **Mogwasha Daphney Makhafola**, Thabang Ronny Somo, Mpitloane Joseph Hato\*, Kerileng M. Molapo, Emmanuel I. Iwuoha, Kwena Desmond Modibane\*. “Fabrication of graphene oxide/metal organic framework nanocomposites with improved compatibility for hydrogen evolution reaction”. *Book Chapter accepted in Intech-Open (Appendix 1).*
- (iii) Emmanuel I. Iwuoha, **Mogwasha Daphney Makhafola**, Thabang Ronny Somo, Mpitloane Joseph Hato, Kerileng M. Molapo, Kwena Desmond Modibane\*. “Graphene oxide/metal organic framework nanocomposite with improved electrocatalytic activity for hydrogen evolution reaction”. *Published as a Book Chapter in Conference Proceeding in the 3rd International Hydrogen Technologies Congress (IHTEC-2018), March 15-18, 2018, Alanya/Antalya, Turkey (Appendix 2).*
- (iv) **Mogwasha Daphney Makhafola**, Thabang Ronny Somo, Mpitloane Joseph Hato\*, Kerileng M. Molapo, Emmanuel I. Iwuoha, Kwena Desmond Modibane\*. “Palladium supported graphene oxide based metal organic framework nanocomposite with improved electrocatalytic efficiency for hydrogen evolution reaction”. *Manuscript pending submission.*
- (v) Emmanuel I. Iwuoha, Gobeng R. Monama, Kabelo E. Ramohlola, **Mogwasha D. Makhafola**, Gloria Mashao, Siyabonga B. Mdluli, Mpitloane J. Hato, Kerileng

M. Molapo, Katlego Makgopa, Kwena D. Modibane\*. Copper(II) phthalocyanine/metal organic framework composite with improved electrocatalytic efficiency for hydrogen production. *Published as a Proceeding in the 3rd International Hydrogen Technologies Congress (IHTEC-2018), March 15-18, 2018, Alanya/Antalya, Turkey (Appendix 3).*

(vi) Thabiso C. Maponya, Kabelo E. Ramohlola, Mpitloane J. Hato\*, **Mogwasha D. Makhafola**, Gobeng R. Monama, Arjun Maity, Kwena D. Modibane\*, "Polyaniline based nanocomposites for environmental remediation". *Submitted as a Book Chapter for possible publication to IntechOpen (Appendix 4).*

(vii) G. R. Monama, S. B. Mdluli, G. Mashao, **M. D. Makhafola**, K. E. Ramohlola, K. M. Molapo, M. J. Hato\*, K. Makgopa, E. I. Iwuoha, and K. D. Modibane\*, "Palladium deposition on copper(II) phthalocyanine/metal organic framework composite and electrocatalytic activity of the modified electrode towards the hydrogen evolution reaction," *Renewable Energy*, vol. 119, pp. 62–72, 2018 (Appendix 5).

## PRESENTATIONS

(i) **Mogwasha Daphney Makhafola**, Thabang Ronny Somo, Mpitloane Joseph Hato\*, Kerileng M. Molapo, Emmanuel I. Iwuoha, Kwena Desmond Modibane\*. Fabrication of graphene oxide/metal organic framework nanocomposites with improved compatibility for hydrogen evolution reaction. Oral Presentation. Faculty of Science and Agriculture Research Day, Bolivia Lodge, Polokwane, South Africa on the 19<sup>th</sup> October 2017. The presentation was awarded second prize.

(ii) **Mogwasha Daphney Makhafola**, Thabang Ronny Somo, Mpitloane Joseph Hato\*, Kerileng M. Molapo, Emmanuel I. Iwuoha, Kwena Desmond Modibane\*. Fabrication of graphene oxide/metal organic framework nanocomposites with improved compatibility for hydrogen evolution reaction. Poster Presentation, 7<sup>th</sup>

SANI–NYRS Symposium, TUT (Arcardia Campus), Pretoria, South Africa on the 20<sup>th</sup> October 2017.

(iii) **Mogwasha Daphney Makhafola**, Thabang Ronny Somo, Mpitloane Joseph Hato\*, Kerileng M. Molapo, Emmanuel I. Iwuoha, Kwena Desmond Modibane\*. Fabrication of graphene oxide/metal organic framework nanocomposites with improved compatibility for hydrogen evolution reaction. Flash Poster Presentation. INORG2017 SACI conference, Western Cape, Cape Town, South Africa on the 25-30<sup>th</sup> June 2017. The presentation was awarded first prize in silver awards.

(iv) **Mogwasha Daphney Makhafola**, Thabang Ronny Somo, Mpitloane Joseph Hato\*, Kerileng M. Molapo, Emmanuel I. Iwuoha, Kwena Desmond Modibane\*. Fabrication of graphene oxide/metal organic framework nanocomposites with improved compatibility for hydrogen evolution reaction. Poster Presentation. SANI–NanoAfrica 2018 Conference, Salt Rock, Durban, South Africa on the 22<sup>nd</sup>-25<sup>th</sup> April 2018.

# TABLE OF CONTENTS

---

DEDICATION .....	ii
ACKNOWLEDGEMENTS .....	iv
ABSTRACT .....	vi
RESEARCH OUTPUTS .....	viii
PUBLICATIONS .....	viii
PRESENTATIONS .....	ix
TABLE OF CONTENTS .....	xi
LIST OF FIGURES.....	xvi
LIST OF SCHEMES.....	xix
LIST OF TABLES.....	xix
LIST OF ABBREVIATIONS.....	xx
LIST OF SYMBOLS .....	xxii
CHAPTER ONE .....	1
INTRODUCTION.....	1
1.1. BACKGROUND .....	1
1.1.1. Energy .....	1
1.1.2. Hydrogen energy technology.....	3
1.2. PROBLEM STATEMENT .....	4
1.3. RATIONALE.....	5
1.4. RESEARCH AIM AND OBJECTIVES.....	6
1.4.1. Aim.....	6
1.4.2. Objectives .....	7

1.4. DISSERTATION OUTLINE .....	7
1.5. REFERENCES.....	8
CHAPTER TWO.....	13
A COMPREHENSIVE REVIEW OF SYNERGETIC EFFECT ON GRAPHENE OXIDE AND METAL ORGANIC FRAMEWORK NANOCOMPOSITES AS ELECTROCATALYSTS FOR HYDROGEN EVOLUTION REACTION .....	13
CHAPTER SUMMARY .....	13
2.1. INTRODUCTION .....	14
2.1.1. Hydrogen energy background.....	14
2.1.2. Hydrogen storage.....	16
2.1.3. Production of hydrogen .....	18
2.2. GRAPHENE OXIDE .....	25
2.2.1. Background.....	25
2.2.2. Structure of graphene oxide.....	26
2.2.3. Synthesis of GO .....	27
2.2.4. GO based materials for HER.....	28
2.3. METAL ORGANIC FRAMEWORK .....	31
2.3.1. Background.....	31
2.3.2. Structure of MOF.....	32
2.3.3. Synthesis of MOF.....	34
2.3.4 MOF based materials as HER electrocatalyst.....	36
2.4. CONCLUSIONS .....	38
2.6. REFERENCES .....	39
CHAPTER THREE .....	54
ANALYTICAL TECHNIQUES.....	54

3.1. INTRODUCTION .....	54
3.2. SPECTROSCOPY .....	54
3.2.1. Fourier transform infrared spectroscopy .....	54
3.3. MICROSCOPY .....	55
3.3.1. Scanning electron microscopy .....	56
3.3.2. Transmission electron microscopy .....	57
3.4. PHYSICAL METHODS .....	59
3.4.1. X-ray diffraction .....	59
3.4.2. Simultaneous thermal analysis (STA) .....	60
3.5. ELECTROANALYTICAL METHODS .....	61
3.5.1. Cyclic voltammetry .....	62
3.6. CONCLUSIONS .....	63
3.7. REFERENCES .....	64
CHAPTER FOUR .....	67
GRAPHENE OXIDE/METAL ORGANIC FRAMEWORKS NANOCOMPOSITE WITH IMPROVED ELECTROCATALYTIC EFFICIENCY FOR HYDROGEN PRODUCTION AND STORAGE .....	67
CHAPTER SUMMARY .....	67
4.1. INTRODUCTION .....	68
4.2. EXPERIMENTAL .....	70
4.2.1. Materials .....	70
4.2.2. Synthesis of GO, MOF and GO/MOF composite .....	70
4.2.3. Material characterisations .....	71
4.3. RESULTS AND DISCUSSION .....	72
4.3.1. Structural Properties .....	72

4.3.2. Morphological characterisation.....	78
4.3.3. Electrochemical characterisation.....	83
4.3.4. Hydrogen studies .....	87
4.4. CONCLUSIONS .....	93
4.5. REFERENCES .....	94
CHAPTER FIVE .....	99
PALLADIUM SUPPORTED GRAPHENE OXIDE BASED METAL ORGANIC FRAMEWORK NANOCOMPOSITE WITH IMPROVED ELECTROCATALYTIC EFFICIENCY FOR HYDROGEN EVOLUTION REACTION.....	99
CHAPTER SUMMARY .....	99
5.1. INTRODUCTION .....	100
5.2. EXPERIMENTAL .....	101
5.2.1. Materials.....	101
5.2.2. Synthesis of MOF and Pd@GO/MOF composite.....	102
5.2.3. Materials characterisation .....	102
5.3. RESULTS AND DISCUSSION .....	103
5.3.1. Structural Characterisation.....	103
5.3.2. Morphological characterisation.....	108
5.3.3. Electrochemical characterisation.....	114
5.3.4. Hydrogen studies .....	119
5.4. CONCLUSIONS .....	127
5.5. REFERENCES .....	127
CHAPTER SIX .....	133
GENERAL DISCUSSION, CONCLUSIONS AND RECOMMENDATIONS .....	133
6.1. GENERAL DISCUSSION AND CONCLUSIONS.....	133

6.2. RECOMMENDATIONS FOR FUTURE WORK .....	136
SUPPORTING INFORMATION .....	139
PALLADIUM SUPPORTED GRAPHENE OXIDE BASED METAL ORGANIC FRAMEWORK NANOCOMPOSITE WITH IMPROVED ELECTROCATALYTIC EFFICIENCY FOR HYDROGEN EVOLUTION REACTION.....	139
S1: EXPERIMENTAL SECTION.....	139
S2: RESULTS.....	140
S2.1: Structural characterisation .....	140
S2.2: Morphological characterisation .....	141
S2.3: Electrochemical characterisation .....	143
S3. REFERENCES.....	144
APPENDIX 1 .....	145
APPENDIX 2 .....	146
APPENDIX 3 .....	147
APPENDIX 4 .....	148
APPENDIX 5 .....	149

## LIST OF FIGURES

---

Figure 1. 1: Chart of the total energy consumption in the world [5].	1
Figure 2. 1: Schematic of PEM fuel cell [7].	15
Figure 2. 2: Schematic representation of the overall photon-induced reaction process for water splitting using a solid photocatalyst [26]	22
Figure 2. 3: Trends in hydrogen evolution reaction activity. Experimental HER activity expressed as the exchange current density, $\log(i_0)$ , for different metal surfaces as a function of the calculated $*H_{ad}$ chemisorption energy, $\Delta E_H$ . The result of a simple theoretical kinetic model is also shown as a dotted line.	25
Figure 2. 4: (i). A typical structure of graphene and (ii). Graphene oxide	27
Figure 2. 5: Schematic diagram for the synthesis of graphene oxide by Hummers method.	28
Figure 2. 6: Linear sweep voltammetry (LSV) curves of RGO, Ni, rGN6 and GN6 in 0.50 M $H_2SO_4$ solution (a) and in 0.50 M $Na_2SO_4$ solution of pH 10 (b). The insets are LSV curves of GN2, GN6, and GN8 composites with reference to Ni [88].	30
Figure 2. 7: Representative examples of some organic ligands used in metal-organic frameworks	32
Figure 2. 8: (a) Tafel plots of blank, MOF and MOF-PABA; and (b) MOF, (c) MOF-3.6wt%-PABA and (d) MOF-5wt%-PABA at $0.10 \text{ V}\cdot\text{s}^{-1}$ in the presence of different $H_2SO_4$ concentration on gold electrode in $0.1 \text{ mol}\cdot\text{L}^{-1}$ DMSO/TBAP electrolytic system.	37
Figure 3.1: Basic components of FTIR [1].	55
Figure 3.2: Overview of scanning electron microscopy.	56
Figure 3.3: Overview of transmission electron microscope.	58
Figure 3. 4: Typical cyclic voltammogram showing the peak cathodic and anodic current respectively for a reversible reaction [19].	63
Figure 4. 1: XRD patterns of MOF, GO, and GO/MOF with reference to MOF CSID.	74

Figure 4. 2: FTIR spectra of MOF, GO and GO/MOF.....	75
Figure 4. 3: TGA analysis of MOF, GO and GO/MOF composite.....	77
Figure 4. 4: DSC analysis of MOF, GO and GO/MOF composite. ....	77
Figure 4. 5: FE-SEM image of (a) MOF, (c) GO (e) GO/MOF composite (inset : magnification on the crystal structure to view the surface of the crystal) and EDS spectrum of (b) MOF, (d) GO, (f) GO/MOF composite. ....	79
Figure 4. 6: TEM image of (a) MOF, (c) GO and (e) GO/MOF; composite and EDX spectrum of (b) MOF, (d) GO and (f) GO/MOF composite. ....	81
Figure 4. 7: HRTEM images of (a) MOF, (c) GO and (e) GO/MOF composite; and SAED patterns of (b) MOF, (d) GO and (f) GO/MOF composite. ....	82
Figure 4. 8: (a) CV curves of Blank, MOF, GO and GO/MOF composite at 0.1 v.s <sup>-1</sup> in 0.1 mol.L <sup>-1</sup> TBAP/DMSO electrolyte solution on Au electrode. (b-d) MOF, GO and GO/MOF at different scan rates (0.02-0.1 v.s <sup>-1</sup> ) in 0.1 mol.L <sup>-1</sup> TBAP/DMSO, respectively. ....	84
Figure 4. 9: (a) The log-log plot of the absolute value of the peak current vs scan rate, (b) peak current as a function of square root of scan rate and (c) peak current as a function of scan rate for MOF, GO and GO/MOF on gold in 0.1 mol.L <sup>-1</sup> DMSO/TBAP electrode system at different scan rates (0.02-0.1 v.s <sup>-1</sup> ).....	86
Figure 4. 10: (a) CV curves of Blank, GO, MOF and GO/MOF composite in the presence of 0.300 mol.L <sup>-1</sup> H <sub>2</sub> SO <sub>4</sub> at 0.10 V.s <sup>-1</sup> and CV curves of (b) MOF (c) GO and (d) GO/MOF composite in different concentration of hydrogen source (0.033-0.450 mol.L <sup>-1</sup> H <sub>2</sub> SO <sub>4</sub> ) at 0.10 V.s <sup>-1</sup> on Au electrode in 0.1 mol.L <sup>-1</sup> TBAP/DMSO electrode system.....	88
Figure 4. 11: Tafel plots of (a) blank, GO, MOF and GO/MOF composite (~2.0x10 <sup>-4</sup> mol.L <sup>-1</sup> ) in the presence 0.300 mol.L <sup>-1</sup> H <sub>2</sub> SO <sub>4</sub> at 0.10 Vs <sup>-1</sup> (b) MOF (c) GO and (d) GO/MOF composite in different concentrations of H <sub>2</sub> SO <sub>4</sub> and 0.10 Vs <sup>-1</sup> scan rate on Au electrode in 0.1 mol.L <sup>-1</sup> TBAP/DMSO electrode system. ....	91
Figure 4. 12: (a) Plot of log current as a function of pH of the solution and (b) Pourbaix diagram of hydrogen evolution reaction .....	93
Figure 5. 1: XRD patterns of MOF, Pd@GO, Pd@MOF and Pd@GO/MOF with reference to MOF CSID.....	105

Figure 5. 2: FTIR spectra of MOF, Pd@GO and Pd@GO/MOF.....	106
Figure 5. 3: TGA analysis of MOF, Pd@GO and Pd@GO/MOF composite.....	107
Figure 5. 4: DSC analysis of MOF, Pd-GO and Pd@GO/MOF composite.....	108
Figure 5. 5: FE-SEM image of (a) MOF, (c) Pd@GO (e) Pd@GO/MOF composite (inset : magnification on the crystal structure to view the surface of the crystal) and EDS spectrum of (b) MOF, (d) Pd@GO, (f) Pd@GO/MOF composite.....	110
Figure 5. 6: TEM image of (a) MOF, (c) Pd@GO (e) Pd@GO/MOF composite (inset : magnification on the crystal structure to view the surface of the crystal) and EDX spectrum of (b) MOF, (d) Pd@GO, (f) Pd@GO/MOF composite. ....	112
Figure 5. 7: HRTEM images of (a) MOF, (c) Pd@GO (e) Pd@GO/MOF composite and SAED patterns of (b) MOF, (d) Pd@GO, (f) Pd@GO/MOF composite. ....	113
Figure 5. 8: (a). CV curves of Blank, MOF, Pd@GO, Pd@MOF and Pd@GO/MOF composite at $0.1 \text{ v.s}^{-1}$ in $0.1 \text{ mol.L}^{-1}$ TBAP/DMSO electrolyte solution on Au electrode. (b-d). MOF, Pd@GO and Pd@GO/MOF at different scan rates ( $0.02\text{-}0.1 \text{ v.s}^{-1}$ ) in $0.1 \text{ mol.L}^{-1}$ TBAP/DMSO, respectively. ....	115
Figure 5. 9: (a) The log-log plot of the absolute value of the peak current vs scan rate, (b) peak current as a function of square root of scan rate and (c) peak current as a function of scan rate for MOF, Pd@GO and Pd@GO/MOF on gold in $0.1 \text{ mol.L}^{-1}$ DMSO/TBAP electrode system at different scan rates ( $0.02 - 0.10 \text{ V.s}^{-1}$ ). ....	118
Figure 5. 10: (a) CV curves of Blank, MOF, Pd@GO and Pd@GO/MOF composite in the presence of $0.300 \text{ mol.L}^{-1} \text{ H}_2\text{SO}_4$ at $0.10 \text{ Vs}^{-1}$ and CV curves of (b) MOF and (c) Pd@GO/MOF composite in different concentration of hydrogen source ( $0.033\text{-}0.450 \text{ mol.L}^{-1} \text{ H}_2\text{SO}_4$ ) at $0.10 \text{ Vs}^{-1}$ on Au electrode in $0.1 \text{ mol.L}^{-1}$ TBAP/DMSO electrode system.....	121
Figure 5. 11: Tafel plots of (a) blank, MOF and Pd@GO/MOF composite ( $\sim 2.0 \times 10^{-4} \text{ mol.L}^{-1}$ ) in the presence $0.300 \text{ mol.L}^{-1} \text{ H}_2\text{SO}_4$ at $0.10 \text{ V.s}^{-1}$ (b) MOF and (c) Pd@GO/MOF composite in different concentrations of $\text{H}_2\text{SO}_4$ and $0.10 \text{ Vs}^{-1}$ scan rate on Au electrode in $0.1 \text{ mol.L}^{-1}$ TBAP/DMSO electrode system.....	124
Figure 5. 12: (a) Plot of log current as a function of pH of the solution and (b) Pourbaix diagram of hydrogen evolution reaction .....	126

## LIST OF SCHEMES

---

<b>Scheme 1. 1:</b> Proposed hydrogen spillover mechanism on Pd@GO/MOF. ....	6
<b>Scheme 4.1:</b> Synthesis of MOF and GO/MOF composite through hydrothermal and impregnation method, respectively. ....	72
<b>Scheme 4.2:</b> Proposed mechanisms involved in the HER kinetics of the composite .....	89
<b>Scheme 5.1:</b> Proposed mechanisms involved in the HER kinetics of the composite. ....	121

## LIST OF TABLES

---

Table 1. 1: Types of renewable energies and their disadvantages .....	2
Table 2. 1: Comparison between the ability of various GO or rGO electrocatalysts toward HER. ....	30
Table 2. 2: Comparison between the ability of various MOF electrocatalysts towards HER. ....	38
Table 4. 1: Experimental values of Tafel slope ( $b$ ), charge transfer coefficient ( $1-\alpha$ ), exchange current density ( $i_0$ ) and TOF of MOF, GO and GO/MOF composite. ....	92
Table 5.1: Electrochemical parameters of MOF, Pd@GO, Pd@MOF and Pd@GO/MOF composite. ....	119
Table 5.2: Experimental values of tafel slope ( $b$ ), charge transfer coefficient ( $1-\alpha$ ), exchange current density ( $i_0$ ) and TOF of MOF and Pd@GO/MOF composite. ....	125

## LIST OF ABBREVIATIONS

---

Cat	: Catalyst
CFG	: Cobalt iron oxide graphene
CNTs	: Carbon nanotubes
CSID	: Crystal structure information data
CV	: Cyclic voltammetry
CuPc	: Copper(II) phthalocyanine
DMF	: Dimethylformamide
DMSO	: Dimethyl sulfoxide
DSC	: Differential scanning calorimetry
DST	: Department of Science and Technology
EDS, EDX	: Energy dispersive X-ray spectroscopy
EMU	: Electron microscope unit
FESEM	: Field Emission Scanning Electron Microscope
FTIR	: Fourier transform infrared
GGNR	: Graphene/graphene nanoribbon
GHG	: Greenhouse gases
GO	: Graphene oxide
H <sub>3</sub> BTC	: Trimesic acid, 1,3,5-benzenetricarboxylic acid
H <sub>ad</sub>	: Adsorbed hydrogen atom
HER	: Hydrogen evolution reaction
HFC	: Hydrogen fuel cell
HKUST-1	: Hong Kong University of Science and Technology-1
HRTEM	: High Resolution Transmittance Electron Microscope
HySA	: Hydrogen South Africa
IR	: Infrared
IRMOF	: Isorectecular metal organic framework
LMCT	: Ligand metal charge transfer

LSV	: Linear sweep voltammetry
M	: Metal
MIL	: Materials of Institute Lavoisier
MOFs	: Metal organic frameworks
NFG	: Nickel iron oxide graphene
NFO	: Nickel ferrite
NPs	: Nanoparticles
NU	: Northwestern University
PANI	: Polyaniline
PABA	: Poly(3-aminobenzoic acid)
PGMs	: Platinum group metals
RHE	: Reference hydrogen electrode
rGO	: Reduced graphene oxide
SAED	: Selected area electron diffraction
SBUs	: Secondary building units
SEM	: Scanning electron microscope
SMR	: Steam methane reforming
STA	: Simultaneous thermal analysis
TBAP	: Tetrabutylammonium percholate
TEM	: Transmission electron microscope
TGA	: Thermogravimetric analysis
TOF	: Turnover frequency
XRD	: X-ray diffraction

## LIST OF SYMBOLS

---

$A$	: Area of the electrode
$C$	: Concentration
$D$	: Diffusion coefficient
$E_{final}$	: Final potential
$E_{initial}$	: Initial potential
$E^{\circ}$	: Formal electrode potential
$E_p$	: Peak potential
$E_{p,a}$	: Anodic peak potential
$E_{p,c}$	: Cathodic peak potential
$F$	: Faraday constant
$I$	: Current
$I_p$	: Peak current
$I_{p,a}$	: Current for the anodic reaction
$I_{p,c}$	: Current for the cathodic reaction
$n$	: Number of electrons transferred
$Q$	: Charge
$R$	: Sample resistance
$\Gamma$	: Surface coverage
$v$	: Scan rate
$V$	: Applied voltage
$M$	: Mass percentage
$m$	: Mass of per square centimeter

# CHAPTER ONE

## INTRODUCTION

### 1.1. BACKGROUND

#### 1.1.1. Energy

Energy drives human life and is extremely crucial for continuous human development. The global demand for energy is rapidly increasing with growth in human population, urbanisation and modernisation [1]. Since developing countries depend on fossil fuels to meet their energy requirements; oil, gas and coal provide almost 90% of the global energy demands (Figure 1.1) [2]. On the other hand, renewable and nuclear energy contribute only 7% [3] and 9% [4] of the total energy needs, respectively. This has resulted in elevated greenhouse gases emission and an increase in fuel prices, which are the main driving forces behind efforts to utilise renewable energy sources more effectively [4].

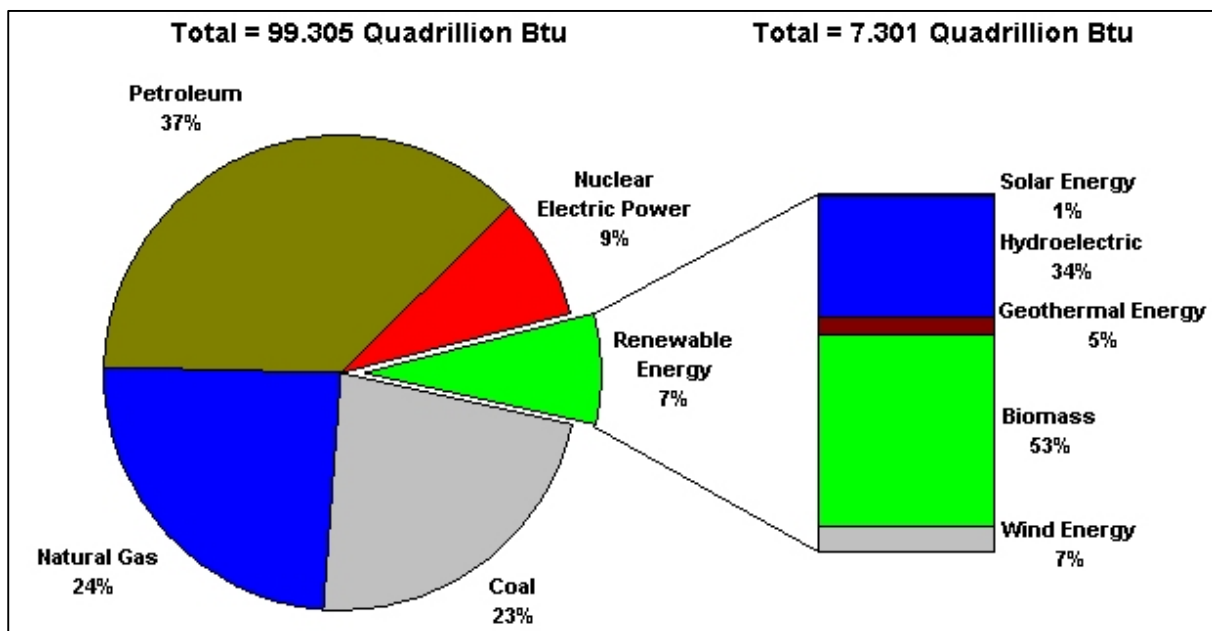


Figure 1. 1: Chart of the total energy consumption in the world [5].

Renewable energy systems have obvious advantages such as providing energy services with no greenhouse gas emissions and polluting the air. Despite the advantages of these systems, they present considerable drawbacks. As indicated in the Table 1.1. below, most renewable energy resources depend on the climate, hence, their use requires complex design, planning and controlled optimisation methods [6,8]. Amongst these renewable sources, hydrogen as an energy carrier energy has been identified as a candidate to counter those limitations through the hydrogen technology process [11,12].

**Table 1.1:** Types of renewable energies and their disadvantages.

<b>Type of renewable energy</b>	<b>Disadvantage(s)</b>
<b>Wind power</b>	This system may not be technically viable in all locations because of low wind speeds (Areas where winds are stronger and more constant are most preferred) [5].
<b>Hydropower</b>	Its construction requires a large area and it poses a threat to the aquatic ecosystem [6].
<b>Bioenergy</b>	May lead to deforestation and it requires a lot of water [7].
<b>Solar energy</b>	It depends on the weather and requires a lot of space [8]
<b>Geothermal energy</b>	May cause surface instability and requires very high temperatures [9].
<b>Hydrogen energy</b>	It is difficult to produce and store hydrogen [10].

### 1.1.2. Hydrogen energy technology

The idea of using hydrogen as an energy carrier was strengthened noticeably after the global energy crisis [4, 13]. Hydrogen holds the promise as an alternative fuel with many social, economic and environmental benefits to its credit [10]. This is supported by the following facts: it is renewable; has a high energy yield of  $122 \text{ kJg}^{-1}$ , which is 2.75 times greater than hydrocarbon fuels [14]; it has a very low density in the gaseous state; its consumption comes with minimal harmful emissions (e.g. nitrous oxides) and the by-product is only water [15], regardless of the method of utilisation. However, there are significant challenges hindering the large scale applications and commercialisation of hydrogen fuel. These problems include the lack of safe handling and effective methods for hydrogen production and storage [12]. In South Africa, the commitment to energy security is identified as one of the few priority areas in the Department of Science and Technology's (DST) ten-year innovation plan [16]. Within the DST's grand challenge on energy security, the interest in hydrogen falls under the national hydrogen and fuel cell technologies research, development and innovation strategies, branded as Hydrogen South Africa (HySA), which was initiated in 2008 [16]. The strategy stimulates and guides innovation along value of hydrogen production, storage and infrastructure in fuel cell technology. However, the primary route for hydrogen production is through conversion of natural gas and other light hydrocarbons, which contributes to greenhouse emissions. The new search for a feasible technology is underway and water splitting electrolysis is deemed as an alternative route for hydrogen production. Water splitting electrolysis gives off clean hydrogen, however since the process requires a lot of energy, the increase in electricity prices hindered the application of the process. Sustainable production of hydrogen through electrochemical water splitting is one of the most environmentally friendly techniques towards energy storage and conversion. The quest for utilising hydrogen as a future energy carrier may be met through efficient hydrogen evolution reaction (HER), which still remains a technically challenging issue due to the choice of an electrocatalyst to be used. On the other hand, hydrogen gas can be stored in three ways, and this is through liquefaction, compression of hydrogen or storage in a

solid material [17]. The large amount of energy consumed during liquefaction and the continuous boil-off of hydrogen limits the possible use of liquid-hydrogen storage system [18]. Hydrogen compression into tanks also consumes energy and requires a very high pressure to obtain sufficient hydrogen fuel for a reasonable driving cycle of 300 miles [19]. This leads to safety issues related to tank rupture in case of accidents and the weight penalty [19]. To overcome these challenges, the current attention is focused on solid state hydrogen storage materials [20–22]. The great advantage of using solid materials for hydrogen technology lies mostly in cost and efficiency of materials and may be monitored using HER mechanism.

## **1.2. PROBLEM STATEMENT**

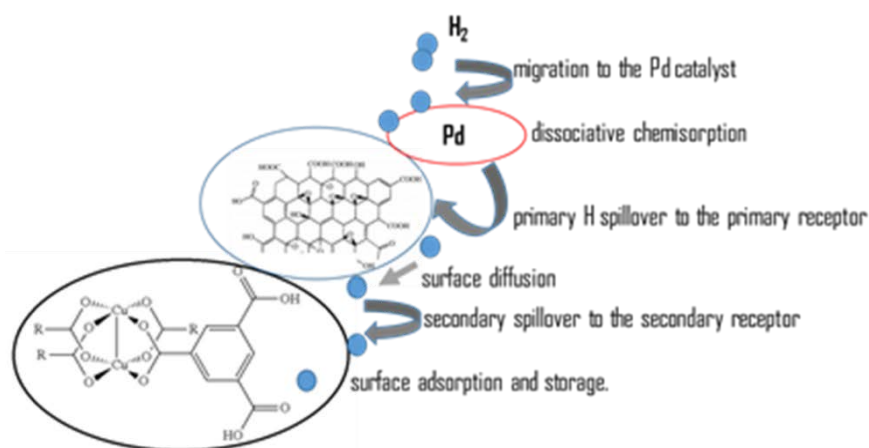
Hydrogen evolution reaction has been identified as an electrochemical process to monitor hydrogen production and storage in solid materials [23]. Solid catalysts such as platinum (Pt) based materials have shown great potential as electrocatalysts for HER due to their good conductivity and high catalytic activity (possessing high current density at low potentials) [24–26]. However, limited reserve in earth and high cost restrict their wide application in industry, which is a major challenge for commercialisation of the fuel cell devices. Therefore, many efforts were made to find the other materials for HER in order to replace or reduce the use of Pt [27-29]. Taking these into consideration, several porous materials such as carbon nanotubes [30], carbon nanofiber [24], metal sulfides [30, 31] and metal organic frameworks [21, 28] have been proposed as electrocatalysts for HER. Amongst these materials, MOFs have shown to be very promising hydrogen adsorbents mainly due to their adjustable pore sizes as well as defined hydrogen occupation sites [32]. Furthermore, these materials possess 3D structural features and large surface areas with many active sites [32]. However, the MOF materials possess drawbacks such as H<sub>2</sub> embrittlement, moisture instability and poor H<sub>2</sub> adsorption and desorption at ambient conditions (the high H<sub>2</sub> adsorption amounts of this material were measured only at 77 K and declined dramatically at ambient temperature, due to weak physisorption of hydrogen on MOFs)

[33]. Recently, the spillover effect for enhanced uptakes of hydrogen at ambient temperature (298K) on adsorbents has attracted much attention from the viewpoint of practical applications. This spillover of hydrogen is a process in which hydrogen dissociates onto the metal catalyst and hydrogen atoms formed migrate onto the support surface/material [34,35]. The process involves the transfer of electrons to acceptor within the support and also enhances the chemical nature of the support and again activates an inactive material [34,35]. Hence, there is a need for fabrication of porous material-based carbon/MOF composites to enhance their structural properties and hydrogen spillover.

### 1.3. RATIONALE

Several MOFs [36–38] and their composites [39–42] have been reported for hydrogen uptakes. In relation to this, Li and Yang [22,43] reported bridged isorecticular metal organic framework (IRMOF)-1 and IRMOF-8 to have enhanced hydrogen uptakes at 298 K compared to unbridged MOFs. Moreover, Petit and Bandoz [44] reported graphene oxide/ Hong Kong University of Science and Technology (GO/HKUST-1) to be a very efficient composite. It is hypothesised that the reaction of the HKUST-1 units with the functionalities of GO (mainly OH, COOH and O) leads to the creation of new pores, and the additional porosity is responsible for the enhancement in the hydrogen uptake [44]. This composite provides individual attribution, wherein the GO will provide the rich functional groups to form an interaction between oxygen and the metal centres of MOF, and this will also assist in enhancing the adsorption properties of the individual materials [38,44,45]. To date, the GO/MOF composite has not been used as an electrocatalyst for HER studies. Furthermore, to improve the feasibility of this approach, we introduce a dissociator, palladium (Pd) to form a composite Pd@GO/MOF composite to facilitate hydrogen spillover through HER processes. The choice of the dissociator (Pd) is because of being unique material with a strong affinity to hydrogen, owing to both its catalytic and hydrogen absorbing properties, and it plays important roles in hydrogen economy [35]. This composite formation was motivated

by the work of Zhou *et al.* [42], who showed the merits of combining the GO/MOF composites and hydrogen spillover mechanism (using platinum as a dissociation source). Their composite Pt@GO/MOF was prepared using the in-situ synthesis method between Pt@GO and MOF. In this regard, we aim to disperse the palladium nanoparticles (NPs) onto the GO surface and then later incorporate with MOF using impregnation method, as to increase the dissociation ability of the metal and hence the quantity of hydrogen to be adsorbed/produced. As a result (proposed mechanism, Scheme 1.1), hydrogen protons from the hydrogen source will first be chemisorbed and dissociated on the surface of palladium and then be migrated to the surface of the primary spillover receptor GO. Subsequently, hydrogen atoms further diffuse into the secondary spillover receptor MOF with high porosity and new pores at the interface between primary layers and secondary units [34,35].



**Scheme 1. 1:** Proposed hydrogen spillover mechanism on Pd@GO/MOF.

## 1.4. RESEARCH AIM AND OBJECTIVES

### 1.4.1. Aim

This study aims to prepare porous GO/MOF and Pd@GO/MOF composites for efficient and safe hydrogen production and storage applications.

### 1.4.2. Objectives

The objectives are to:

- I. synthesise GO, MOF, GO/MOF
- II. optimise structures of the synthesised materials by introduction of Pd to form Pd@GO, Pd@MOF and Pd@GO/MOF composites for enhanced hydrogen production and spillover mechanism at reasonable operating temperatures
- III. carry out structural characterisation of the samples using powder X-ray diffraction (PXRD) and Fourier transform infrared (FTIR)
- IV. evaluate the thermal stability of the samples by thermogravimetric analysis (TGA/DSC)
- V. perform morphological and elemental characterisations using scanning electron microscopy/energy dispersive spectroscopy (SEM/EDS), transmission electron microscopy/energy dispersive X-ray spectroscopy (TEM/EDX) and high resolution transmission electron microscopy/selected area electron diffraction (HRTEM/SAED)
- VI. study electrochemical behaviour of the synthesised materials using cyclic voltammetry (CV)
- VII. evaluate HER studies of synthesised porous systems at room temperature through Tafel parameters and turn over frequency (TOF).

## 1.4. DISSERTATION OUTLINE

This MSc dissertation consists of six chapters. All these chapters channel the electrocatalytic properties and hydrogen storage capacities of graphene oxide-metal organic framework composites. The outline of the remaining chapters in the dissertation is as follows:

- Chapter two: it concentrates on the comprehensive review of synergetic effect on graphene oxide and metal organic framework nanocomposites as electrocatalysts for hydrogen evolution reaction, wherein it introduces the

theoretical considerations of hydrogen technology, hydrogen evolution reaction, Hydrogen storage systems, metal organic frameworks, graphene oxide and graphene oxide-metal organic framework composite.

- Chapter three: It focuses on the review of analytical techniques used for structural, thermal, morphological and electrochemical characterisations.
- Chapter four: focuses on the synthesis of metal organic frameworks, graphene oxide and graphene oxide-metal organic framework composite and their catalytic hydrogen production and storage.
- Chapter five: focuses on the synthesis of palladium loaded graphene oxide - metal organic framework, its hydrogen storage ability and capacity.
- Chapter six: Summary of the main conclusions and recommendations.

## 1.5. REFERENCES

- [1] J. Goudsblom, "Energy and civilization," *Int. Rev. Sociol.*, vol. 3, pp. 405–411, 2012.
- [2] P. Laha and B. Chakraborty, "Energy model – A tool for preventing energy dysfunction," *Renew. Sustain. Energy Rev.*, vol. 73, pp. 95–114, 2017.
- [3] J. Goldemberg, "Ethanol for a sustainable energy future," *Sci.*, vol. 315, pp. 808–810, 2007.
- [4] M. Asif and T. Muneer, "Energy supply, its demand and security issues for developed and emerging economies," *Renew. Sustain. Energy Rev.*, vol. 11, pp. 1388–1413, 2007.
- [5] R. Baños, F. Manzano-Agugliaro, F. G. Montoya, C. Gil, A. Alcayde, and J. Gómez, "Optimization methods applied to renewable and sustainable energy: A review," *Renew. Sustain. Energy Rev.*, vol. 15, pp. 1753–1766, 2011.
- [6] C. Zarfl, A. E. Lumsdon, J. Berlekamp, L. Tydecks, and K. Tockner, "A global boom in hydropower dam construction," *Aquat. Sci.*, vol. 77, pp. 161–170, 2014.
- [7] S. Meher Kotay and D. Das, "Biohydrogen as a renewable energy resource-

- Prospects and potentials,” *Int. J. Hydrogen Energy*, vol. 33, pp. 258–263, 2008.
- [8] D. Bahnemann, “Photocatalytic water treatment: Solar energy applications,” *Sol. Energy*, vol. 77, pp. 445–459, 2004.
- [9] M. F. Akorede, H. Hizam, and E. Pouresmaeil, “Distributed energy resources and benefits to the environment,” *Renew. Sustain. Energy Rev.*, vol. 14, pp. 724–734, 2010.
- [10] A. Midilli, M. Ay, I. Dincer, and M. A. Rosen, “On hydrogen and hydrogen energy strategies I: Current status and needs,” *Renew. Sustain. Energy Rev.*, vol. 9, pp. 255–271, 2005.
- [11] K. Schoots, F. Ferioli, G. J. Kramer, and B. C. C. van der Zwaan, “Learning curves for hydrogen production technology: An assessment of observed cost reductions,” *Int. J. Hydrogen Energy*, vol. 33, pp. 2630–2645, 2008.
- [12] S. G. Chalk and J. F. Miller, “Key challenges and recent progress in batteries, fuel cells, and hydrogen storage for clean energy systems,” *J. Power Sources*, vol. 159, pp. 73–80, 2006.
- [13] M. Momirlan and T. . Veziroglu, “Current status of hydrogen energy,” *Renew. Sustain. Energy Rev.*, vol. 6, pp. 141–179, 2002.
- [14] H. Fayaz, R. Saidur, N. Razali, F. S. Anuar, A. R. Saleman, and M. R. Islam, “An overview of hydrogen as a vehicle fuel,” *Renew. Sustain. Energy Rev.*, vol. 16, pp. 5511–5528, 2012.
- [15] K. Bennaceur, B. Clark, F. M. Orr Jr, T. S. Ramakrishnan, C. Roulet, and E. Stout. “Hydrogen: a future energy carrier?.” *Gas*, vol. 25, pp. 3-15, 2005.
- [16] A. B. Sebitosi and P. Pillay, “Renewable energy and the environment in South Africa: A way forward,” *Energy Policy*, vol. 36, pp. 3312–3316, 2008.
- [17] H. Barthelemy, “Hydrogen Storage - Recent improvements and industrial perspectives,” *Proc. Int. Conf. Hydrog. Safety*, vol. 13, pp. 1–19, 2013.
- [18] J. Sakamoto, J. Nakayama, T. Nakarai, N. Kasai, T. Shibutani, and A. Miyake, “Effect of gasoline pool fire on liquid hydrogen storage tank in hybrid hydrogen-gasoline fueling station,” *Int. J. Hydrogen Energy*, vol. 41, pp. 2096–2104, 2016.
- [19] K. O'Malley, G. Ordaz, J. Adams, K. Randolph, C. C. Ahn, and N. T. Stetson, “Applied hydrogen storage research and development: A perspective from the

- U.S. Department of Energy," *J. Alloys Compd.*, vol. 645, pp. S419–S422, 2015.
- [20] B. Sakintuna, F. Lamari-Darkrim, and M. Hirscher, "Metal hydride materials for solid hydrogen storage: A review," *Int. J. Hydrogen Energy*, vol. 32, pp. 1121–1140, 2007.
- [21] P. Q. Liao, J. Q. Shen, and J. P. Zhang, "Metal-organic frameworks for electrocatalysis," *Coord. Chem. Rev.*, vol. 2, pp. 1-27, 2017.
- [22] H. W. Langmi, J. Ren, B. North, M. Mathe, and D. Bessarabov, "Hydrogen storage in metal-organic frameworks: A review," *Electrochim. Acta*, vol. 128, pp. 368–392, 2014.
- [23] K. E. Ramohlola, M. Masikini, S. B. Mdluli, G. R. Monama, M. J. Hato, K. M. Molapo, E. I. Iwuoha, and K. D. Modibane, "Electrocatalytic Hydrogen Evolution Reaction of Metal Organic Frameworks decorated with poly (3-aminobenzoic acid)," *Electrochim. Acta*, vol. 246, pp. 1174–1182, 2017.
- [24] Y. Zhang, J. Tan, F. Wen, Z. Zhou, and M. Zhu, "ScienceDirect Platinum nanoparticles deposited nitrogen-doped carbon nanofiber derived from bacterial cellulose for hydrogen evolution reaction," *Int. J. Hydrogen Energy*, vol. 43, pp. 6167–6176, 2018.
- [25] F. J. Vidal-Iglesias, J. Solla-Gullón, V. Montiel, J. M. Feliu, and A. Aldaz, "Screening of electrocatalysts for direct ammonia fuel cell: Ammonia oxidation on PtMe (Me: Ir, Rh, Pd, Ru) and preferentially oriented Pt(1 0 0) nanoparticles," *J. Power Sources*, vol. 171, pp. 448–456, 2007.
- [26] F. Ye, C. Xua, G. Liub, J. Lid, X. Wangd, X. Dua, and J. K. Leeb, "A novel PtRuIr nanoclusters synthesized by selectively electrodepositing Ir on PtRu as highly active bifunctional electrocatalysts for oxygen evolution and reduction," *Energy Convers. Manag.*, vol. 155, no. October 2017, pp. 182–187, 2018.
- [27] Y. Liu, C. M. Brown, D. A. Neumann, D. B. Geohegan, A. A. Puretzky, C. M. Rouleau, H. Hu, D. Styers-Barnett, P. O. Krasnov, B. I. Yakobson, "Metal-assisted hydrogen storage on Pt-decorated single-walled carbon nanohorns," *Carbon N. Y.*, vol. 50, pp. 4953–4964, 2012.
- [28] Y. Z. Chen, R. Zhang, L. Jiao, and H. L. Jiang, "Metal–organic framework-derived porous materials for catalysis," *Coord. Chem. Rev.*, vol. 362, pp. 1–23,

- 2018.
- [29] C. O. Ania, M. Seredych, E. Rodriguez-Castellon, and T. J. Bandosz, "New copper/GO based material as an efficient oxygen reduction catalyst in an alkaline medium: The role of unique Cu/rGO architecture," *Appl. Catal. B Environ.*, vol. 163, pp. 424–435, 2015.
- [30] D. Y. Wang, M. Gong, H.L. Chou, C.J. Pan, H.A. Chen, Y. Wu, M.C. Lin, M. Guan, J. Yang, C.W. Chen, Y.L. Wang, B.J. Hwang, C.C. Chen, and H. Dai, "Highly active and stable hybrid catalyst of cobalt-doped FeS<sub>2</sub> nanosheets-carbon nanotubes for hydrogen evolution reaction," *J. Am. Chem. Soc.*, vol. 137, pp.1587–1592, 2015.
- [31] M. R. Gao *et al.*, "An efficient molybdenum disulfide/cobalt diselenide hybrid catalyst for electrochemical hydrogen generation," *Nat. Commun.*, vol. 6, pp. 1–7, 2015.
- [32] B. Valizadeh, T. N. Nguyen, and K. C. Stylianou, "Shape engineering of metal-organic frameworks," *Polyhedron*, vol. 145, pp. 1–15, 2018.
- [33] G. R. Monama, S. B. Mdluli, G. Mashao, M. D. Makhafola, K. E. Ramohlola, K. M. Molapo, M. J. Hato, K. Makgopa, E. I. Iwuoha, and K. D. Modibane, "Palladium deposition on copper(II) phthalocyanine/metal organic framework composite and electrocatalytic activity of the modified electrode towards the hydrogen evolution reaction," *Renew. Energy*, vol. 119, pp. 62–72, 2018.
- [34] A. D. Lueking and R. T. Yang, "Hydrogen spillover to enhance hydrogen storage — study of the effect of carbon physicochemical properties," vol. 265, pp. 259–268, 2004.
- [35] S. K. Konda and A. Chen, "Palladium based nanomaterials for enhanced hydrogen spillover and storage," *Biochem. Pharmacol.*, vol. 19, pp. 100–108, 2016.
- [36] W. Liu and X. B. Yin, "Metal-organic frameworks for electrochemical applications," *TrAC - Trends Anal. Chem.*, vol. 75, pp. 86–96, 2016.
- [37] B. Xiao and Q. Yuan, "Nanoporous metal organic framework materials for hydrogen storage," *Particuology*, vol. 7, pp. 129–140, 2009.
- [38] N. Stock, and S. Biswas, "Synthesis of Metal-Organic Frameworks (MOFs):

- Routes to Various,” *Chem. Revs.*, vol. 112, pp. 933–969, 2012.
- [39] S. Kempahanumakkagari, K. Vellingiri, A. Deep, E. E. Kwon, N. Bolan, and K. Kim, “Metal – organic framework composites as electrocatalysts for electrochemical sensing applications,” *Coord. Chem. Rev.*, vol. 357, pp. 105–129, 2018.
- [40] J. Chen, G. Xia, P. Jiang, Y. Yang, R. Li, R. Shi, J. Su, and Q. Chen, “Active and Durable Hydrogen Evolution Reaction Catalyst Derived from Pd-Doped Metal-Organic Frameworks,” *ACS Appl. Mater. Interfaces*, vol. 8, pp. 13378–13383, 2016.
- [41] H. Zhou, J. Zhang, D. Ji, A. Yuan, and X. Shen, “Microporous and Mesoporous Materials Effect of catalyst loading on hydrogen storage capacity of ZIF-8 / graphene oxide doped with Pt or Pd via spillover,” *Microporous Mesoporous Mater.*, vol. 229, pp. 68–75, 2016.
- [42] H. Zhou, X. Liu, J. Zhang, X. Yan, and Y. Liu, “ScienceDirect Enhanced room-temperature hydrogen storage capacity in Pt-loaded graphene oxide / HKUST-1 composites,” *Int. J. Hydrogen Energy*, vol. 39, pp. 2160–2167, 2013.
- [43] L. Wang and R. T. Yang, “New sorbents for hydrogen storage by hydrogen spillover: A review,” *Energy Environ. Sci.*, vol. 1, pp. 268–279, 2008.
- [44] C. Petit, B. Levasseur, B. Mendoza, and T. J. Bandosz, “Reactive adsorption of acidic gases on MOF/graphite oxide composites,” *Microporous Mesoporous Mater.*, vol. 154, pp. 107–112, 2012.
- [45] H. Zhou, J. Zhang, J. Zhang, X. Yan, X. Shen, and A. Yuan, “Spillover enhanced hydrogen storage in Pt-doped MOF / graphene oxide composite produced via an impregnation method,” *INOCHE*, vol. 54, pp. 54–56, 2015.

## CHAPTER TWO

### A COMPREHENSIVE REVIEW OF SYNERGETIC EFFECT ON GRAPHENE OXIDE AND METAL ORGANIC FRAMEWORK NANOCOMPOSITES AS ELECTROCATALYSTS FOR HYDROGEN EVOLUTION REACTION

---

*This chapter is pending submission as a book chapter for possible publication:*

#### CHAPTER SUMMARY

Exploiting low-cost and efficient electrocatalysts for hydrogen evolution reaction (HER) is an important route to resolve the energy crisis and environmental pollution. HER process plays a vital role in many energy storage and conversion systems, including water splitting, rechargeable metal-air batteries, and the unitised regenerative fuel cells. The platinum based catalysts are regarded as best electrocatalysts for the HER, however, they suffer from high price and scarcity problems. Therefore, it is urgently necessary to develop efficient electrocatalyst of carbon based materials. Graphene oxide (GO) is an atom-thick sheet of  $sp^2$ -hybridised carbons, possesses an excellent electron transfer ability and large specific surface area. It can be easily manufactured by simple and scalable chemical oxidation approaches from graphite, the reduction of GO into reduced graphene oxide (rGO) is a widely-used method to obtain graphene. In HER, GO can also be incorporated with metals and porous materials for synergetic effect as co-catalysts for enhancement of electrocatalytic activities. On the other hand, metal-organic frameworks (MOFs) are crystalline materials with porous network structure. They possess various compositions, large specific surface area, tunable pore structures, and they are easily functionalised. Recently, MOF-based electrocatalysts for HER have been rapidly developed where they exhibit excellent catalytic performance for HER, demonstrating a promising application prospect in

HER. In this chapter, the background of hydrogen energy and hydrogen evolution reaction structure, category, and synthesis of GO and MOFs are introduced briefly. Then, the applications of the GO- and MOFs-based electrocatalysts for HER in recent years are discussed in detail. Their HER parameters such as Tafel slope and current density are emphatically discussed and followed by the synergetic effect of HER studies of GO/MOF composites as an alternative electrocatalyst for future hydrogen production and storage via HER mechanism.

## **2.1. INTRODUCTION**

### **2.1.1. Hydrogen energy background**

The global energy crisis and environment pollution are becoming more serious due to the utilisation of fossil fuel [1]. Developing a new, efficient and clean energy source based on renewable energy is extremely urgent [2]. Conversion of hydrogen gas into energy is the most promising strategy to resolve these crises. Hydrogen is a colorless and tasteless element which is abundant on the universe [3], but may be found in chemical compound such water and hydrocarbons [4]. Unlike conventional petroleum-based fuels and natural gas derivatives, hydrogen gas has high energy density and light molecular structure. In this regard, hydrogen is expected to play an important role in the future energy economy. This is because hydrogen is carbon-free, non-toxic, and its thermal or electrochemical combustion with oxygen yields nothing but energy and water - although its combustion in air might generate nitric oxide air pollutants in controllable amounts [5].

As it can be produced from a range of renewable and non-renewable sources, hydrogen has the potential to form the basis of a clean and virtually limitless energy system [6]. Another advantage is that the main source of hydrogen is water, which is essentially an unlimited resource. To utilise hydrogen gas as an energy source, there must be a technology that converts the chemical form of hydrogen to electrical energy. The convenient form of electrical energy conversions is through hydrogen fuel cell

(HFC) technology. This technology generates electrical energy from an electrochemical process and gives water as a by-product [7,8]. The hydrogen fuel cells are not just environmental friendly, but their energy efficiency is two times more than the traditional combustion technologies. A basic fuel cell setup (Figure 2.1) consists of two electrodes (anode and cathode) separated by an electrolyte and a membrane that conducts ions. In HFC principle, hydrogen gas flows through the channel of anode, where oxidation takes place.

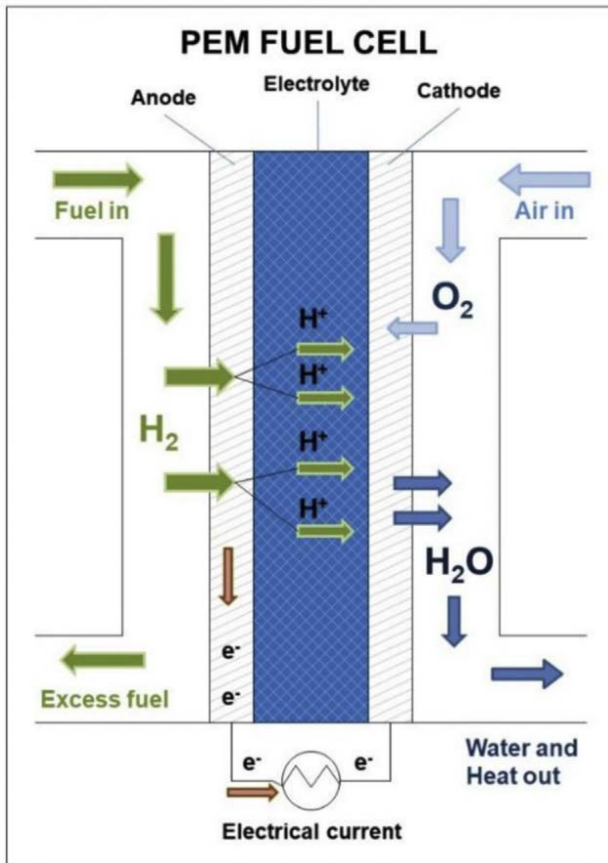


**Figure 2.1:** Schematic of PEM fuel cell [7].

The oxidation process takes place when an electrocatalyst (e.g. platinum) causes hydrogen molecule to separate into protons and electrons. The membrane which differs from fuel cell to fuel cell allows protons to pass through. Those protons will combine with oxidised air to form water. The electrons flow to the cathode to generate electricity or power [1,9,10]. Commercialisation of HFC is hampered by demand and

supply of pure hydrogen gas. The demand and supply of pure hydrogen gas can be addressed by tackling two major concepts of hydrogen technology, thus production and storage. Several technologies or processes are currently employed to address this and they are briefly discussed below.

## **2.1.2. Hydrogen storage**

When hydrogen is produced, it needs to be stored in order to overcome daily and seasonal discrepancies between energy source availability and demand. Depending on storage size and application, several types of hydrogen storage systems are available.

### **2.1.2.1. Compressed gas storage**

The most common method which is employed to store hydrogen is through compression of gas [11]. This method of storing hydrogen brings several advantages such as high H<sub>2</sub> fraction, rapid refuelling capability and excellent dormancy characteristics [12]. Their major challenge is the system volume which does not reach the target and an ideal cylinder which is cylindrical shape makes it difficult to conform storage to available space and the weight/energy penalties. The other inconvenient issue is the safety measures such as rapid loss of H<sub>2</sub> in an accident which can cause explosion [13]. Another gaseous hydrogen storage method is using glass microspheres which have more advantages than compression gaseous method. The process of storage occurs in three stages: charging, filling and discharging. In principle, hollow glass spheres are filled with hydrogen gas at high pressures and temperatures by permeation in high pressure vessels. After that process, the sphere is cooled to ambient temperatures and stored in vehicle tanks. Finally, the microspheres are heated to release hydrogen gas. The major setback in utilising this method are low volumetric density, high pressure needed for filling and high temperatures for releasing hydrogen [14].

### **2.1.2.2. Liquid hydrogen storage**

Unlike compressed hydrogen storage, liquid hydrogen has high density at low pressure, which enables light and compact vehicular storage and efficient delivery by truck [15]. Liquefying hydrogen is a way of increasing volumetric energy density by cooling hydrogen gas below its boiling temperature of  $-253\text{ }^{\circ}\text{C}$ . A major problem associated with the liquefaction process is the transformation of hydrogen from the ortho- to para- state during cooling [16]. Hydrogen in liquid form has a considerably higher energy density than in its gaseous form, making it an attractive storage medium [16,17]. Although it is an energy expensive process, it increases  $\text{H}_2$  volumetric energy density from  $5\text{ MJ}\cdot\text{L}^{-1}$  for compressed  $\text{H}_2$  at 345 atm to  $8\text{ MJ}\cdot\text{L}^{-1}$  for liquid hydrogen [17]. This clearly means that liquid hydrogen has a much better energy density than the compressed gas since it can store high energy at low pressures. The main limitation with liquid hydrogen is the efficiency of the liquefaction process and the boil-off of the liquid [18], because of the low critical temperature of hydrogen (33 K), the liquid form can only be stored in open systems, as there is no liquid phase existent above the critical temperature [15].

### **2.1.2.3. Hydrogen storage in solid materials**

The development of efficient methods for hydrogen storage is a major hurdle that must be overcome to enable the use of hydrogen as an alternative energy carrier [19]. The development of high capacity, hydrogen storage materials that can be recharged under moderate conditions is a key barrier to the realisation of a hydrogen economy [20,21]. In solid storage materials, hydrogen can bind/ interact with the adsorbent in two ways, *i.e.* physisorption or chemisorption. In physisorption, hydrogen can adsorb on the surface of the materials (adsorbent) and stored in a much convenient and safer way. The main advantage of adsorption over other physical storage systems (compressed gas and liquid hydrogen) is that it stores large quantity of hydrogen [22]. The adsorbed hydrogen does not chemically react with the adsorbent, since hydrogen binds via weak van der Waal forces and therefore does not accumulate impurities

which can poison operations of fuel cell [22,23]. In chemisorption, hydrogen predominately binds stronger in an adsorbent than in physisorption, However, physisorption has a great advantage to chemisorption since it has fast kinetics (during release of hydrogen) and it is fully reversible [24]. The problem with physisorption-based hydrogen storage is that, due to weak interaction between hydrogen and adsorbent the hydrogen density at ambient temperature is small [24]. In relation to this, several studies report the development of hydrogen storage materials such as metal hydrides [25], carbon- based materials [26], boron compounds [27], metal organic frameworks [22,28], etc. An optimum hydrogen storage material must have the following characteristics: (1) high volumetric/gravimetric hydrogen storage capacity, (2) fast absorption kinetics, (3) near room temperature and ambient pressure operation, (4) lightweight materials, and (5) low cost materials. However, some of these storage materials do not meet the above requirements.

### **2.1.3. Production of hydrogen**

A wide range of methods are being used to generate hydrogen from different resources and they are discussed below.

#### **2.1.3.1. Fossil fuels**

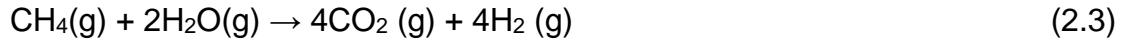
##### **(i) Steam methane reforming (SMR)**

Steam reforming of natural gas is the most widely used process for industrial hydrogen generation. In this method, hydrogen production is through extraction, by breaking the bonds between hydrogen and carbon content [3]. Basically, the SMR process consists of two main steps: in the first step endothermic SMR reaction (Equation 2.1) takes place at a high temperature (~800-1000 °C, at 20-35 atm) and in the second step (Equation 2.2), the exothermic water gas shift (WGS) reaction runs at a lower temperature (~200-400 °C, at 10-15 atm).





The overall reaction of this process is given by Equation 2.3:



Reasonable production price [29] and possibility of mass production [3] are the main advantages of fossil fuel based hydrogen production. However, this approach of hydrogen production suffers from problems which are mainly based on its pollution ratings (emission of CO or CO<sub>2</sub>) and limited resources [3,30].

#### (ii) Partial oxidation

In the partial oxidation process which is mainly known as a gasification, hydrogen is produced from a range of hydrocarbon fuels which include coal and oils. In this process, coal is first reacted with oxygen and steam under high pressures and temperatures to form synthesis gas, a mixture consisting primarily of carbon monoxide and hydrogen [31]. The synthesis gas is cleaned of impurities and the carbon monoxide in the gas mixture is reacted with steam through the water-gas shift reaction to produce additional hydrogen and carbon dioxide. Hydrogen is removed by a separation system and the highly concentrated CO<sub>2</sub> stream can subsequently be captured and sequestered. The hydrogen can be used in a combustion turbine or solid oxide fuel cell to produce power, or utilised as a fuel or chemical feedstock [25,32]. The fact that fossil-based production of hydrogen is associated with the emission of such enormous quantities of CO<sub>2</sub> and other greenhouse gases, may diminish the environmental appeal of hydrogen as an ecologically clean fuel.

#### **2.1.3.2. Biomass**

Hydrogen can be obtained from biomass by a pyrolysis/gasification process [33]. The biomass preparation step involves heating of the biomass/water slurry to high temperatures under pressure in a reactor. This process decomposes and partially oxidises the biomass, producing a gas product consisting of hydrogen, methane, CO<sub>2</sub>, CO and nitrogen. Mineral matter is removed from the bottom of the reactor. The gas

stream goes to a high-temperature shift reactor where the hydrogen content is increased [34]. However, biomass utilisation is not common in developed countries because of its high cost and the large area required for its production [35,36]. The reason for the high cost for biomass production is partly attributed to labour cost. Another reason for the high cost is that effective production of biomass requires fuels for machines and fertilisers produced by petroleum chemistry [42]. Utilisation of agricultural residue and city wastes such as sewage sludge is expected to reduce this cost to a large extent because of their negative costs [37,38]. Using land for biomass cropping rather than food production could also cause problems, since an increase in world population will result in increased food demand [35,36,43]. Thus, fertile land in the world will be required for food production, and it is questionable if sufficient land area will be left for biomass production.

#### **2.1.3.3. Photolysis**

Photolysis (or direct extraction of hydrogen from water using only sunlight as an energy source) can be accomplished by employing photobiological systems, photochemical assemblies or photoelectron-chemical cells. Intensive research activities are opening new perspectives for photo-conversion, where new redox catalysts, colloidal semiconductors, immobilised enzymes, and selected microorganisms could provide means of large-scale solar energy harvesting and conversion into hydrogen [32]. However, the enzyme hydrogenase is very sensitive to oxygen, which inhibits hydrogenase activity and stops it from producing hydrogen [32].

#### **2.1.3.4. Electrolysis**

Electrochemical/photochemical water splitting has been regarded as a promising approach for energy storage and conversion to address the energy crisis and environmental issues [39]. In this method, water is subjected to an electric current in order to force its molecules to decompose into hydrogen and oxygen [39,40].The

occurring half-reactions at the electrodes are given by the following Equation 2.4 and 2.5:



The overall chemical reaction of a water electrolysis process is given by:



This method however has several barriers to the commercialisation of water electrolysis: (1) water electrolysis is expensive as compared to hydrocarbon reforming which is the most widely used technology for hydrogen production, (2) hydrogen evolution reaction (HER) can be started at large overpotential and (3) the water electrolysis system suffers a stability problem over long-term and shut down operations [41].

#### *2.1.3.4.1. Photo-electrocatalytic water splitting*

Development of efficient processes to utilise naturally available solar energy directly to generate hydrogen by water splitting has emerged as a strong contender, thus electrolysis of water has always had a central role in the realm of electrochemistry because of its industrial importance. This process can be employed for the energy storage if the required energy is supplied from a renewable resource [42]. In a simple cell design, a photovoltaic (PV) cell generating appropriate voltage can be coupled with an electrolysis cell to produce hydrogen and oxygen by the solar energy conversion [43]. Various criteria have been used to evaluate the performance of a photocatalyst, typically for photo-electrochemical (PEC) water splitting [43] and HER [44,45]. Photocatalytic water splitting involves an extremely complex series of photophysical and electrocatalytic steps. During water splitting hydrogen generation (Figure 2.2), incident light is irradiated on the catalyst, generating electrons and holes in the conduction and valence bands. The generated electrons and holes cause redox

reactions similar to electrolysis. Water molecules are adsorbed at the electron-holes and oxidised to form protons and O<sub>2</sub>. The generated protons are further reduced to H<sub>2</sub>, leading to overall water splitting [42-45].

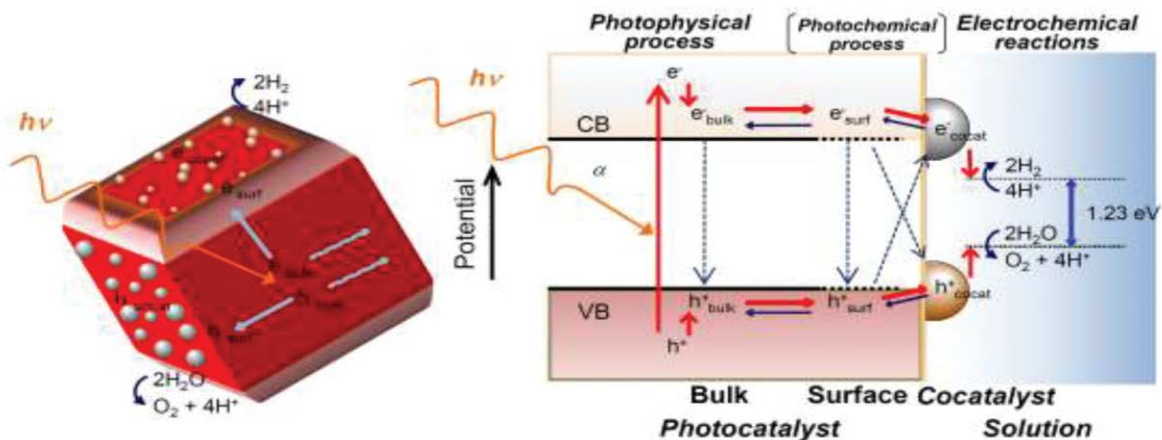


**Figure 2.2:** Schematic representation of the overall photon-induced reaction process for water splitting using a solid photocatalyst [26].

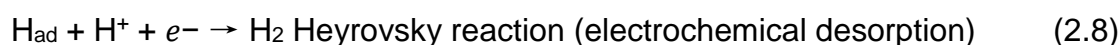
The primary challenge is, of course, finding the most appropriate materials with highest efficiencies for photon absorption and electrocatalysis. The choice of photo/electrocatalyst to exploit the visible light regime and near infrared region, thus, becomes crucial. Since this technology is deemed the future hydrogen production method, there is a need for intense study on it to find the best semiconductor/catalysts that can overcome the challenges imposed by this technology.

#### 2.1.3.4.2. Hydrogen evolution reaction

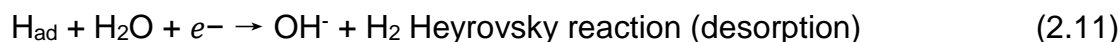
A hydrogen evolution reaction is the production of hydrogen through the process of water electrolysis. The evolution of hydrogen is possibly limited and based on the desorbing of molecules coming from the cathode surface [46]. This process is a crucial step in electrochemical water splitting and demands an efficient, durable and cheap catalyst if it is to succeed in real applications [46,47]. For an energy-efficient HER, a catalyst must be able to trigger proton reduction with minimal overpotential and have fast kinetics [48]. However, catalyst surface having too weak bonding strength with

hydrogen atoms cannot efficiently adsorb the reactant to initiate the HER and a catalyst surface having too strong bonding strength would have a difficulty in releasing the product towards completion of the HER [49,50].

The mechanism of the HER in aqueous acid or alkaline solutions proceeds in a series of three elementary reaction steps which comprises of two electrochemical steps and one chemical step [48–51]. The three elementary reaction steps in acidic medium give in Equation 2.7-2.12:



And in alkaline solution are:



In an acidic solution, the first step (Equation 2.7) is the Volmer reaction in which a proton receives an electron and generates an adsorbed hydrogen atom ( $\text{H}_{\text{ad}}$ ) at the active site as an intermediate [46]. Then the second step can be Heyrovsky or Tafel reaction. In Heyrovsky mechanism, a proton reacts with one adsorbed hydrogen to form  $\text{H}_2$  as illustrated in Equation 2.8. In the Tafel mechanism, two adsorbed surface hydrogens next to each other react to form  $\text{H}_2$  molecule as illustrated in Equation 2.9 [46,49,50]. Since HER involves the adsorption and desorption of the hydrogen atoms on the surface of the catalyst, a suitable catalyst for HER should have a good balance between the two steps [49,50].

The efficiency and commercialisation of HER depends mostly on the electrocatalyst, hence, most studies have been conducted in electrocatalysis with the great hope of finding a best suitable electrocatalyst for HER [52–55]. The advanced and ideally electrocatalyst should reduce the overpotential and increase the hydrogen production

efficiency [53]. In addition, the efficient electrocatalyst must encounter different characteristics such as high thermal and mechanical stability as well as low cost [56,57]. The HER activities of various catalysts can be summarised in the “Volcano plot” as shown in Figure 2.3 below, where the exchange current density for different catalysts in acid are plotted as a function of the Gibbs free energy of adsorbed atomic hydrogen on catalyst [53]. Platinum group metals (PGMs) such as Pt, Pd, Ir and Rh can be found on the apex of the Volcano plot and are the frequently used electrocatalysts for HER [52,56,58,59]. PGMs especially Pt-based electrocatalysts meet various requirements for HER electrocatalyst as they exhibit low overpotential, high catalytic activity, fast kinetics and are most stable. However, their extremely high cost and limited abundance or scarcity is the major obstacles for industrial applications [58,59]. Thus, the important goal of the modern electrocatalysis is to completely replace PGM based electrocatalysts with low cost and catalytic active materials [60,61]. Although non-platinum active metals such as Fe, Ni, Mo or Co are considerably cheaper, they suffer from corrosion and passivation under reaction conditions [44,49,62]. Electrocatalysts based carbons (graphene oxide) and/or metal organic frameworks have been rarely investigated for HER. These materials have shown great catalytic activity as well as low cost and have a great ranges of potential windows [28,63,64]. With these properties, they can be used to replace the PGM-based electrocatalysts.

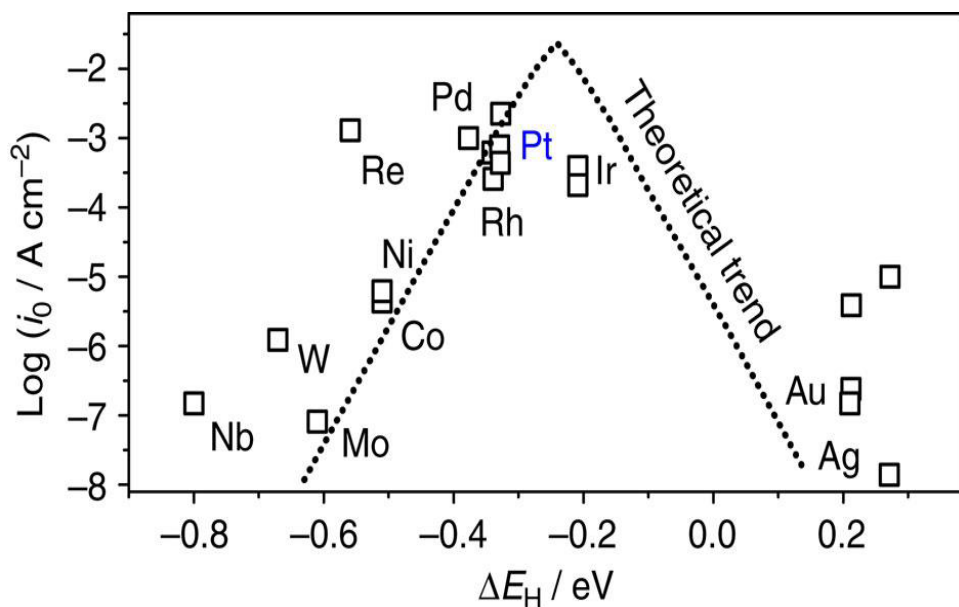


**Figure 2.3:** Trends in hydrogen evolution reaction activity. Experimental HER activity expressed as the exchange current density,  $\log(i_0)$ , for different metal surfaces as a function of the calculated  $^*H_{ad}$  chemisorption energy,  $\Delta E_H$ . The result of a simple theoretical kinetic model is also shown as a dotted line.

## 2.2. GRAPHENE OXIDE

### 2.2.1. Background

Graphene oxide (GO), also called graphitic acid, attracts the attention of many research groups [65-70]. GO is a component in composite materials with photochemical, electric or adsorptive properties [65] and it is a layered material formed by the oxidation of graphite [66]. In comparison to pristine graphite, the graphene-derived sheets in graphite oxide (graphene oxide sheets) are heavily oxygenated [66,67]. Oxidation of graphite enables the incorporation of oxygen atoms on the basal planes and edges of graphene layers. These oxygen functional groups identified so far on the surface of GO are epoxide, keto and hydroxylic groups on the basal planes, and carboxylic groups on the edges [68]. Direct incorporation of oxygen atoms into the graphene layers was also observed in other studies [69-72]. Indeed, owing to its oxygen functional groups, GO has a hydrophilic character and molecules of water can

easily be intercalated between the graphene layers [73,74]. This hydrophilic character is also responsible for the easy dispersion of GO in water, alkaline solutions or alcoholic media [75,76]. Not only does the oxidation of graphite enable the incorporation of oxygen groups, but it also leads to the formation of defects [77,78]. These defects usually correspond to vacancies or adatoms in the graphene layers [77,78]. Considering this, GO is commonly represented as distorted/corrugated graphene layers stacked in a more or less ordered fashion [70–72].

### **2.2.2. Structure of graphene oxide**

GO is obtained from chemical exfoliation of graphite in which graphite powder is oxidized with strong oxidising agents such as  $\text{KMnO}_4$  in the presence of concentrated sulfuric acid [79]. The oxidation of graphite breaks up the extended two-dimensional  $\pi$ -conjugation of the stacked graphene sheets into nanoscale graphitic  $\text{sp}^2$  domains surrounded by disordered, highly oxidised  $\text{sp}^3$  domains as well as defects of carbon vacancies [80]. The resulting GO sheets are derivatised by carboxylic acid at the edges, and phenol, hydroxyl and epoxide groups mainly at the basal plane (Figure 2.4(ii)). After centrifugation, the graphene oxide can be reduced to regular graphene by thermal or chemical methods (Figure 2.4(i)) [74,81]. It is hardly possible to remove all the oxygen containing groups, depending on the reducing agent used. Therefore, a wide range of reducing agents are available and each with its own different reducing ability/capacity.

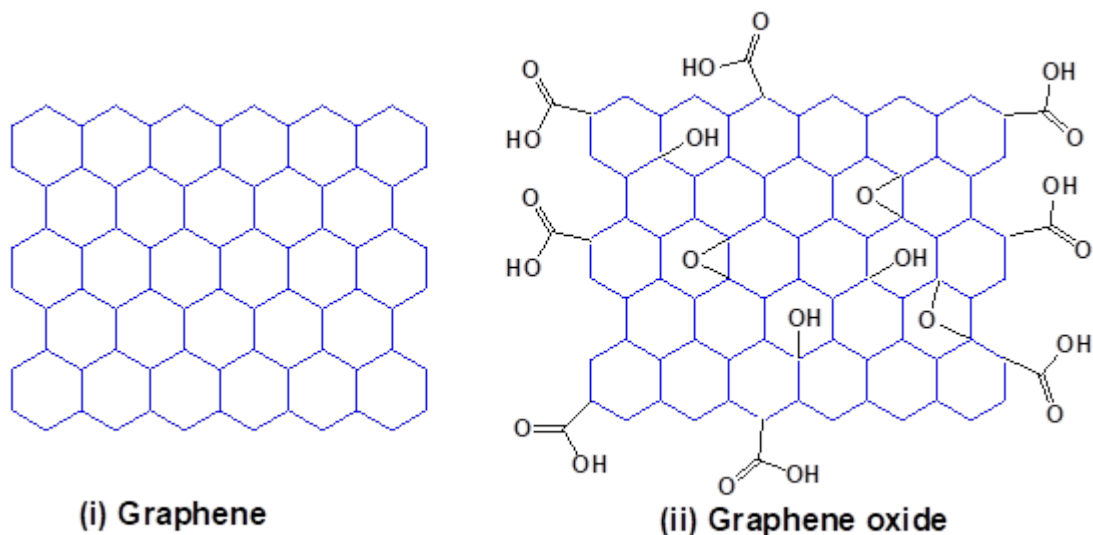


**Figure 2.4:** (i). A typical structure of graphene and (ii). Graphene oxide.

### 2.2.3. Synthesis of GO

The most important and widely applied method for the synthesis of GO is the one developed by Hummers and Offeman [71,82,83]. This method, at least, has three important advantages over previously used techniques. First, the reaction can be completed within a few hours. Second,  $\text{KClO}_3$  was replaced by  $\text{KMnO}_4$  to improve the reaction safety, avoiding the evolution of explosive  $\text{ClO}_2$ . And lastly, the use of  $\text{NaNO}_3$  instead of fuming  $\text{HNO}_3$  eliminates the formation of acid fog. In brief, the method involves the oxidation of graphite powder with a mixture of potassium permanganate ( $\text{KMnO}_4$ ) and concentrated sulfuric acid ( $\text{H}_2\text{SO}_4$ ), wherein Potassium permanganate serves as an oxidant [73] (Figure 2.5). The oxidative treatment of graphite helps to increase the interlayer distance between graphene sheets in graphite for an easy exfoliation, since the sheets are usually held by strong van der Waals forces [71,84]. The produced graphite oxide can be exfoliated directly in several polar solvents, such as water, ethylene glycol, N,N-dimethylformamide (DMF), N-methylpyrrolidone (NMP) and tetrahydrofuran (THF) [84]. This process results in the formation of various oxide-containing species including carboxyls, lactones, and ketones [85]. Finally, resulting GO has a nonstoichiometric and amorphous structure [69]. Due to these functional

groups, graphene oxide is hydrophilic and can be dissolved in water by sonication or stirring [79,86,87]. Thereby the layers become negatively charged and thus a recombination is inhibited by the electrical repulsion.

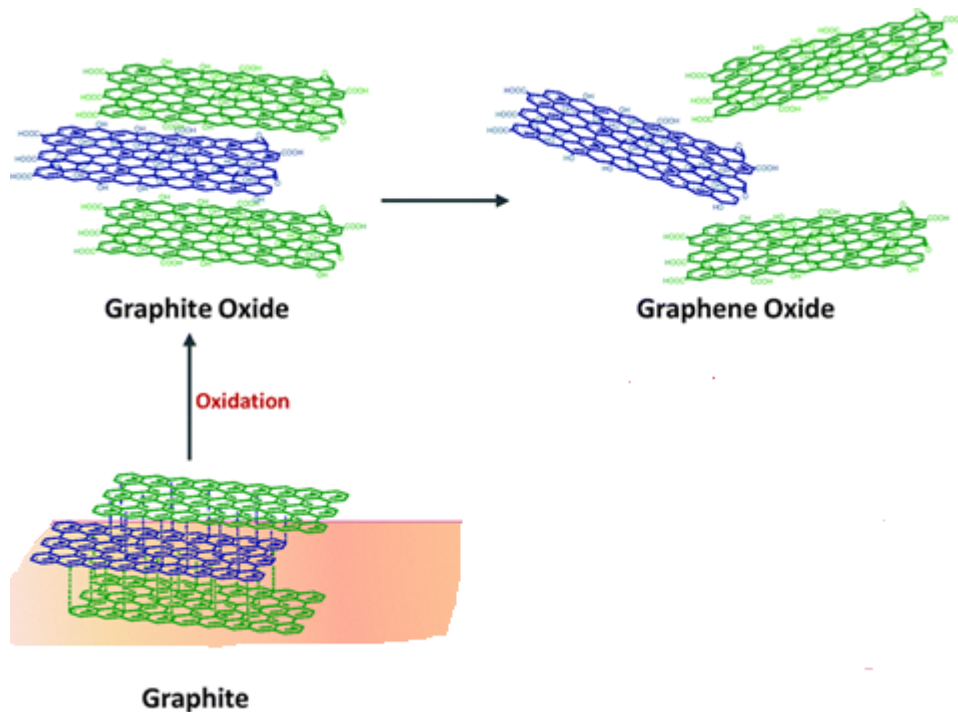


**Figure 2.5:** Schematic diagram for the synthesis of graphene oxide by Hummers method [79].

This material has been applied in several fields such use in composite materials, as the electrode materials for electrochemical sensors, as absorbers for both gases and liquids, and as electrode materials for devices involved in electrochemical energy storage and conversion. This review focuses on its use as electrocatalyst for hydrogen evolution reaction.

#### 2.2.4. GO based materials for HER

The nanostructured and carbonaceous material are the most fruitful nominees for enhanced electrochemical performance. Recently, hydrogen evolution reaction on GO-based materials as electrocatalysts has been widely studied in both acidic and

alkaline conditions [88-92]. For example, the Tafel slopes for Ni metal and graphene oxide (GN) (Figure 2.6 and Table 2.1), were found to be 85, 64, and 68  $\text{mV.dec}^{-1}$  for Ni to GO ratios of 2.0 (GN2), 6.0 (GN6), and 8.0 wt.% (GN8), respectively, which did not correspond to any simple kinetic model (Volmer, Heyrovsky or Tafel reaction), indicating complex mechanisms for hydrogen evolution on the GN hybrids [88]. Furthermore, the Tafel slope for GN2 was higher, while the slope for GN6 was close to that for GN8, probably due to the difference in the interaction between the carbon-vacancy defects and Ni nanoparticles (NPs), and the difference in their sandwich structures [88]. Moreover, Zhen Sun *et al.* [61] showed GGNR@MoS<sub>2</sub> hybrid exhibiting good HER performance, with a low onset potential of -105 mV, a small Tafel slope of 49 mV per decade and a large current density (10.0  $\text{mA.cm}^{-2}$  at  $\eta = 183$  mV), making this composite promising and highly efficient electrocatalyst for hydrogen evolution reaction. The NFO/RGO catalyst exhibited HER activity than bare NFO and other reported catalysts such as sulfides, carbides, phosphides, bimetals of molybdenum and iron-cobalt. With a low onset overpotential of 5 mV (vs. reference hydrogen electrode (RHE)), high cathodic current density, low Tafel slope of 58  $\text{mV.dec}^{-1}$ , low charge transfer resistance and turnover frequency of 0.48  $\text{s}^{-1}$  [89]. Another study [90] showed HER activity of nanocomposites (CFG and NFG) which were tested for hydrogen evolution at an applied potential of -1.2 to 0.8 V in acidic electrolyte. It revealed good exchange current density of 47.9 and 41.2  $\text{mA.cm}^{-2}$  at over potential of 248.3 and 259 mV and Tafel slopes of 116.6 and 121.4  $\text{mV.dec}^{-1}$  for CFG and NFG nanocomposite respectively [90].

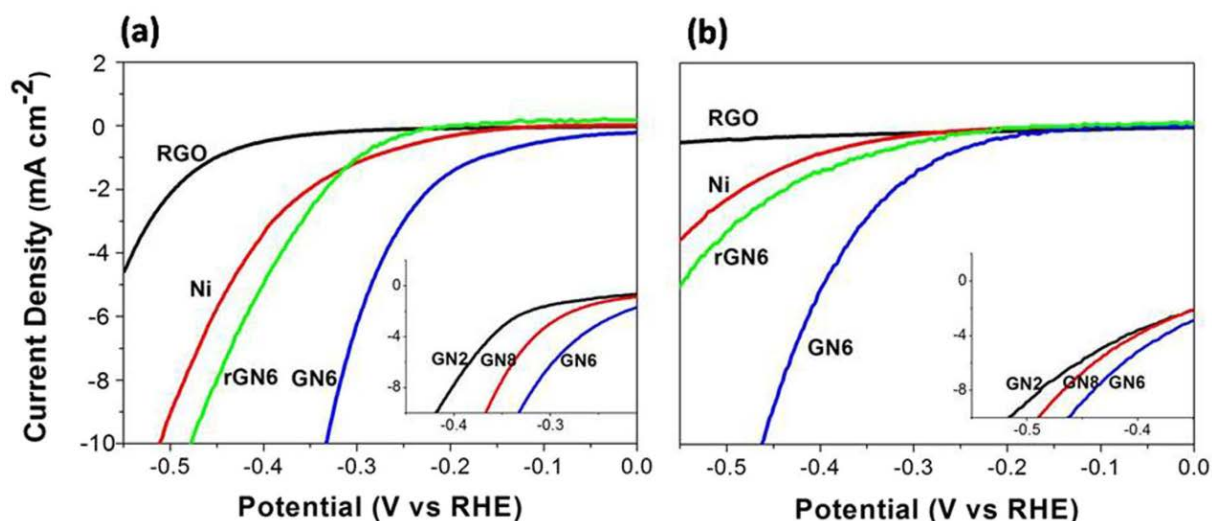


**Figure 2.6:** Linear sweep voltammetry (LSV) curves of RGO, Ni, rGN6 and GN6 in 0.50 M H<sub>2</sub>SO<sub>4</sub> solution (a) and in 0.50 M Na<sub>2</sub>SO<sub>4</sub> solution of pH 10 (b). The insets are LSV curves of GN2, GN6, and GN8 composites with reference to Ni [88].

**Table 2. 1:** Comparison between the ability of various GO or rGO electrocatalysts toward HER.

Material	H <sub>2</sub> source in Electrolyte	Tafel slope/ mV.dec <sup>-1</sup>	Current density( <i>i</i> <sub>0</sub> )/ mA.cm <sup>-2</sup>	References
PdNPs-GO	0.5 M H <sub>2</sub> SO <sub>4</sub>	-	5.2	[82]
NFO/RGO	0.5 M H <sub>2</sub> SO <sub>4</sub>	58	25.2 x 10 <sup>-2</sup>	[89]
GGNR@MoS <sub>2</sub>	0.5 M H <sub>2</sub> SO <sub>4</sub>	49	10.0	[61]
rGO-Au <sub>48</sub> Pd <sub>52</sub>	0.5 M H <sub>2</sub> SO <sub>4</sub>	149	-	[91]
CFG	0.5 M H <sub>2</sub> SO <sub>4</sub>	116.6	47.9	[90]
NFG	0.5 M H <sub>2</sub> SO <sub>4</sub>	121.4	41.2	[90]

As observed in the Table 2.1 above, few electrochemists paid more consideration to GO or rGO because of their admirable conductivity, less weight, strong mechanical

properties, high surface area and good chemical stability [68,79,92]. However, the electrochemical applications of these materials have some hitches due to their insulation properties which are interrelated to the manifestation of oxygen functionalities. To overcome this issue, GO was composite with metal particles, metal oxide, conductive polymers, and biopolymers [93–96]. As mentioned above, small sized metal particles have been acknowledged as a good mediator on the fabrication of electrochemical applications due to their biocompatibility, fast electron transfer rate, and excellent conductivity. Therefore, decoration of small-sized metal nanoparticles and/or organometallic compounds on the surface of GO sheets is proposed to not only further resolve the insulation properties problem of GO but also significantly increase the electrochemical activity.

## **2.3. METAL ORGANIC FRAMEWORK**

### **2.3.1. Background**

Metal-organic frameworks (MOFs) are class of adsorbent materials, consisting of metal ions and organic ligands that involve O and N [97]. As there was no accepted standard nomenclature during the development of this new class of hybrid solids, several names have been proposed and are in use [28,97]; examples include porous coordination polymers [98] and networks [99], microporous coordination polymers [22], zeolite-like MOFs [100], and isorecticular MOFs [98,101,102]. In MOFs, the inorganic and organic building units are linked via coordination bonds. Generally, the inorganic units are metal ions or metal cluster, and the organic units (known as linkers or bridging- ligands) are di-, tri-, or tetradentate organic ligands [100,103,104] such as carboxylates or other organic anions (phosphonate, sulfonate, and heterocyclic compounds). A lot of features of these types of crystalline materials caught the eyes of many scientists in different fields (physicists, biologists, environmental engineers etc.) due to their adjustable pore size and high surface area [105].

### 2.3.2. Structure of MOF

MOF materials are formed by assembling metal nodes and organic ligands [28,45]. The metal node precursors mainly come from metal nitrates or chlorides, while the organic ligands mainly include benzimidazolate, dicarboxylic acid, and others.

#### 2.3.2.1. Organic ligands

Organic ligands are known for their complex nature and ability to form coordination bonds [22, 28,97]. They exist mostly in anionic states and, thus, are helpful in forming bonds with metal ions. The most commonly used organic ligands in making MOFs are benzene 1,3,5-tricarboxylic acid ( $H_3btc$ ), benzene 1,4-dicarboxylic acid ( $H_2bdc$ ), 4,5-imidazole dicarboxylic acid and pyrazine-2-carboxylic acid (Figure 2.7) [98].

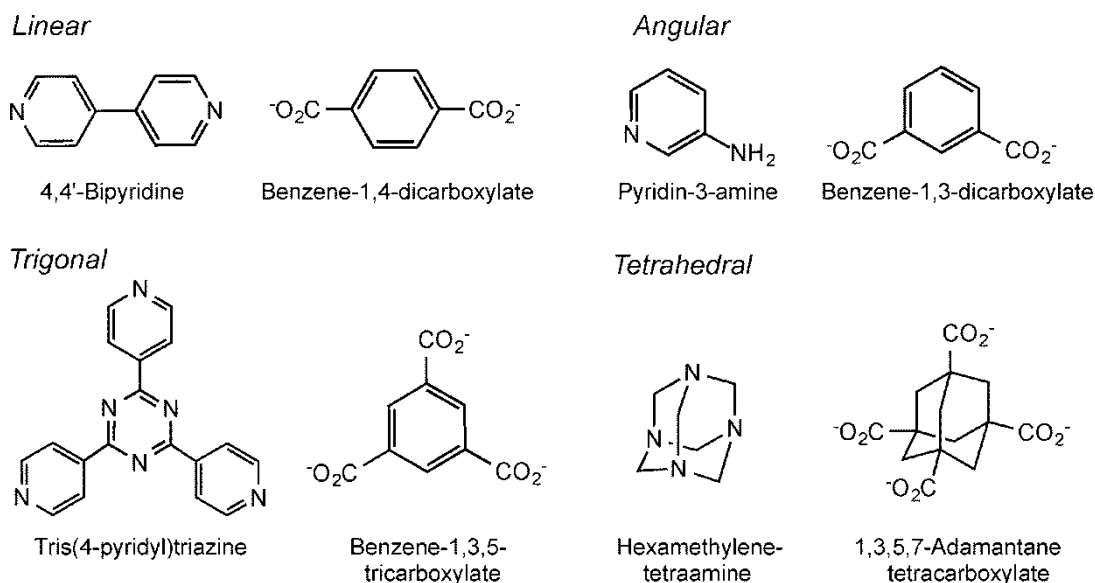


**Figure 2.7:** Representative examples of some organic ligands used in metal-organic frameworks.

#### 2.3.2.2. Metal sites

Metal sites have tremendous influence on the adsorption and catalytic properties of MOFs [106]. The metals act as Lewis acids and can activate the coordinated organic substrate for subsequent organic transformation [107]. Furthermore, the metal sites have been reported to enhance H<sub>2</sub> adsorption in MOFs [106,107]. These commonly used transition metals give different geometries depending on their number of oxidation states. For example, copper – Electron configuration of zero-valent metal is [Ar]3d<sup>10</sup>4s<sup>1</sup>. Copper nodes are often in distorted octahedral and square-planar geometries which assist in rapid electron transfer to facilitate electron mobility in HER process [63]. The distortion occurs mainly due to Jahn-Teller distortion commonly resulting in octahedral geometries having four short bonds and two longer bonds as the dz<sup>2</sup> orbital is filled whilst the dx<sup>2</sup>-y<sup>2</sup> orbital is only partially filled.

#### **2.3.2.3. Secondary building units**

Secondary building units (SBUs) play an important role as it dictates the final topology of MOFs. The geometry and chemical attributes of the SBUs and organic linkers lead to the prediction of the design and the synthesis of MOFs [23,106,107]. It was reported that under carefully selected conditions, multidentate linkers could aggregate and lock metal ions at certain positions, forming SBUs [107,108]. These SBUs will subsequently be joined by rigid organic links to produce MOFs that exhibit high structural stability [109]. Studies have proved that the geometry of the SBU depends on metal-to-ligand ratio, the solvent and the source of anions to balance the charges of the metal ions [106,110].

#### **2.3.2.4. Pores in MOFs**

Pores are empty space formed within MOFs upon the removal of guest molecules. The wide open MOF structures with pores of internal diameter of up to 4.8 nm provide extra-large free space that can be used for H<sub>2</sub> storage [111]. The ideal pore size for porous adsorbents should give an optimal interaction of the adsorbate gas with the

potential surface of all the surrounding walls. The pore size should be close to the kinetic diameter of H<sub>2</sub> molecule (0.289 nm) to promote stronger interaction between H<sub>2</sub> molecules and the framework. For example, NU-100 contains micropores (<2 nm) and have storage capacity of 8 wt.%[112], while MOF-5 have micropores of (0.77 nm) and stores close to 7 wt.% [108] . Generally, the larger the pore size the more likely that the structural collapse could occur, and is more difficult to achieve permanent porosity. Nevertheless, this kind of structures may lead to improved performance in some application such as H<sub>2</sub> storage [108] .

### **2.3.3. Synthesis of MOF**

The most preparation methods for MOFs are liquid-phase syntheses, whereby metal salt and ligand solutions are mixed together in a reaction vial [113].

#### ***2.3.3.1. Microwave assisted synthesis***

Microwave (MW)-assisted synthesis relies on the interaction of electromagnetic waves with mobile electric charges. These can be polar solvent molecules/ions in a solution or electrons/ions in a solid. In the solid, an electric current is formed and heating is due to electric resistance of the solid [114,115]. In solution, polar molecules try to align themselves in an electromagnetic field and in an oscillating field so that the molecules change their orientations permanently [116,117]. Thus, applying the appropriate frequency, collision between the molecules will take place, which leads to an increase in kinetic energy, *i.e.* temperature of the system. Furthermore, several metal(III) carboxylate-based MOFs (M = Fe, Al, Cr, V, Ce) have been prepared by MW-assisted synthesis route [116–119].

#### ***2.3.3.2. Mechanochemical synthesis***

In mechanochemical synthesis, there are mechanical breakage of intramolecular bonds followed by a chemical transformation. Mechanochemistry has a long history in

synthetic chemistry [120] and it has recently been employed in multicomponent (ternary and higher) reactions to form pharmaceutically active co-crystals and in inorganic solid-state chemistry, organic synthesis, and polymer science [113,120,121]. Its use for the synthesis of porous MOFs was first reported in 2006 [116] and results of selected mechanochemical studies were summarized recently [113,120].

### **2.3.3.3. Electrochemical synthesis**

The electrochemical synthesis of MOFs was first reported in 2005 [122]. The main objective was the exclusion of anions, such as nitrate, perchlorate, or chloride, during the syntheses, which are of concern to large-scale production processes. Rather than using metal salts, the metal ions are continuously introduced through anodic dissolution to the reaction medium, which contains the dissolved linker molecules and a conducting salt [23,122]. The metal deposition on the cathode is avoided by using protic solvents, but in the process H<sub>2</sub> is formed [123]. Other advantages of the electrochemical route for industrial process are the possibility to run a continuous process and the possibility to obtain a higher solids content compared to normal batch reactions [123].

### **2.3.3.4. Solvo/hydrothermal synthesis**

The solvo/hydrothermal method is a process of crystallisation in which the compounds are synthesised depending on the solubility of compound in water at autogenous pressure [112,124]. The crystallisation process is done in a vessel called an autoclave [112,124]. The autoclave is usually made of thick-walled steel cylinders, which can withstand high temperatures and pressures for prolonged periods of time [97,119,122,125]. The autoclave is especially designed to withstand corrosiveness and also has protective seals. The inside of the autoclave is layered with Teflon or titanium or glass depending on the nature of the solvent used. The samples are first placed within the Teflon bags. The bags are sealed and kept in the Teflon cup. The Teflon cup is closed with a cap on the top and then this cup is placed into the autoclave.

The autoclave is tightly closed and placed within the oven for high temperatures [117,122].

### 2.3.4 MOF based materials as HER electrocatalyst

The electrochemical water-splitting process includes two half-reactions: HER and oxygen evolution reaction (OER). Given that the water splitting needs high activation energy and large overpotential, high-performance electrocatalysts with low cost are highly desired to enhance the performance of electrocatalytic water splitting. Complexes with precise structures are beneficial for mechanism studies by using various electrochemical measurements and other techniques [25,40,126,127]. Such homogeneous catalysts can also fully utilise all catalytic sites, when they are used at low concentrations, giving particularly high activity in the term of turnover frequency (TOF). Such catalysts usually suffer from low stability [65,98,128,129]. Combining the advantages of conventional heterogeneous and homogeneous catalysts, MOF-derived inorganic materials can solve many of the above-mentioned problems [83,96,130]. In this regard, Sandra Loera-Serna *et al.* [131] showed the electrochemical behaviour Cu-MOF, confirming that this material has a high catalytic activity. Furthermore, Jie Lin *et al.* [64] constructed metal-organic frameworks derived cobalt diselenide (MOF-CoSe<sub>2</sub>) with CoSe<sub>2</sub> nanoparticles anchored into nitrogen-doped (N-doped) graphitic carbon through in-situ selenisation of Co-based MOFs. It was detected that the MOF-CoSe<sub>2</sub> delivered excellent HER performance with an onset potential of approximately 150 mV and high current density of 80 mA.cm<sup>-2</sup> at about -0.33 V (vs. RHE), which behaved better than bare CoSe<sub>2</sub>. The Tafel slope of the MOF-CoSe<sub>2</sub> was 42 mV.dec<sup>-1</sup>, which is much smaller than that of bare CoSe<sub>2</sub> of 72 mV.dec<sup>-1</sup>. Moreover, Ramohlola *et al.* [132] showed the merits of combining MOF material with conductive polymers to produce a highly active material with Tafel plots presented in Figure 2.8. Table 2.2 presents the Tafel parameters of MOF-polyaniline (PANI), MOF-3.6wt%poly(3-aminobenzoic acid) (PABA), PABA-MOF and MOF-5wt%PABA composite with high exchange current densities of 7.943 [132], 31.62 [133], 35.48

[134] and  $50.12 \text{ A.m}^{-2}$  [133] and Tafel slopes of  $199.3$  [132],  $166.7$  [133],  $130.5$  [134] and  $153.5 \text{ mV.dec}^{-1}$  [133], respectively. .

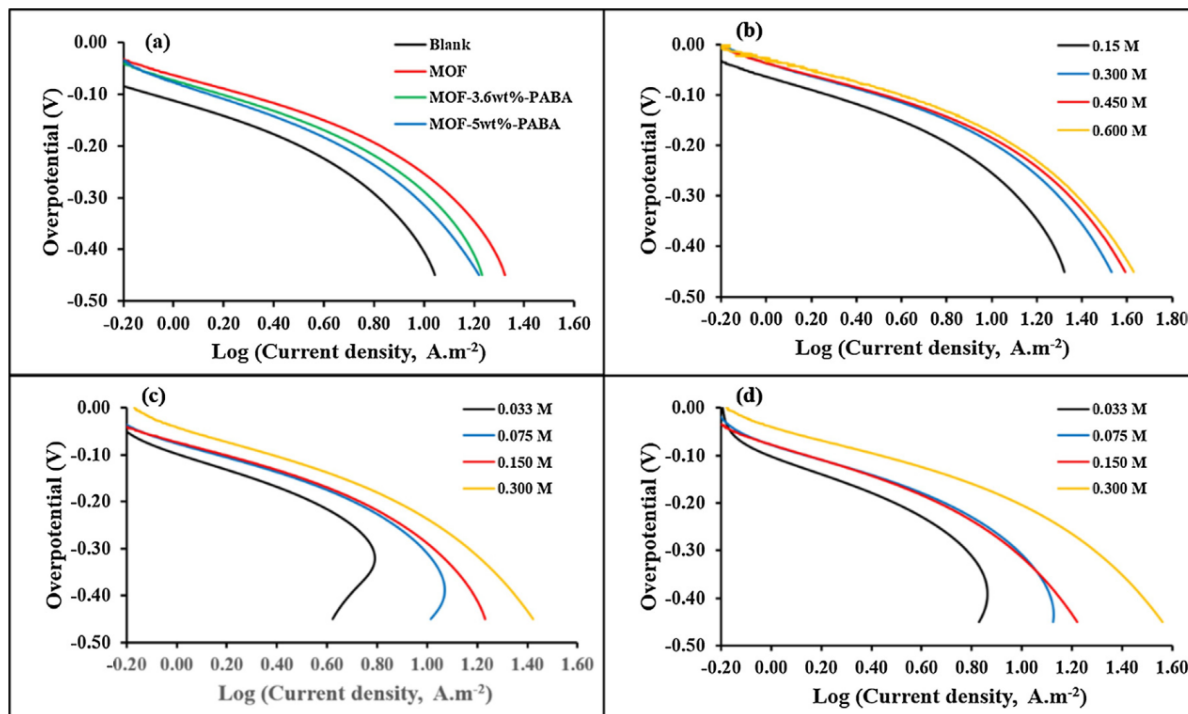


**Figure 2.8:** (a) Tafel plots of blank, MOF and MOF- PABA; and (b) MOF, (c) MOF-3.6wt%-PABA and (d) MOF-5wt%-PABA at  $0.10 \text{ V.s}^{-1}$  in the presence of different  $\text{H}_2\text{SO}_4$  concentration on gold electrode in  $0.1 \text{ mol.L}^{-1}$  (DMSO/TBAP) electrolytic system [133].

The integration of Cu-MOF with graphene oxide (GO) can effectively enhance the electron transfer, which further significantly improve HER activity [135]. It was also found that the GO content affected the HER activity of the nanocomposite catalysts. The optimised GO content was about 8 wt.%. The HER current density of the (GO 8wt%) Cu-MOF (Table 2.2) was high up to  $-30 \text{ mA.cm}^{-2}$  at an overpotential of  $-2.0 \text{ V}$  in  $\text{N}_2$  saturated  $0.5 \text{ M H}_2\text{SO}_4$ , whereas the overpotential of 30 wt% Pt was  $-0.06 \text{ V}$  at the current density of  $-30 \text{ mA.cm}^{-2}$  [135]. The electrochemical hydrogen evolution reaction performance of the Pd@CuPc/MOF and Tafel analysis were evaluated by Monama *et al.*[63]. The Tafel slope of this composite was found to be  $176.9 \text{ mV/dec}$

and the transfer coefficient of 0.67, with the exchange current density of  $8.9 \text{ A.m}^{-2}$  (Table 2.2) The HER results revealed that the Pd@CuPc/MOF composite has better catalytic characteristic such as high catalytic activity and lowest onset potential compared to MOF. More importantly, they reported the significant enhancement of HER performance at ambient temperature for the composite with Pd content to be ascribed to the hydrogen spillover mechanism in such a system.

**Table 2. 2:** Comparison between the ability of various MOF electrocatalysts towards HER.

<b>Material</b>	<b>H<sub>2</sub> source in Electrolyte</b>	<b>Tafel slope mV.dec<sup>-1</sup></b>	<b>Current density(<i>i</i><sub>0</sub>)/ A.m<sup>-2</sup></b>	<b>Refs.</b>
MOF-CoSe <sub>2</sub>	0.5 M H <sub>2</sub> SO <sub>4</sub>	42	0.080	[64]
MOF-5wt.%- PABA	0.3 M H <sub>2</sub> SO <sub>4</sub>	153.5	50.12	[133]
PABA/MOF	0.3 M H <sub>2</sub> SO <sub>4</sub>	130.5	35.48	[134]
Pd@CuPc/MOF	0.3 M H <sub>2</sub> SO <sub>4</sub>	176.9	8.900	[63]
MOF-3.6wt.%-PABA	0.3 M H <sub>2</sub> SO <sub>4</sub>	166.7	31.62	[133]
MOF/PANI	0.3 M H <sub>2</sub> SO <sub>4</sub>	199.3	7.943	[132]
Cu-MOF/8 wt.% GO	0.5 M H <sub>2</sub> SO <sub>4</sub>	-	-300	[135]

## 2.4. CONCLUSIONS

This review work focused on resolving energy scarcity problem via hydrogen technology. Major problem of hydrogen energy such as hydrogen storage and production has been highlighted and their mitigation can be achieved through fabrication of graphene based metal organic framework nanocomposite. The reaction mechanisms of HER, the transfer and diffusion properties of reactants and products, and the effects of electrolyte on the catalytic performance of MOFs based catalysts

were identified in the review as the alternative methods to study the hydrogen storage and production behaviour of the materials. Recently, hydrogen evolution reaction on GO-based composite with metals as electrocatalysts has been widely studied in both acidic and alkaline conditions for hydrogen production due to the electron and functional groups enrichment character of the GO. However, the electrochemical applications of these materials have some drawbacks owing to their insulation properties caused by oxygen functionalities. On the other hand, MOFs-based electrocatalysts for HER are rapidly established due to extraordinary structures of MOFs because of the pore structures and functions are tunable and devisable, it is convenient to directly design and construct the active sites for HER in MOFs during the synthesis process. However, the vast majority of the synthesised MOFs suffer from poor electronic conductivity, leading to low electron transfer efficiency, which restricts catalytic performance. There are still a lot of scientific and technical problems to solve in MOFs electrocatalysts before meeting the requirements for commercialisation. The problems mainly involve how to improve the electronic conductivity of MOFs, enlarge pore channels of MOFs to accommodate more electrolytes, limit the collapse of pore structure of MOFs, and maintain high specific surface area during pyrolysis. It was seen that the integration of MOF with graphene oxide (GO) can effectively enhance the electron transfer, which further significantly improve HER activity. Furthermore, the HER mechanisms, transfer and diffusion properties of GO based MOF electrocatalysts need to be investigated as future alternative route in hydrogen production and storage technologies to meet energy demands.

## 2.6. REFERENCES

- [1] M. Balat, "Potential importance of hydrogen as a future solution to environmental and transportation problems," vol. 33, pp. 4013–4029, 2008.
- [2] P. Laha and B. Chakraborty, "Energy model – A tool for preventing energy dysfunction," *Renew. Sustain. Energy Rev.*, vol. 73, pp. 95–114, 2017.
- [3] K. Mazloomi and C. Gomes, "Hydrogen as an energy carrier: Prospects and

- challenges,” *Renew. Sustain. Energy Rev.*, vol. 16, pp. 3024–3033, 2012.
- [4] S. Dunn, “Hydrogen futures: Toward a sustainable energy system,” *Int. J. Hydrogen Energy*, vol. 27, pp. 235–264, 2002.
- [5] H. Fayaz, R. Saidur, N. Razali, F. S. Anuar, A. R. Saleman, and M. R. Islam, “An overview of hydrogen as a vehicle fuel,” *Renew. Sustain. Energy Rev.*, vol. 16, , pp. 5511–5528, 2012.
- [6] K. O’Malley, G. Ordaz, J. Adams, K. Randolph, C. C. Ahn, and N. T. Stetson, “Applied hydrogen storage research and development: A perspective from the U.S. Department of Energy,” *J. Alloys Compd.*, vol. 645, pp. S419–S422, 2015.
- [7] D. Ross, "Hydrogen storage: the major technological barrier to the development of hydrogen fuel cell cars," *Vacuum*, vol. 80 , pp. 1084-1089, 2006.
- [8] A. Yilanci, I. Dincer, and H. K. Ozturk, “A review on solar-hydrogen / fuel cell hybrid energy systems for stationary applications,” *Prog. Energy Combust. Sci.*, vol. 35, pp. 231–244, 2009.
- [9] A. C. Yakaryilmaz, “A review : Exergy analysis of PEM and PEM fuel cell based CHP systems,” *Int. J. Hydrogen Energy*,  
doi: 10.1016/j.ijhydene.2018.01.106
- [10] S. M. Haile, “Fuel cell materials and components ,” *Acta mater*, vol. 51, pp. 5981–6000, 2003.
- [11] I. Hadjipaschalis, A. Poullikkas, and V. Efthimiou, “Overview of current and future energy storage technologies for electric power applications,” *Renew. Sustain. Energy Rev.*, vol. 13, pp. 1513–1522, 2009.
- [12] L. Schlapbach, and A. Züttel, “Hydrogen storage materials for mobile applications,” *Nature* vol. 414, pp. 353–358, 2001.
- [13] R. K. Brow and M. L. Schmitt, “A survey of energy and environmental applications of glass,” *J. Eur. Ceram. Soc.*, vol. 29, pp. 1193–1201, 2009.
- [14] R. K. Ahluwalia, T.Q. Hua, J. K. Peng, S. Lasher, K. McKenney, J. Sinha, and M. Gardiner, “Technical assessment of cryo-compressed hydrogen storage tank systems for automotive applications,” *Int. J. Hydrogen Energy*, vol. 35, pp. 4171–4184, 2010.
- [15] H. Barthelemy, M. Weber, and F. Barbier, "Hydrogen storage: Recent

- improvements and industrial perspectives". *Int. J. Hydrogen Energy*, 42, pp. 7254-7262, 2017.
- [16] L. Li, M. Yang, Y. Dong, P. Mei, and H. Cheng, "Hydrogen storage and release from a new promising Liquid Organic Hydrogen Storage Carrier (LOHC): 2-methylindole," *Int. J. Hydrogen Energy*, vol. 41, pp. 16129–16134, 2016.
- [17] S. Y. Liu, P. Kundu, T.W. Huang, Y.J. Chuang, F. G. Tseng, Y. Lu, M. L. Sui and F. R. Chen "Quasi-2D liquid cell for high density hydrogen storage," *Nano Energy*, vol. 31, pp. 218–224, 2017.
- [18] J. Sakamoto, J. Nakayama, T. Nakarai, N. Kasai, T. Shibutani, and A. Miyake, "Effect of gasoline pool fire on liquid hydrogen storage tank in hybrid hydrogen-gasoline fueling station," *Int. J. Hydrogen Energy*, vol. 41, pp. 2096–2104, 2016.
- [19] S. A. Sherif, F. Barbir, and T. N. Veziroglu, "Towards a hydrogen economy", *Electric. J.*, vol. 18, p.p. 62-76. 2005.
- [20] B. Sakintuna, F. Lamari-Darkrim, and M. Hirscher. "Metal hydride materials for solid hydrogen storage: a review." *Int. J. hydrogen energy*, vol. 32, pp. 1121-1140, 2007.
- [21] F. H. Yang and R. T. Yang, "Ab initio molecular orbital study of adsorption of atomic hydrogen on graphite: Insight into hydrogen storage in carbon nanotubes," *Carbon*, vol. 40, pp. 437–444, 2002.
- [22] H. W. Langmi, J. Ren, B. North, M. Mathe, and D. Bessarabov, "Hydrogen storage in metal-organic frameworks: A review," *Electrochim. Acta*, vol. 128, pp. 368–392, 2014.
- [23] B. Xiao and Q. Yuan, "Nanoporous metal organic framework materials for hydrogen storage," *Particuology*, vol. 7, pp. 129–140, 2009.
- [24] D. P. Broom, C. J. Webb, K. E. Hurst, P. A. Parilla, T. Gennett, C. M. Brown, R. Zacharia, E. Tylianakis, E. Klontzas, G. E. Froudakis, T. A. Steriotis, P. N. Trikalitis, D. L. Anton, B. Hardy, D. Tamburello, C. Corgnale, B. A. van Hassel, D. Cossement, R. Chahine, and M. Hirscher, "Outlook and challenges for hydrogen storage in nanoporous materials," *Appl. Phys. A Mater. Sci. Process.*, vol. 122, pp. 1–21, 2016.
- [25] B. Sakintuna, F. Lamari-Darkrim, and M. Hirscher, "Metal hydride materials for

- solid hydrogen storage: A review," *Int. J. Hydrogen Energy*, vol. 32, pp. 1121–1140, 2007.
- [26] W. Zhou, J. Jia, J. Lu, L. Yang, D. Hou, G. Li, and S. Chen, "Recent developments of carbon-based electrocatalysts for hydrogen evolution reaction," *Nano Energy*, vol. 28, pp. 29–43, 2016.
- [27] T. Autrey, "Boron-nitrogen-hydrogen (BNH) compounds : recent developments in hydrogen storage , applications in hydrogenation and catalysis , and new syntheses," *Energy and Enviro. Sci.*, vol. 5, pp. 9257–9268, 2012.
- [28] Y. Z. Chen, R. Zhang, L. Jiao, and H. L. Jiang, "Metal–organic framework-derived porous materials for catalysis," *Coord. Chem. Rev.*, vol. 362, pp. 1–23, 2018.
- [29] K. Schoots, F. Ferioli, G. J. Kramer, and B. C. C. van der Zwaan, "Learning curves for hydrogen production technology: An assessment of observed cost reductions," *Int. J. Hydrogen Energy*, vol. 33, pp. 2630–2645, 2008.
- [30] A. M. Kler, E. A. Tyurina, Y. M. Potanina, and A. S. Mednikov, "Estimation of efficiency of using hydrogen and aluminum as environmentally-friendly energy carriers," *Int. J. Hydrogen Energy*, vol. 40, pp. 14775–14783, 2015.
- [31] A. Sharma and S. K. Arya, "Hydrogen from algal biomass: A review of production process," *Biotechnol. Rep.*, vol. 15, pp. 63-69, 2017.
- [32] D. D. Burnette, G. G. Kremer, and D. J. Bayless, "The use of hydrogen-depleted coal syngas in solid oxide fuel cells," *J. Power Sources*, vol. 182, pp. 329–333, 2008.
- [33] A. Demirbaş, "Biomass resource facilities and biomass conversion processing for fuels and chemicals," *Energy Convers. Manag.*, vol. 42, pp. 1357–1378, 2001.
- [34] A. V Puga, "Photocatalytic production of hydrogen from biomass-derived feedstocks," *Coord. Chem. Rev.*, vol. 315, pp. 1–66, 2016.
- [35] H. Lund, "Renewable energy strategies for sustainable development," *Energy*, vol. 32, pp. 912–919, 2007.
- [36] H. Lund and B. V. Mathiesen, "Energy system analysis of 100% renewable energy systems-The case of Denmark in years 2030 and 2050," *Energy*, vol. 34,

- pp. 524–531, 2009.
- [37] M. Asif and T. Muneer, “Energy supply, its demand and security issues for developed and emerging economies,” *Renew. Sustain. Energy Rev.*, vol. 11, pp. 1388–1413, 2007.
- [38] O. Ellabban, H. Abu-Rub, and F. Blaabjerg, “Renewable energy resources: Current status, future prospects and their enabling technology,” *Renew. Sustain. Energy Rev.*, vol. 39, pp. 748–764, 2014.
- [39] J. Chi and H. Yu, “Water electrolysis based on renewable energy for hydrogen production,” *Chinese J. Catal.*, vol. 39, pp. 390–394, 2018.
- [40] K. Zeng and D. Zhang, “Recent progress in alkaline water electrolysis for hydrogen production and applications,” *Prog. Energy Combust. Sci.*, vol. 36, pp. 307–326, 2010.
- [41] C. R. P. Patel, P. Tripathi, A. K. Vishwakarma, M. Talat, P. K. Soni, T.P. Yadav, and O.N. Srivastava, “Enhanced hydrogen generation by water electrolysis employing carbon nano-structure composites,” *Int. J. Hydrogen Energy*, vol. 43, pp. 3180–3189, 2018.
- [42] Y. Yan, Y. Xia, and X. Wang, “A review on noble-metal-free bifunctional heterogeneous catalysts for overall electrochemical water splitting,” *J. Mater. Chem. A Mater. energy Sustain.*, vol. 4, pp. 17587–17603, 2016.
- [43] M. Momirlan and T. . Veziroglu, “Current status of hydrogen energy,” *Renew. Sustain. Energy Rev.*, vol. 6, pp. 141–179, 2002.
- [44] C. F. Leung, Y. Z. Chen, H. Q. Yu, S. M. Yiu, C. C. Ko, and T. C. Lau, “Electro- and photocatalytic hydrogen generation in acetonitrile and aqueous solutions by a cobalt macrocyclic Schiff-base complex,” *Int. J. Hydrogen Energy*, vol. 36, pp. 11640–11645, 2011.
- [45] R. Lin, L. Shen, Z. Ren, W. Wu, Y. Tan, H. Fu, J. Zhang, and L. Wu, “Enhanced photocatalytic hydrogen production activity via dual modification of MOF and reduced graphene oxide on CdS,” *Chem. Commun.*, vol. 50, pp. 8533-8535, 2014.
- [46] T. Jesionowski, “Influence of aminosilane surface modification and dyes adsorption on zeta potential of spherical silica particles formed in emulsion

- system,” *Colloids Surfaces A Physicochem. Eng. Asp.*, vol. 222, pp. 87–94, 2003.
- [47] J. K. Nørskov, T. Bligaard, A. Logadottir, J.R. Kitchin, J.G. Chen, S. Pandelov, and U. Stimming, “Trends in the Exchange Current for Hydrogen Evolution,” *J. Electrochem. Soc.*, vol. 152, pp. J23-J26, 2005.
- [48] O. Azizi, M. Jafarian, F. Gobal, H. Heli, and M. G. Mahjani, “The investigation of the kinetics and mechanism of hydrogen evolution reaction on tin,” *Int. J. Hydrogen Energy*, vol. 32, pp. 1755–1761, 2007.
- [49] F. Rosalbino, S. Delsante, G. Borzone, and E. Angelini, “Electrocatalytic behaviour of Co-Ni-R (R = Rare earth metal) crystalline alloys as electrode materials for hydrogen evolution reaction in alkaline medium,” *Int. J. Hydrogen Energy*, vol. 33, pp. 6696–6703, 2008.
- [50] R. Bocutti, M. J. Saeki, A. O. Florentino, C. L. F. Oliveira, and A. C. D. Ângelo, “Hydrogen evolution reaction on codeposited Ni-hydrogen storage intermetallic particles in alkaline medium,” *Int. J. Hydrogen Energy*, vol. 25, pp. 1051–1058, 2000.
- [51] F. Rosalbino, G. Borzone, E. Angelini, and R. Raggio, “Hydrogen evolution reaction on Ni-RE (RE = rare earth) crystalline alloys,” *Electrochim. Acta*, vol. 48, pp. 3939–3944, 2003.
- [52] D. N. Li, A. J. Wang, J. Wei, Q. L. Zhang, and J. J. Feng, “Facile synthesis of flower-like Au@AuPd nanocrystals with highly electrocatalytic activity for formic acid oxidation and hydrogen evolution reactions,” *Int. J. Hydrogen Energy*, vol. 42, pp. 19894–19902, 2017.
- [53] M. Schalenbach, F. D. Speck, M. Ledendecker, O. Kasian, D. Goehl, A. M. Mingers, B. Breitbach, H. Springer, S. Cherevko, and K. J. J. Mayrhofer, “Nickel-Molybdenum alloy catalysts for the hydrogen evolution reaction: Activity and stability revised,” *Electrochim. Acta*, vol. 259, 1154-1161, 2018.
- [54] M. Seredych, E. Rodriguez-Castellon, and T. J. Bandosz, “New CuxSy/nanoporous carbon composites as efficient oxygen reduction catalysts in alkaline medium,” *J. Mater. Chem. A*, vol. 2, npp. 20164–20176, 2014.
- [55] P. E. Karthik, K. A. Raja, S. S. Kumar, K.L.N. Phani, Y. Liu, S. X. Guo, J. Zhang

- and A. M. Bond, "Electroless deposition of iridium oxide nanoparticles promoted by condensation of  $[\text{Ir}(\text{OH})_6]^{2-}$  on an anodized Au surface: application to electrocatalysis of the oxygen evolution reaction," *RSC Adv.*, vol. 5, pp. 3196–3199, 2015.
- [56] F. Ye, C. Xua, G. Liub, J. Lid, X. Wangd, X. Dua, and J. K. Leeb, "A novel PtRuIr nanoclusters synthesized by selectively electrodepositing Ir on PtRu as highly active bifunctional electrocatalysts for oxygen evolution and reduction," *Energy Convers. Manag.*, vol. 155, pp. 182–187, 2018.
- [57] S. Kempahanumakkagari, K. Vellingiri, A. Deep, E. E. Kwon, N. Bolan, and K. Kim, "Metal – organic framework composites as electrocatalysts for electrochemical sensing applications," *Coord. Chem. Rev.*, vol. 357, pp. 105–129, 2018.
- [58] Q. Ye. A. Chen, W. Huang, J. Zhang, X. Liu, G. Xu, and Z. Zhou, "Titanium-supported nanoporous bimetallic Pt-Ir electrocatalysts for formic acid oxidation," *Electrochem. commun.*, vol. 9, no. 7, pp. 1513–1518, 2007.
- [59] J. B. Raoof, R. Ojani, S. A. Esfeden, and S. R. Nadimi, "Fabrication of bimetallic Cu/Pt nanoparticles modified glassy carbon electrode and its catalytic activity toward hydrogen evolution reaction," *Int. J. Hydrogen Energy*, vol. 35, pp. 3937–3944, 2010.
- [60] C. O. Ania, M. Seredych, E. Rodriguez-Castellon, and T. J. Bandosz, "New copper/GO based material as an efficient oxygen reduction catalyst in an alkaline medium: The role of unique Cu/rGO architecture," *Appl. Catal. B Environ.*, vol. 163, pp. 424–435, 2015.
- [61] Z. Sun, W. Fan, and T. Liu, "Graphene/graphene nanoribbon aerogels as tunable three-dimensional framework for efficient hydrogen evolution reaction," *Electrochim. Acta*, vol. 250, pp. 91–98, 2017.
- [62] M. R. Gao *et al.*, "An efficient molybdenum disulfide/cobalt diselenide hybrid catalyst for electrochemical hydrogen generation," *Nat. Commun.*, vol. 6, pp. 1–7, 2015.
- [63] G. R. Monama, S. B. Mdluli, G. Mashao, M. D. Makhafola, K. E. Ramohlola, K. M. Molapo, M. J. Hato, K. Makgopa, E. I. Iwuoha, and K. D. Modibane,

- “Palladium deposition on copper(II) phthalocyanine/metal organic framework composite and electrocatalytic activity of the modified electrode towards the hydrogen evolution reaction,” *Renew. Energy*, vol. 119, pp. 62–72, 2018.
- [64] J. Lin, J. He, F. Qi, B. Zheng, X. Wang, B. Yu, K. Zhou, W. Zhang, Y. Li, and Y. Chen, “Electrochimica Acta In-situ Selenization of Co-based Metal-Organic Frameworks as a Highly Efficient Electrocatalyst for Hydrogen Evolution Reaction,” *Electrochim. Acta*, vol. 247, pp. 258–264, 2017.
- [65] F. Li, X. Jiang, J. Zhao, and S. Zhang, “Graphene oxide : A promising nanomaterial for energy and environmental applications,” *Nano Energy*, vol. 16, pp. 488–515, 2015.
- [66] C. Petit, M. Seredych, and T. J. Bandosz, “Revisiting the chemistry of graphite oxides and its effect on ammonia adsorption,” *J. Mater. Chem.*, vol. 19, pp. 9176, 2009.
- [67] A. Energy, E. S. May, D. C. Higgins, Z. Chen, and J. Zhang, “A Review of graphene and graphene oxide sponge : material synthesis and applications to energy and the environment,” *Energy Environ. Sci.*, vol.7, pp. 1564–1596, 2014.
- [68] D. R. Dreyer, S. Park, W. Bielawski, and R. S. Ruoff, “The chemistry of graphene oxide,” 2010.
- [69] J. Song, X. Wang, and C.T. Chang, “Preparation and characterization of graphene oxide paper.,” *J. Nanomater.*, vol. 448, pp. 457–60, 2007.
- [70] G. Wang. Y. Ma, L. Zhang, J. Mu, Z. Zhang, X. Zhang, H. Che, Y. Bai, and J. Hou., “Facile synthesis of manganese ferrite/graphene oxide nanocomposites for controlled targeted drug delivery,” *J. Magn. Mater.*, vol. 401, pp. 647–650, 2016.
- [71] R. M. N. M. Rathnayake, H. W. M. A. C. Wijayasinghe, H. M. T. G. A. Pitawala, M. Yoshimura, and H. H. Huang, “Synthesis of graphene oxide and reduced graphene oxide by needle platy natural vein graphite,” *Appl. Surf. Sci.*, vol. 393, pp. 309–315, 2017.
- [72] C. K. Chua and M. Pumera, “Chemical reduction of graphene oxide : a synthetic chemistry viewpoint,” *Chem Soc Rev*, vol. 43, pp. 291–312, 2014.
- [73] J. Song, X. Wang, and C.-T. Chang, “Preparation and Characterization of

- Graphene Oxide,” *J. Nanomater.*, vol. 2014, pp. 1–6, 2014.
- [74] F. Mindivan, “The synthesis and characterization of graphene oxide ( GO ) and reduced graphene oxide ( rGO ),” *Machines , Technologies , Materials.*, vol. 6, pp. 32-35, 2017.
- [75] J. Lee, H. R. Chae, Y. J. Won, K. Lee, C.H. Lee, H. H. Lee, I. C. Kim, and J.M. Lee, “Graphene oxide nanoplatelets composite membrane with hydrophilic and antifouling properties for wastewater treatment,” *J. Memb. Sci.*, vol. 448, pp. 223–230, 2013.
- [76] G. Wang, X. Shen, B. Wang, J. Yao, and J. Park, “Synthesis and characterisation of hydrophilic and organophilic graphene nanosheets,” *Carbon N. Y.*, vol. 47, pp. 1359–1364, 2009.
- [77] A. L. Higginbotham, D. V Kosynkin, A. Sinitskii, Z. Sun, and J. M. Tour, “Lower-Defect Graphene Oxide Nanotubes,” *ACS Nano*, vol. 4, pp. 2059–2069, 2010.
- [78] D. C. Marcano, D. V. Kosynkin, J. M. Berlin, A. Sinitskii, Z. Sun, A. Slesarev, L. B. Alemany, W. Lu, and J. M. Tour, “Improved Synthesis of Graphene Oxide,” *ACS Nano*, vol. 4, pp. 183–191, 2010.
- [79] L. Shahriary and A. A. Athawale, “Graphene Oxide Synthesized by using Modified Hummers Approach,” *Int. J. Renew. Energy Environ. Eng.*, vol. 2, pp. 58–63, 2014.
- [80] J. Chen, B. Yao, C. Li, and G. Shi, “An improved Hummers method for eco-friendly synthesis of graphene oxide,” *Carbon N. Y.*, vol. 64, pp. 225–229, 2013.
- [81] Y. Gao, D. Ma, C. Wang, J. Guan, and X. Bao, “Reduced Graphene Oxide as Catalyst for Hydrogenation of Nitrobenzene,” *Structure*, vol. 47, pp. 2432–2434, 2011.
- [82] X. Chen, G. Wu, J. Chen, X. Chen, Z. Xie, and X. Wang, “Synthesis of ‘clean’ and well-dispersive pd nanoparticles with excellent electrocatalytic property on graphene oxide,” *J. Am. Chem. Soc.*, vol. 133, pp. 3693–3695, 2011.
- [83] C. Petit, J. Burrell, and T. J. Bandoz, “The synthesis and characterization of copper-based metal-organic framework/graphite oxide composites,” *Carbon N. Y.*, vol. 49, pp. 563–572, 2011.
- [84] J. Liu, H. Jeong, J. Liu, K. Lee, J. Y. Park, Y.H. Ahn, and S. Lee., “Reduction of

- functionalized graphite oxides by trioctylphosphine in non-polar organic solvents,” *Carbon N. Y.*, vol. 48, pp. 2282–2289, 2010.
- [85] V. Gupta, N. Sharma, U. Singh, M. Arif, and A. Singh, “Higher oxidation level in graphene oxide,” *Optik (Stuttg.)*, vol. 143, pp. 115–124, 2017.
- [86] S. Stankovich, D. A. Dikin, R. D. Piner, K. A. Kohlhaas, A. Kleinhammes, Y. Jia, Y. Wu, S. T. Nguyen, and R. S. Ruoff, “Synthesis of graphene-based nanosheets via chemical reduction of exfoliated graphite oxide,” *Carbon*, vol. 45, pp. 1558–1565, 2007.
- [87] B. M. Ganesh, A. M. Isloor, and A. F. Ismail, “Enhanced hydrophilicity and salt rejection study of graphene oxide-polysulfone mixed matrix membrane,” *Desalination*, vol. 313, pp. 199–207, 2013.
- [88] W. Zhang, Y. Li, X. Zeng, and S. Peng, “Synergetic effect of metal nickel and graphene as a cocatalyst for enhanced photocatalytic hydrogen evolution via dye sensitization,” *Sci. Rep.*, vol. 5, pp. 1–12, 2015.
- [89] A. Mukherjee, S. Chakrabarty, W. N. Su, and S. Basu, “Nanostructured nickel ferrite embedded in reduced graphene oxide for electrocatalytic hydrogen evolution reaction,” *Mater. Today Energy*, vol. 8, pp. 118–124, 2018.
- [90] R. Nivetha, S. Chella, P. Kollu, S. K. Jeong, A. Bhatnagar, and N. G. Andrews, “Cobalt and nickel ferrites based graphene nanocomposites for electrochemical hydrogen evolution,” *J. Magn. Magn. Mater.*, vol. 448, pp. 165–171, 2018.
- [91] J. A. S. B. Cardoso, L. Amaral, O. Metin, D.S.P. Cardoso, M. Sevim, T. Sener, C.A.C. Sequeira, D.M.F. Santos, “Reduced graphene oxide assembled Pd-based nanoalloys for hydrogen evolution reaction,” *Int. J. Hydrogen Energy*, vol. 42, pp. 3916–3925, 2017.
- [92] S. Lee, S. Hun, J. Suk, and S. Hyun, “Large-scale production of high-quality reduced graphene oxide,” *Chem. Eng. J.*, vol. 233, pp. 297–304, 2013.
- [93] P. C. Banerjee, D. E. Lobo, R. Middag, W. K. Ng, M. E. Shaibani, and M. Majumder, “Electrochemical Capacitance of Ni-Doped Metal Organic Framework and Reduced Graphene Oxide Composites : More than the Sum of Its Parts,” *ACS Appl. Mater. Interfaces*, vol. 7, pp. 3655–3664, 2015.
- [94] Z.S. Wu, G. Zhou, L.C. Yin, W. Ren, F. Li, and H.M. Cheng, “Graphene/metal

- oxide composite electrode materials for energy storage,” *Nano Energy*, vol. 1, pp. 107–131, 2012.
- [95] S. Stankovich, D. A. Dikin, G. H. B. Dommett, K. M. Kohlhaas, E. J. Zimney, E. A. Stach, R. D. Piner, S. T. Nguyen, and R. S. Ruoff, “Graphene-based composite materials,” *Letters*, vol. 442, pp.282-286, 2006.
- [96] V. Gargiulo, L. Lisi, R. Di, and M. Alf, “Synthesis and characterization of conductive copper-based metal-organic framework / graphene-like composites,” *Mater. Chem. Phys.*, vol. 147, pp. 744–750, 2014.
- [97] B. Valizadeh, T. N. Nguyen, and K. C. Stylianou, “Shape engineering of metal–organic frameworks,” *Polyhedron*, vol. 145, pp. 1–15, 2018.
- [98] P. Q. Liao, J. Q. Shen, and J. P. Zhang, “Metal-organic frameworks for electrocatalysis,” *Coord. Chem. Rev.*, vol. 2, pp. 1-27, 2017.
- [99] K. A. Lin, S. Chen, and A. P. Jochems, “Zirconium-based metal organic frameworks : Highly selective adsorbents for removal of phosphate from water and urine,” *Mater. Chem. Phys.*, vol. 160, pp. 168–176, 2015.
- [100] N. Stock, and S. Biswas, “Synthesis of Metal-Organic Frameworks (MOFs): Routes to Various,” *Chem. Revs.*, vol. 112, pp. 933–969, 2012.
- [101] L. Wang and R. T. Yang, “New sorbents for hydrogen storage by hydrogen spillover – a review,” *Energy Environ. Sci.*, vol. 1, pp. 268–279, 2008.
- [102] H. W. Langmia, J. Rena, B. Northa, M. Mathea, and D. Bessarabov, “Hydrogen storage in metal-organic frameworks: A Review,” *Electrochim. Acta*, vol. 128, pp. 368–392 2014.
- [103] Z. Hasan and S. H. Jhung, “Removal of hazardous organics from water using metal-organic frameworks (MOFs): Plausible mechanisms for selective adsorptions,” *J. Hazard. Mater.*, vol. 283, pp. 329–339, 2015.
- [104] C. Petit and T. J. Bandoz, “Engineering the surface of a new class of adsorbents: metal-organic framework/graphite oxide composites,” *J. Colloid Interface Sci.*, vol. 447, pp. 139–51, 2015.
- [105] H. Zhou, J. Zhang, J. Zhang, X. Yan, X. Shen, and A. Yuan, “Spillover enhanced hydrogen storage in Pt-doped MOF / graphene oxide composite produced via an impregnation method,” *INOCHÉ*, vol. 54, pp. 54–56, 2015.

- [106] H.C. Joe Zhou and S. Kitagawa, "Metal–Organic Frameworks (MOFs)," *Chem. Soc. Rev.*, vol. 43, pp. 5415–5418, 2014.
- [107] R. J. T. Houk, B. W. Jacobs, F. E. Gabaly, N. N. Chang, A. A. Talin, D. D. Graham, S. D. House, I. M. Robertson, and M. D. Allendorf, "Silver Cluster Formation , Dynamics , and Chemistry in Metal - Organic Frameworks," *Nano letters*, vol. 9, pp. 3413-3418 2009.
- [108] A. G. Wong-Foy, A. J. Matzger, and O. M. Yaghi, "Exceptional H<sub>2</sub> saturation uptake in microporous metal-organic frameworks," *J. Am. Chem. Soc.*, vol. 128, pp. 3494–3495, 2006.
- [109] F. Ke, L. G. Qiu, Y. P. Yuan, F. M. Peng, X. Jiang, A. J. Xie, Y. H. Shen, and J. F. Zhu, "Thiol-functionalization of metal-organic framework by a facile coordination-based postsynthetic strategy and enhanced removal of Hg<sup>2+</sup> from water," *J. Hazard. Mater.*, vol. 196, pp. 36–43, 2011.
- [110] M. Eddaoudi, D. B. Moler, H. Li, B. Chen, T. M. Reineke, T. M. O'keeffe, and O.M. Yaghi, "Modular chemistry: Secondary building units as a basis for the design of highly porous and robust metal-organic carboxylate frameworks," *Acc. Chem. Res.*, vol. 34, pp. 319–330, 2001.
- [111] M. Eddaoudi, J. Kim, N. Rosi, D. Vodak, J. Wachter, M. O'keeffe, and O. M. Yaghi, "Systematic Design of Pore Size and Functionality in Isorecticular MOFs and Their Application in Methane Storage," *Sci*, vol. 295, pp. 469–472, 2016.
- [112] F. N. Azad, M. Ghaedi, K. Dashtian, S. Hajati, and V. Pezeshkpour, "Ultrasonically assisted hydrothermal synthesis of activated carbon-HKUST-1-MOF hybrid for efficient simultaneous ultrasound-assisted removal of ternary organic dyes and antibacterial investigation: Taguchi optimization," *Ultrason. Sonochem.*, vol. 31, pp. 383–393, 2016.
- [113] M. Pilloni, F. Padella, G. Ennas, S. Lai, M. Bellusci, E. Rombi, F. Sini, M. Pentimalli, C. Delitala, A. Scano, and V. Cabras, "Liquid-assisted mechanochemical synthesis of an iron carboxylate Metal Organic Framework and its evaluation in diesel fuel desulfurization," *Microporous Mesoporous Mater.*, vol. 213, pp. 14–21, 2015.
- [114] P. Amo-Ochoa, G. Givaja, P. J. S. Miguel, O. Castillo, and F. Zamora,

- “Microwave assisted hydrothermal synthesis of a novel CuI-sulfate-pyrazine MOF,” *Inorg. Chem. Commun.*, vol. 10, pp. 921–924, 2007.
- [115] X. Wu, Z. Bao, B. Yuan, J. Wang, Y. Sun, H. Luo, and S. Deng, “Microwave synthesis and characterization of MOF-74 (M = Ni, Mg) for gas separation,” *Microporous Mesoporous Mater.*, vol. 180, pp. 114–122, 2013.
- [116] J. Y. Choi, J. Kim, S. H. Jung, H. Kim, J. Chang, and H. K. Chae, “Microwave Synthesis of a Porous Metal-Organic Framework , Zinc Terephthalate MOF-5,” *Bull Korean Chem. Soc.*, vol. 27, pp. 1523–1524, 2006.
- [117] C. M. Lu, J. Liu, K. Xiao, and A. T. Harris, “Microwave enhanced synthesis of MOF-5 and its CO<sub>2</sub> capture ability at moderate temperatures across multiple capture and release cycles,” *Chem. Eng. J.*, vol. 156, pp. 465–470, 2010.
- [118] R. Vakili, S. Xu, N. Al-Janabi, P. Gorgojo, S. M. Holmes, and X. Fan, “Microwave-assisted synthesis of zirconium-based metal organic frameworks (MOFs): Optimization and gas adsorption,” *Microporous Mesoporous Mater.*, vol. 260, pp. 45–53, 2018.
- [119] Y. Chen, D. Ni, X. Yang, C. Liu, J. Yin, and K. Cai, “Electrochimica Acta Microwave-assisted synthesis of honeycomblike hierarchical spherical Zn-doped Ni-MOF as a high-performance battery-type supercapacitor electrode material,” *Electrochim. Acta*, vol. 278, pp. 114–123, 2018.
- [120] N. K. Singh, S. Gupta, V. K. Pecharsky, and V. P. Balema, “Solvent-free mechanochemical synthesis and magnetic properties of rare-earth based metal-organic frameworks,” *J. Alloys Compd.*, vol. 696, pp. 118–122, 2017.
- [121] Y. R. Lee, J. Kim, and W. S. Ahn, “Synthesis of metal-organic frameworks: A mini review,” *Korean J. Chem. Eng.*, vol. 30, pp. 1667–1680, 2013.
- [122] H. M. Yang, X. Liu, X. L. Song, T. L. Yang, Z. H. Liang, and C. M. Fan, “In situ electrochemical synthesis of MOF-5 and its application in improving photocatalytic activity of BiOBr,” *Trans. Nonferrous Met. Soc. China*, vol. 25, pp. 3987–3994, 2015.
- [123] T. R. C. Van Assche, N. Campagnol, T. Muselle, H. Terryn, J. Fransaer, and J. F. M. Denayer, “On controlling the anodic electrochemical film deposition of HKUST-1 metal-organic frameworks,” *Microporous Mesoporous Mater.*, vol.

- 224, pp. 302–310, 2016.
- [124] Y. S. Song, B. Yan, and Z. X. Chen, “Hydrothermal synthesis, crystal structure and luminescence of four novel metal-organic frameworks,” *J. Solid State Chem.*, vol. 179, pp. 4037–4046, 2006.
- [125] J. Gascon, S. Aguado, and F. Kapteijn, “Manufacture of dense coatings of  $\text{Cu}_3(\text{BTC})_2$  (HKUST-1) on  $\alpha$ -alumina,” *Microporous Mesoporous Mater.*, vol. 113, pp. 132–138, 2008.
- [126] J. Yang, F. Cheng, J. Liang, and J. Chen, “Hydrogen generation by hydrolysis of ammonia borane with a nanoporous cobalt-tungsten-boron-phosphorus catalyst supported on Ni foam,” *Int. J. Hydrogen Energy*, vol. 36, pp. 1411–1417, 2011.
- [127] M. Ma, L. Wang, Y. Wang, W. Xiang, P. Lyu, B. Tang, and X. Tan, “Effect of hydrogen content on hydrogen desorption kinetics of titanium hydride,” *J. Alloys Compd.*, vol. 709, pp. 445–452, 2017.
- [128] Y. Zhang, J. Tan, F. Wen, Z. Zhou, and M. Zhu, “ScienceDirect Platinum nanoparticles deposited nitrogen-doped carbon nanofiber derived from bacterial cellulose for hydrogen evolution reaction,” *Int. J. Hydrogen Energy*, vol. 43, pp. 6167–6176, 2018.
- [129] J. R. Mckone, S. C. Marinescu, B. S. Brunshwig, J. R. Winkler, and H. B. Gray, “Earth-abundant hydrogen evolution electrocatalysts,” *Chemical Science* vol. 5, pp. 865–878, 2014.
- [130] H. Zhou, J. Zhang, D. Ji, A. Yuan, and X. Shen, “Microporous and Mesoporous Materials Effect of catalyst loading on hydrogen storage capacity of ZIF-8 / graphene oxide doped with Pt or Pd via spillover,” *Microporous Mesoporous Mater.*, vol. 229, pp. 68–75, 2016.
- [131] S. Loera-serna, M. A. Oliver-Telentino, M. L. Lopez-Nunez, A. Santana-Cruz, A. Guzman-Vargas, R. Cabrera-Sierra, H. I. Beltran, and J. Flores, “Electrochemical behavior of [  $\text{Cu}_3(\text{BTC})_2$  ] metal – organic framework : The effect of the method of synthesis,” *J. Alloys Compd.*, vol. 540, pp. 113–120, 2012.
- [132] K. E. Ramohlola, G. R. Monama, M. J. Hato, K. D. Modibane, K. M. Molapo, M.

- Masikini, S. B. Mdluli, and E. I. Iwuoha, "Polyaniline-metal organic framework nanocomposite as an efficient electrocatalyst for hydrogen evolution reaction," *Compos. Part B Eng.*, vol. 137, pp. 129–139, 2018.
- [133] K. E. Ramohlola, M. Masikini, S. B. Mdluli, G. R. Monama, M. J. Hato, K. M. Molapo, E. I. Iwuoha, and K. D. Modibane, "Electrocatalytic Hydrogen Evolution Reaction of Metal Organic Frameworks decorated with poly (3-aminobenzoic acid)," *Electrochim. Acta*, vol. 246, pp. 1174–1182, 2017.
- [134] K. E. Ramohlola, M. Masikini, S. B. Mdluli, G. R. Monama, M. J. Hato, K. M. Molapo, E. I. Iwuoha, and K. D. Modibane, "Electrocatalytic Hydrogen Production Properties of Poly(3- aminobenzoic acid) doped with Metal Organic Frameworks," *Int. J. Electrochem. Sci.*, vol. 12, pp. 4392–4405, 2017.
- [135] M. Jahan, Z. Liu, and K. P. Loh. "A Graphene oxide and copper-centered metal organic framework composite as a tri-functional catalyst for HER, OER, and ORR." *Adv. Funct. Mater.*, vol. 23, pp. 5363-5372, 2013.

## CHAPTER THREE

### ANALYTICAL TECHNIQUES

---

#### 3.1. INTRODUCTION

Analytical techniques are set of instruments used to determine the chemical, physical, morphological or electrochemical nature of a material and also quantify certain species within the material. The analytical techniques can be separated into different categories such as spectroscopy, microscopy and physical methods.

#### 3.2. SPECTROSCOPY

Spectroscopy is the study of the interaction of electromagnetic radiation in all its forms with matter, which can be used for both quantitative and qualitative analysis. The interaction might give rise to molecular vibrations in Infrared (IR).

##### 3.2.1. Fourier transform infrared spectroscopy

Fourier transform infrared spectroscopy (FTIR) is an analytical technique employed to attain an infrared spectrum of absorption or emission of a solid, liquid, or gaseous molecules. The principle behind FTIR involves the absorption of light in the infrared region of the electromagnetic spectrum by molecules. The absorbed light causes the bonds within molecules to vibrate with a certain frequency which corresponds to that specific bond. The frequencies of the vibrations are calculated in terms of wave numbers ranging from  $4000 - 400 \text{ cm}^{-1}$  [1]. The instrument initially records the background emission spectrum, which will be used to correct the spectra reading of analyte, and then secondly the emission spectrum of the IR source of the sample of interest. The ratio between the sample spectrum and background spectrum directly correlates with the sample's absorption spectrum. The resultant absorption spectrum due to the bond natural vibration frequencies designates the presence of those specific

chemical bonds corresponding to functional groups existing in the sample. Figure 3.1 outlines the important features of FTIR and how sample analysis takes place [1,2].

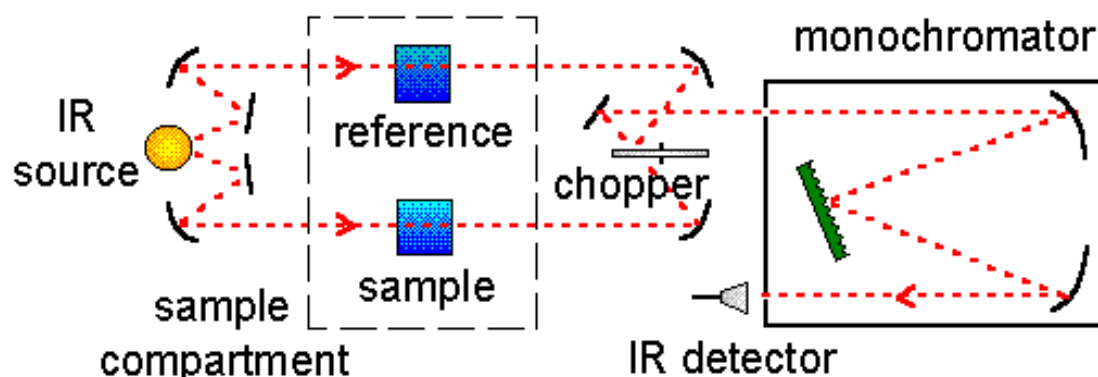


**Figure 3.1:** Basic components of FTIR [1].

FTIR is mostly employed for qualitative analysis to identify which functional groups are present in the sample [3,4]. In this work FTIR was used to confirm the presence of MOF and GO functional groups in the nanocomposite.

### 3.3. MICROSCOPY

Microscopic techniques are set of methods which are used to view objects that cannot be detected by naked eye or simple spectroscopic techniques such as UV-vis or IR. In principle, when an electron beam interacts with the atoms in a sample, individual incident electrons undergo two types of scattering - elastic and inelastic. In the elastic, only the trajectory changes, the kinetic energy and velocity remain constant. Inelastic scattering, some incident electrons will actually collide and displace electrons from their orbits (shells) around nuclei of atoms comprising the sample. This interaction places the atom in an excited (unstable) state. Microscopy can be categorised into three sections, namely:

- optical microscopy which uses visible light to produce enlarged images,

- scanning probe microscopy that involves using a probe to scan object and electron microscopy that uses an electron beams to create an image of an object.

### 3.3.1. Scanning electron microscopy

Scanning electron microscopy (SEM) is a powerful method that utilises focused beam of electrons for high-resolution imaging of surfaces of the materials. The basic principle (Figure 3.2) is that a sample is bombarded with electrons, the strongest region of the electron energy spectrum is due to secondary electrons. These secondary electrons are produced when incident electrons excite electrons in the sample and lose most of the energy in the process [5,6].

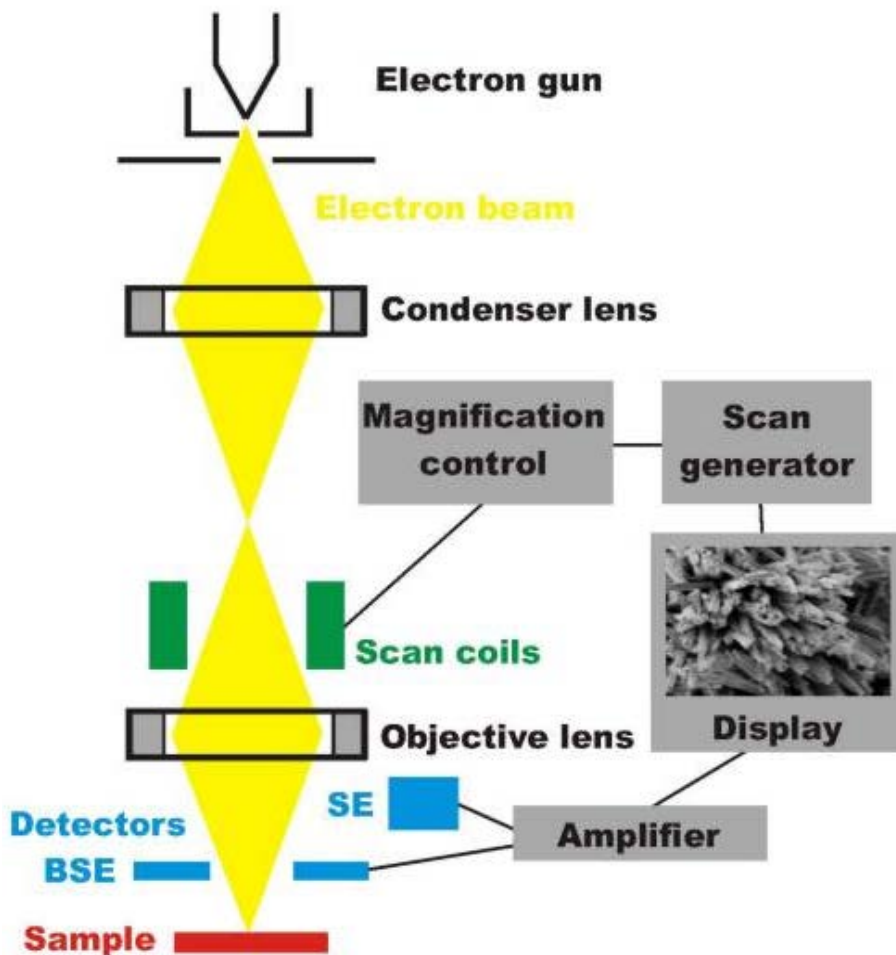


**Figure 3.2:** Overview of scanning electron microscopy [6].

The electron beam is accelerated through a high voltage (e.g. 20 kV) and pass through a system of apertures and electromagnetic lenses to produce a thin beam of electrons [5]. The beam scans the surface of the specimen by means of scan coils. Furthermore, the excited electron moves towards the surface of the sample undergoing elastic and inelastic collisions until it reaches the surface, where it can escape if it still has sufficient energy. Electrons are emitted from the specimen by the action of the scanning beam and collected by a suitably-positioned detector [7]. The relaxation energy is the fingerprint of each element which are measured by Energy Dispersive Spectroscopy detector (also called EDS). In this study, the SEM technique was employed for investigation of the morphology of the synthesised GO and MOF materials as well as composite.

### **3.3.2. Transmission electron microscopy**

Transmission electron microscopy (TEM) is a very powerful tool for material science. A high energy beam of electrons is shone through a very thin sample, and the interactions between the electrons and the atoms can be used to observe features such as the crystal structure and features in the structure like dislocations and grain boundaries [8]. TEM (Figure 3.3) can be used to study the growth of layers, their composition and defects in semiconductors. High resolution can be used to analyse the quality, shape, size and density of quantum wells, wires and dots.

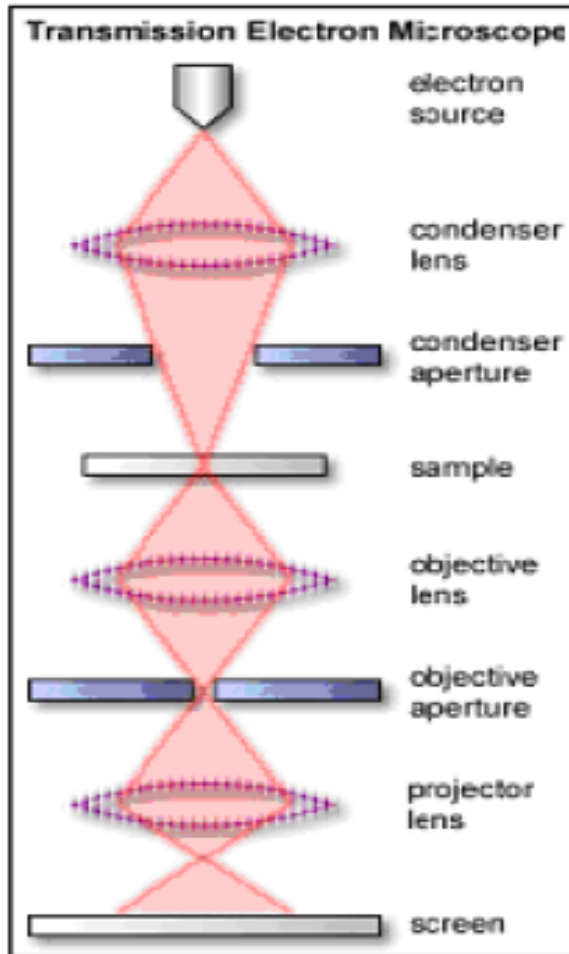


**Figure 3.3:** Overview of transmission electron microscope [8].

In principle, the electrons pass through multiple electromagnetic lenses. The beam passes through the solenoids (tubes with coil wrapped around them), down the column, makes contact with the screen where the electrons are converted to light and form an image. The image can be manipulated by adjusting the voltage of the gun to accelerate or decrease the speed of electrons as well as changing the electromagnetic wavelength via the solenoids [8,9]. The coils focus images onto a screen or photographic plate. During transmission, the speed of electrons directly correlates to electron wavelength; the faster electrons move, the shorter wavelength and the greater the quality and detail of the image. The lighter areas of the image represent the places where a greater number of electrons were able to pass through the sample

and the darker areas reflect the dense areas of the object. These differences provide information on the structure, texture, shape and size of the sample [6,8]. To obtain a TEM analysis, samples need to have certain properties. They need to be sliced thin enough for electrons to pass through, a property known as electron transparency. Samples need to be able to withstand the vacuum chamber and often require special preparation before viewing. A high resolution transmission electron microscope coupled with energy dispersive X-ray (EDX) was used to obtain the structural morphology and elemental analysis for all the synthesised materials.

### 3.4. PHYSICAL METHODS

Physical methods are techniques which are used to determine the physical properties of the materials or compounds. This technique helps in determining the crystallinity of the compounds, surface area and also the mechanical and thermal stability of the materials. In principles this method uses the spectroscopy and microscopy techniques.

#### 3.4.1. X-ray diffraction

X-ray diffraction (XRD) is an analytical technique that is used primarily for phase identification of a crystalline material and can provide information on unit cell dimensions. This technique is based on constructive interference of monochromatic X-rays and a crystalline sample of which interaction of the incident rays with the sample induces constructive interference such that Bragg's law is satisfied which is given by [10]:

$$n\lambda = 2d\sin\theta \quad (3.1)$$

where  $\lambda$  designates the wavelength of the radiation beam,  $d$  is the interplanar spacing between two diffracting lines,  $\theta$  is the diffraction angle, and  $n$  is an interger usually equal to 1. XRD is most widely used for identification of unknown crystalline materials

such as minerals and inorganic compounds, measurements of sample purity, characterisation of crystalline materials, and determination of unit cell dimensions. The technique possesses numerous advantages such as being powerful and rapid (<20 min) for identification of unknown materials and data interpretation is relatively straight forward [10, 11]. However, its disadvantage is that peak overlay may occur and worsens for high angle reflections and that for fixed materials, detection limit is ~2% of sample. In this study, XRD was used to fingerprint the materials using the known reference patterns and also monitor the composite formation [12].

### **3.4.2. Simultaneous thermal analysis (STA)**

STA involves the application of thermogravimetric analysis (TGA) and differential scanning calorimetry (DSC) simultaneously. In brief, the thermogravimetry deals with thermal analysis which is focussed on investigating the change in weight of a material as a function of increasing temperature or time. The profile of weight change is recorded upon sample exposure to a controlled heating or cooling environment. The weight change recorded as a function of time is isothermal mode, whereas the one captured as a function of temperature is scanning mode [13,14]. Thermogravimetric analyses (TGA) is primarily used to understand certain thermal processes such as absorption, adsorption, desorption, vaporization, sublimation, decomposition, oxidation, and reduction. Additionally, this method can be used for evaluating volatiles or gaseous products lost during such chemical reactions for various samples such as nanomaterials, polymers, polymer nanocomposites, fibres etc. [13]. TGA is employed for determining the thermal stability and organic content of samples, degradation mechanism as well as kinetics of chemical reactions. On the other hand, Differential scanning calorimeter (DSC) is a technique in which the difference in the amount of heat required to increase the temperature of a sample and reference are measured as function of temperature. Both the sample and reference are maintained at nearly the same temperature throughout the experiment. Generally, the temperature program for a DSC analysis is designed such that the sample holder temperature increases linearly as a function of time. Only a few mg of material are required to run the analysis. DSC

is the most often used thermal analysis method, primarily because of its speed, simplicity, and availability. It is mostly used for quantitative analysis. Generally, if a material is thermally stable, no change in mass will be observed. Advantages associated with this method include limitations in instrumental error and no series of standards for calculation of an unknown are required. The drawback is that it only allows for single element analysis, or a limited group of elements at a time [15]. The thermal stability of the prepared nanocomposite was studied using STA.

### **3.5. ELECTROANALYTICAL METHODS**

Electroanalytical methods are a class of techniques in analytical chemistry, which study an analyte by measuring the potential (volts) and/or current (amperes) in an electrochemical cell containing the analyte. These methods can be broken down into several categories depending on which aspects of the cell are controlled and which are measured. The three main categories are potentiometry (the difference in electrode potentials is measured), coulometry (the cell's current is measured over time), and voltammetry (the cell's current is measured while actively altering the cell's potential) [16,17]. Electroanalytical techniques follow the basics of electrochemistry whereby redox reactions occur during operations and use the electrochemical cell principles. This means that there is an electron loss and gain between the species in question. The simplest electrochemical cell will consist of two electrodes immersed in an electrolyte solution, which can be separated by a salt bridge. Chemical reactions mostly occur on the surface of the electrodes giving several half reactions. Mostly three compartment electrodes are used which are placed in an electrolytic solution in a glass [18,19]. The reactions occur on the surface of the working electrode. There are several types of working electrodes, which are commonly used, thus glassy carbon, gold and mercury working electrodes. During operations, there must be a standardisation process, which occurs in reference electrode. The potential in reference electrode is fixed and the potential change is monitored on working electrode. The most commonly used reference electrode is saturated calomel electrode (SCE) and silver/silver chloride (Ag/AgCl) electrode. Then lastly there is an

auxillary electrode, which is known as counter electrode. It serves as a sink for electrons so that the current can be passed from the external circuit. The electroanalytical technique used in this work is voltammetry, so next sections will review types of voltammetry methods used in study.

### **3.5.1. Cyclic voltammetry**

Cyclic voltammetry (CV) is an electrochemical technique which measures the current that develops in an electrochemical cell under conditions where voltage is in excess of that predicted by the Nernst equation [17-19]. The CV (Figure 3.4) is performed by cycling the potential of a working electrode and measuring the resulting current. In this technique it is compulsory to have a working, reference, and counter electrode, and an electrolytic solution to be added to the sample solution to ensure sufficient conductivity [19]. It is often used to study a variety of redox processes, to determine the stability of reaction products, the presence of intermediates in redox reactions, reaction and electron transfer kinetics and the reversibility of a reaction [18]. The CV was used to evaluate the electrochemical properties of the materials as well as the hydrogen evolution reaction for hydrogen production.

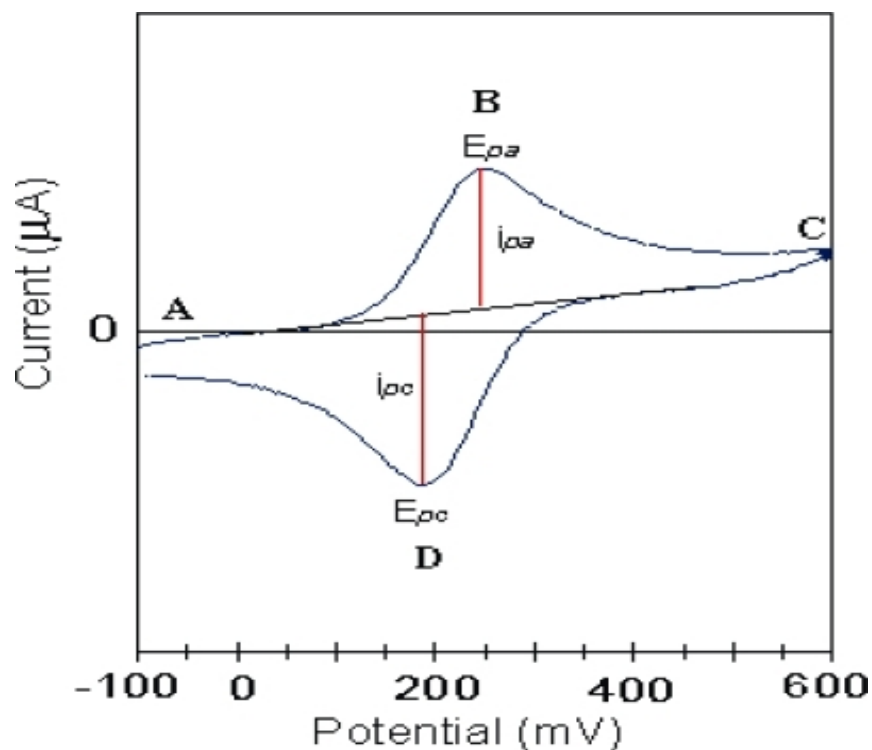


**Figure 3.4:** Typical cyclic voltammogram showing the peak cathodic and anodic current respectively for a reversible reaction [19].

### 3.6. CONCLUSIONS

In summary, several analytical instruments were reviewed in this Chapter with their applications in materials' characterisations. The review chapter explained the principle behind analytical techniques, which will be used to study and understand the chemistry of the prepared materials. The FTIR was detailed to help with the confirmation of the composite by looking at the appearance and disappearance of vibration bands. This technique was adopted in this work for structural elucidation of the nanocomposites. The STA was identified as a suitable thermal technique for thermal stability and moisture characterisation of the materials and also to monitor the formation of the nanocomposite. The crystallinity of the materials was confirmed by XRD, wherein the review of this technique showed further on how to determine the magnetic and polymeric phases of the nanocomposites. On the other hand, the morphological

techniques were reviewed. The FE-SEM and HRTEM techniques provide information about extrinsic and intrinsic structural imaging as well as elemental mapping and composition (using EDX). The CV potentiostat was used to confirm the electrochemical properties of the synthesised materials and to monitor their hydrogen evolution.

### 3.7. REFERENCES

- [1] M. A. Mohamed, J. Jaafar, A. F. Ismail, M. H. D. Othman, and M. A. Rahman, "Fourier Transform Infrared (FTIR) Spectroscopy," In *Membrane Characterization*, pp. 3-29, 2017. doi.org/10.1016/B978-0-444-63776-5.00001-2.
- [2] L. C. Lee, C. Liang, and A. A. Jemain, "A contemporary review on Data Preprocessing (DP) practice strategy in ATR-FTIR spectrum," *Chemom. Intell. Lab. Syst.*, vol. 163, pp. 64–75, 2017.
- [3] M. C. Rehbein, S. Husmann, C. Lechner, C. Kunick, and S. Scholl, "Fast and calibration free determination of first order reaction kinetics in API synthesis using in-situ ATR-FTIR," *Eur. J. Pharm. Biopharm.*, pp. 1–6, 2017. doi.org/10.1016/j.ejpb.2017.09.013.
- [4] G. E. Tranter and U. Kingdom, "FTIR Spectroscopy of Aqueous Solutions," *Encyclopedia of Spectroscopy and Spectrometry*, Third Edition, pp. 762–769, 2017. doi.org/10.1016/B978-0-12-409547-2.12157-2.
- [5] A. Yoshida, Y. Kaburagi, and Y. Hishiyama, "Scanning Electron Microscopy," *Materials Science and Engineering of Carbon: Characterization*, pp. 71-93, 2016. doi.org/10.1016/B978-0-12-805256-3.00005-2.
- [6] M. D. A. Pereira-da-silva and F. A. Ferri, "Scanning Electron Microscopy," *Nanocharacterization Techniques*, pp. 1-35, 2017.
- [7] T. L. Kirk, "A Review of Scanning Electron Microscopy in Near Field Emission Mode," *Advances in Imaging and Electron Physics*, vol. 204, 2017, ISSN 1076-5670, doi.org/10.1016/bs.aiep.2017.09.002

- [8] Z. L. Wang, "Transmission Electron Microscopy of Shape-Controlled Nanocrystals and Their Assemblies," *J. Phys. Chem. B.*, vol.104, pp. 1153–1175, 2000.
- [9] P. G. Callahan et al., J. C. Stinville, E. R. Yao, M. P. Echlin, M. S. Titus, M. Graef, D. S. Gianola and T. M. Pollock, "Ultramicroscopy Transmission scanning electron microscopy: Defect observations and image simulations," *Ultramicroscopy*, vol. 186, pp. 49–61, 2018.
- [10] F. C. Adams, "X-Ray Absorption and Diffraction — Overview," *Encyclopedia of Analytical Science* 3rd ed, pp. 1-14, 2017. doi.org/10.1016/B978-0-12-409547-2.14263-5.
- [11] G. M. Hansford, "Nuclear Instruments and Methods in Physics Research A X-ray diffraction without sample preparation: Proof-of-principle experiments," *Nucl. Inst. Methods Phys. Res. A*, vol. 728, pp. 102–106, 2013.
- [12] D. Rennes and D. Loue, "Powder X-Ray Diffraction, Applications," *Encyclopedia of Spectroscopy and Spectrometry*, Third Edition, pp. 723–731, 2017. doi.org/10.1016/B978-0-12-803224-4.00257-0.
- [13] S. Loganathan, R. B. Valapa, R. K. Mishra, G. Pugazhenthii and S. Thomas, "Thermogravimetric Analysis for Characterization of Nanomaterials," *Thermal and Rheological Measurement Techniques for Nanomaterials Characterization*, pp. 67-108, 2017. doi.org/10.1016/B978-0-323-46139-9.00004-9.
- [14] P. Thirunathan, P. Arnz, J. Husny, A. Gianfrancesco, and J. Perdana, "Thermogravimetric analysis for rapid assessment of moisture diffusivity in polydisperse powder and thin film matrices," *Food Chem.*, vol. 242, pp. 519–526, 2018.
- [15] C. Karakaya, S. Ricote, D. Albin, E. Sánchez-cortezón, B. Linares-zea, and R. J. Kee, "Thermochimica Acta Thermogravimetric analysis of InCl<sub>3</sub> sublimation at atmospheric pressure," *Thermochim. Acta*, vol. 622, pp. 55–63, 2015.
- [16] McMurry, J. *Organic Chemistry*, 7th Edition Brooks/Cole, Thomson Learning, Inc (2008).
- [17] <http://www.chemicool.com/img1/graphics/ir.gi>.

- [18] Bard, A.J., Faulkner, L.R. In: *Electrochemical Methods: Fundamentals and applications*. 2nd edition, John Wiley & Sons Inc (2001).
- [19] [https://openi.nlm.nih.gov/imgs/512/389/2871148/PMC2871148\\_ijms-11-01956f1.png](https://openi.nlm.nih.gov/imgs/512/389/2871148/PMC2871148_ijms-11-01956f1.png).

**CHAPTER FOUR**  
**GRAPHENE OXIDE/METAL ORGANIC FRAMEWORKS NANOCOMPOSITE**  
**WITH IMPROVED ELECTROCATALYTIC EFFICIENCY FOR HYDROGEN**  
**PRODUCTION AND STORAGE**

---

*This chapter has been submitted for publication:*

**CHAPTER SUMMARY**

There are very rare reports on using metal organic framework (MOF) electrocatalysts for hydrogen production and storage through electrochemical hydrogen evolution reaction (HER). In this study, a composite of graphene oxide (GO) and Metal organic framework (MOF) was synthesised by impregnation method, characterised with various techniques and its application as HER electrocatalyst was studied using cyclic voltammetry (CV), Tafel plots and turn over frequencies (TOFs). The X-ray diffraction (XRD) and Fourier Transform Infrared spectroscopy (FTIR) results of the composite demonstrated the crystalline phases and vibrational bands for both parent materials. The simultaneous thermal analysis (thermal gravimetric analysis (TGA) and differential scanning calorimetry (DSC)) results showed enhancement of the thermal stability of the composite as compared to the neat materials. The scanning electron microscopy/Energy dispersive spectroscopy (SEM/EDS) and high resolution transmission electron microscopy/Energy dispersive x-ray spectroscopy (HRTEM/EDX) confirmed the presence of octahedral structure of MOF in the GO sheet-like structure and elemental composition of the synthesised materials. The performance of the proposed electrolytic system for electrochemical HER by Tafel parameters and TOFs showed a drastic increase in catalytic H<sub>2</sub> production in the composite through the Volmer reaction coupled with one of the mechanisms. This disclosed that the addition of GO/MOF in the electrolytic system possessed better

catalytic characteristics with enhanced TOFs which may open a new way for hydrogen production and storage via HER enhancement.

#### 4.1. INTRODUCTION

Currently, energy supplies are mainly based on combustion of fossil fuels accompanied by a number of environmental problems such as greenhouse emission and air pollution. In order to overcome these challenges, hydrogen gas as a renewable energy has been designated as the best energy carrier and alternative non-renewable sources due to its excellent properties (i.e. light weight and high energy density as compared to fossil fuel based sources) [1,2]. However, there are significant challenges hindering the large scale applications and commercialisation of hydrogen fuel especially in mobile transportation. These problems include the lack of safe handling/hydrogen storage materials and effective methods for hydrogen production. With this being noted, electrochemical reduction of water is considered as one of the promising route for hydrogen production due to its simplicity and economical way to produce hydrogen with high purity and large quantity [2]. Even though electrochemical water splitting is regarded as a promising route for hydrogen generations, usage of platinum (Pt) as an excellent cathode electrode hampers its practical applications because of its high cost and low earth abundance [3,4]. Hence, there is a need to look for a suitable alternative material to Pt based on cheap and high earth abundant materials [3]. There are several reports which have attempted to reduce the amount of Pt loaded in the electrode body [4] or replace it with another electrocatalyst[5]. Electrocatalysts such as nanostructured carbons (carbon nanotubes) [6], metal organic frameworks (MOFs) [7] and metal sulphides [6] were proposed as candidates for hydrogen evolution reaction (HER) due to the light weight and high surface areas. Amongst these electrocatalysts, MOFs have shown to be very promising materials for HER mainly due to their adjustable pore sizes as well as defined hydrogen occupation sites [7]. Related to hydrogen energy, MOFs have also been used as hydrogen storage materials [8,9] and there are some reports in hydrogen generation area with photocatalytic method [10], and a few reports on electrochemical hydrogen generation

[7,11]. Nevertheless, MOFs exhibit a few weak points that impact their potential use. These include low electrical conductivity (their use in electrocatalysis is limited), moisture instability, poor H<sub>2</sub> adsorption and desorption at ambient conditions (the high H<sub>2</sub> adsorption amounts of this material were measured only at 77 K and declined dramatically at ambient temperature, due to weak physisorption of hydrogen on MOFs) [12]. Combining MOF materials with other substrates has been proposed in order to mitigate the above-mentioned drawbacks [13-15]. Carbon based/metal-organic frameworks (MOF) composites have recently attracted significant attention as a new class of materials [10-15]. For example, Petit and Bandosz [16] have reported the formation of graphene (GO)/MOF composites via interactions between oxygen groups of GO and metallic centers of MOF using hydrothermal method, where the synergetic effect between MOF units and GO layers was responsible for enhanced adsorption amounts compared to the parent material. Bandosz and other groups have also constructed GO/MOF composites (in-situ hydrothermal synthesis), and the synergistic effect on porosity and chemistry of GO/MOF resulted in an improvement of H<sub>2</sub> absorption [15]. In addition, Ramohlola *et al.* [14] presented poly(3-aminobenzoic acid)/metal organic framework composite with a drastic increase in catalytic H<sub>2</sub> evolution due increase in electron density of the polymer by introduction of MOF. Taking advantages of GO, chemically modified graphene with MOF exhibits numerous active edges and functional groups based on oxygen. It has good electrochemical and mechanical properties, which makes it suitable for energy devices [13,15]. To the best of our knowledge, there are no studies reported on HER using composite of GO/MOF. Hence in this study, a composite of MOF with GO was prepared through impregnation method and applied for electrochemical hydrogen evolution reaction. Structure and morphology of the composite were characterised by various techniques, and its electrochemical hydrogen production and storage performance was compared with bare electrode, MOF and GO.

## 4.2. EXPERIMENTAL

### 4.2.1. Materials

Copper nitrate trihydrate ( $\text{Cu}(\text{NO}_3)_2 \cdot 3\text{H}_2\text{O}$ ), trimesic acid ( $\text{H}_3\text{BTC}$ ), graphite powder, tetrabutylammonium percholate (TBAP), and Sodium nitrate ( $\text{NaNO}_3$ ) were purchased from Sigma Aldrich, South Africa., dimethylformamide (DMF), dimethylsulfoxide (DMSO), phosphoric acid ( $\text{H}_3\text{PO}_4$ ) and sulphuric acid ( $\text{H}_2\text{SO}_4$ ) were purchased from Rochelle chemicals. Potassium permanganate ( $\text{KMnO}_4$ ) and hydrochloric acid (HCl) were purchased from SAARCHEM. Hydrogen peroxide ( $\text{H}_2\text{O}_2$ ) from Moncon.  $\text{H}_2\text{SO}_4$  standard solutions were made in DMSO solution with  $0.1 \text{ mol.L}^{-1}$  TBAP as a supporting electrolyte system unless otherwise stated. Electrochemical measurements were carried out at  $22 \pm 2$  °C.

### 4.2.2. Synthesis of GO, MOF and GO/MOF composite

GO was prepared according to the modified Hummer method [17]. Briefly, 5 g of graphite and 2.5 g of  $\text{NaNO}_3$  were mixed with 108 mL  $\text{H}_2\text{SO}_4$  and 12 mL  $\text{H}_3\text{PO}_4$  and stirred in an ice bath for 10 minutes. Approximately, 15 g of  $\text{KMnO}_4$  was slowly added maintaining the temperature of the mixture below 5 °C. The suspension was then left to react for 2 hours in an ice bath, stirred for 60 minutes and stirred in a 40 °C water bath for 60 minutes. The temperature of the mixture was adjusted to a constant 98 °C for 60 minutes while water was added dropwisely. Deionised water was further added so that the volume of the suspension was 400 mL. Again, 15 mL of  $\text{H}_2\text{O}_2$  was added after 5 minutes. The reaction product was centrifuged and washed with deionised water and 5% HCl solution repeatedly. Finally, the product was dried at 60 °C.

MOF was synthesised by following a hydrothermal procedure [18]. Briefly, 4.5 mmol (1.087 g) of  $\text{Cu}(\text{NO}_3)_2 \cdot 3\text{H}_2\text{O}$  was dissolved in 10 mL of distilled water and then mixed with 2.5 mmol (0.525 g) of  $\text{H}_3\text{BTC}$  (trimesic acid) dissolved in 10 mL of ethanol. The mixture was stirred for 30 minutes and then transferred to a 23 mL Teflon stainless-steel autoclave and sealed to react for 36 hours at 120 °C in thermostatic drying oven.

After cooling to room temperature, the mother liquor was then filtered. The product was washed by ethanol repeatedly, and then dried at 50 °C for overnight.

GO/MOF composite was prepared through impregnation method of directly mixing of GO and MOF. Briefly, 0.1 g of as-synthesized MOF sample was dehydrated at 150 °C for 1 hour. It was then suspended in 10 ml DMF. In a separate beaker, 0,1 g of graphene oxide (50 wt.%) was dispersed in 1,4 mL DMF, and then the two mixtures were mixed together and stirred magnetically for 24 hours at 50 °C. The resulting product was recovered by filtration and washed with ethanol and then dried overnight at 50 °C.

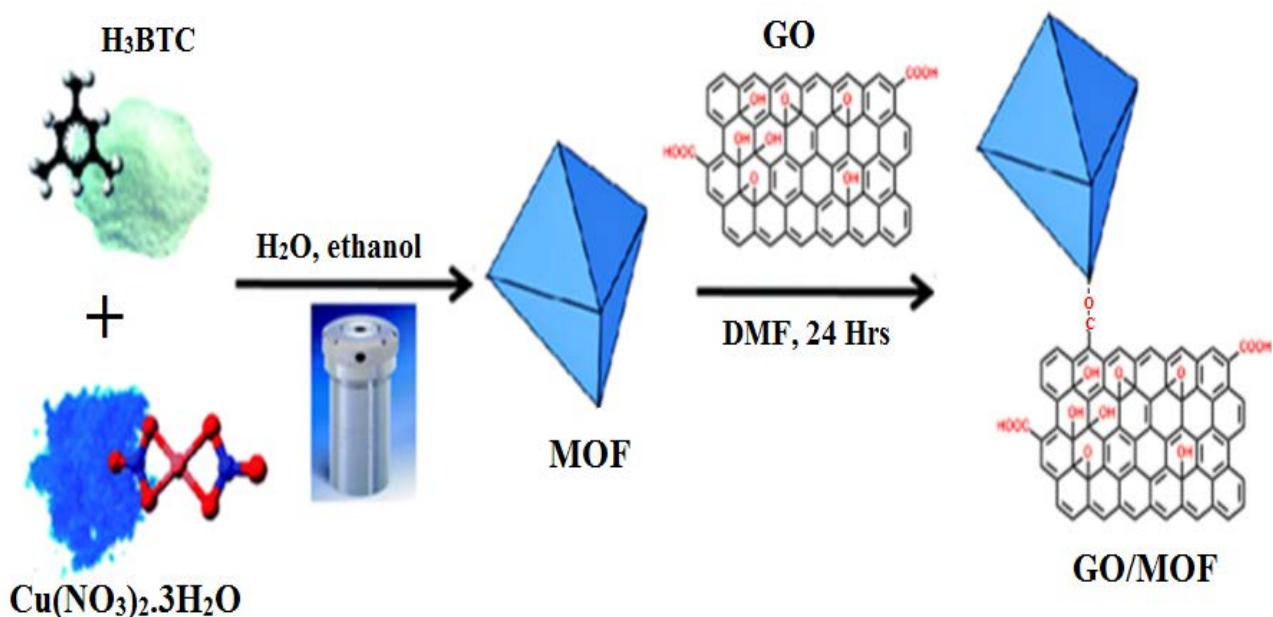
#### **4.2.3. Material characterisations**

FTIR spectra were recorded on Spectrum II spectrometer (PerkinElmer) in the wavenumber range between 400 and 4500  $\text{cm}^{-1}$  at room temperature and X-ray diffraction (XRD Phillips PW 1830,  $\text{CuK}\alpha$  radiation,  $\lambda = 1.5406 \text{ \AA}$ ). The thermal stability was studied by a thermogravimetric analyser (STA Perkin-Elmer 4000). Samples ranging between 1 to 4 mg were heated from 30-500 °C at a heating rate of 20 °C.min<sup>-1</sup> under N<sub>2</sub> environment. Morphological characterisations were performed using Auriga Field Emission Scanning Electron Microscope (FESEM) coupled with EDS detector for elemental analysis. The internal morphology was carried out using a FEI Tecnai G2 20 transmission electron microscope (TEM) coupled with EDX, operated at an accelerating voltage of 200 kV. Electrochemical measurements were performed using EPSILON electrochemical workstation. The data were collected using gold (3 mm diameter, 0.071  $\text{cm}^2$  area), Pt and Ag/AgCl electrode as working electrode, counter electrode and reference electrode, respectively. Repetitive scanning of the solutions of GO, MOF, and GO/MOF composite ( $\sim 2.0 \times 10^{-4} \text{ mol.L}^{-1}$ ) was from -2.0 to 1.25 V at scan rate of 0.02 - 0.10  $\text{V.s}^{-1}$ . Electrochemical experiments were performed in 25 mL of 0.1  $\text{mol.L}^{-1}$  TBAP/DMSO electrolytic system. HER studies were done using different concentrations of 0.03 - 0.45  $\text{mol.L}^{-1}$  H<sub>2</sub>SO<sub>4</sub> as H<sub>2</sub> source in 0.1  $\text{mol.L}^{-1}$  TBAP/DMSO system and  $\sim 2.0 \times 10^{-4} \text{ mol.L}^{-1}$  of GO, MOF and GO/MOF composite as electrocatalysts.

## 4.3. RESULTS AND DISCUSSION

### 4.3.1. Structural Properties

It was well documented that Hummer's method involves oxidation of graphene by strong oxidising agents to obtain graphite oxide [19,20]. Through exfoliation and ultra-sonication, a black powdered graphene oxide was obtained. Scheme 4.1 presents the synthetic route followed for preparation of MOF and GO/MOF via hydrothermal and impregnation methods, respectively. The synthesised materials were confirmed by XRD, FTIR, TGA, DSC, SEM/EDS, TEM/EDX and SAED analyses.



**Scheme 4.1:** Synthesis of MOF and GO/MOF composite through hydrothermal and impregnation method, respectively.

The XRD diffraction pattern of MOF presented in Figure 4.1, is in accordance with the one reported in the literature [21] and this is also supported by the reference MOF CSID [18]. The characteristics peaks of the MOF pattern appeared at small  $2\theta$  angles which are characteristics of microporous materials, which possess numerous tiny

pores or cavities that are in accordance with typical MOF structure [21]. One of the main intense peak of the pattern appeared at  $2\theta=11.5^\circ$ , which accounts for the reflection (222) when calculating the lattice plane with interplanar d spacing of 7.68 Å (estimated using Bragg's equation:  $n\lambda=2d\sin\theta$ ) [18]. On the XRD pattern of GO in Figure 1 (blue pattern), it is observed that there is a strong peak at around  $2\theta = 10.5^\circ$  ( $d = 8.42$  Å), corresponding to GO (002) crystal face [22]. This peak is ascribed to the introduction of oxygen-containing functional groups on the graphite sheet surfaces. However, depending on its water content, GO was reported to have the interplanar spacing of 8.8 Å [23] which is much larger than that of pristine graphite. Furthermore, the broadening of the peak is due to the decrease of the crystal size into the nanoscale during the synthesis process [24]. It is interesting to notice that the diffraction pattern of the composite is similar to those of parents MOF and GO, however, they were observed at high  $2\theta$  values. This indicates that the well-defined MOF structure has been preserved with the reduction of d spacing to 7.61 Å on 222 crystal plane. In addition, the existence of GO in the composite is represented by a shoulder peak at  $2\theta = 10.9^\circ$  (corresponding to the 002 crystal plane) with a d-spacing of 8.12 Å. It was seen that the incorporation of GO component did not destroy the linkages between copper dimers and benzene tricarboxylic acid (BTC) bridges. Moreover, it should be noted here that the intensity of diffraction peaks for composites decreased with introduction of GO content. This observation is attributed to the oxygen functional groups from excessive GO flakes reacting with copper from MOF sites to form a uniform new structure [13–15].

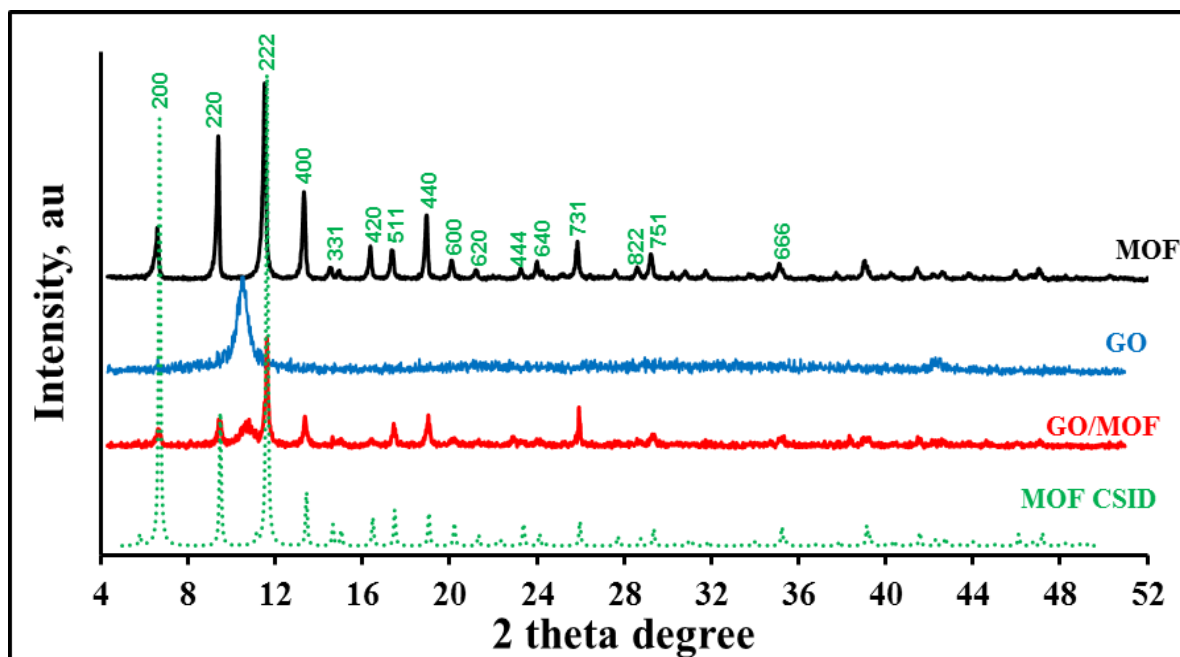


**Figure 4.1:** XRD patterns of MOF, GO, and GO/MOF with reference to MOF CSID.

Figure 4.2 shows FTIR spectra of MOF, GO and GO/MOF. The characteristic bands of MOF are well observed on the spectrum. Since MOF consisted of benzene-1,3,5-tricarboxylic acid ( $H_3BTC$ ), the bands of the spectrum are essentially derived from  $H_3BTC$ . The spectrum shows separate and different regions; the region below  $1300\text{ cm}^{-1}$ , shows various bands assigned to a bridging bidentate coordination of the carboxylate group in the organic linker ; and between  $1300\text{-}1700\text{ cm}^{-1}$  with the bands at  $1645$  and  $1590\text{ cm}^{-1}$  correspond to the asymmetric and at  $1450$  and  $1370\text{ cm}^{-1}$  for the symmetric stretching vibrations of the  $C=O$  groups in BTC [25,26]. The band centred at  $530\text{ cm}^{-1}$  is assigned to a vibrational mode directly involving the Cu centre and the organic ligand (Cu-O) [20]. The FTIR spectrum of GO is similar to the one reported in the literature [19]. Vibration of C–O appears at  $1060\text{ cm}^{-1}$  and the vibration of O–H bond in water and/or oxygen surface groups is observed at  $1450\text{ cm}^{-1}$  [26]. C=O vibration from carboxyl and/or carbonyl groups is detected at  $1735\text{ cm}^{-1}$  [15]. Two other bands observed at  $800$  and  $810\text{ cm}^{-1}$  to epoxy/peroxide groups and C=O asymmetric stretching vibration in sulfonic groups and/or vibration of C–O in epoxides, respectively [15]. The bands of both GO and MOF are clearly observed in the FTIR

spectrum of the composite GO/MOF and there is a new band appearing at  $617\text{ cm}^{-1}$ , which is attributed to the Cu-O stretching vibration [15], due to the oxygen of graphene oxide and copper metal centres on MOF. This confirms that the interaction between the two parent materials is electrostatic as observed in XRD analysis.

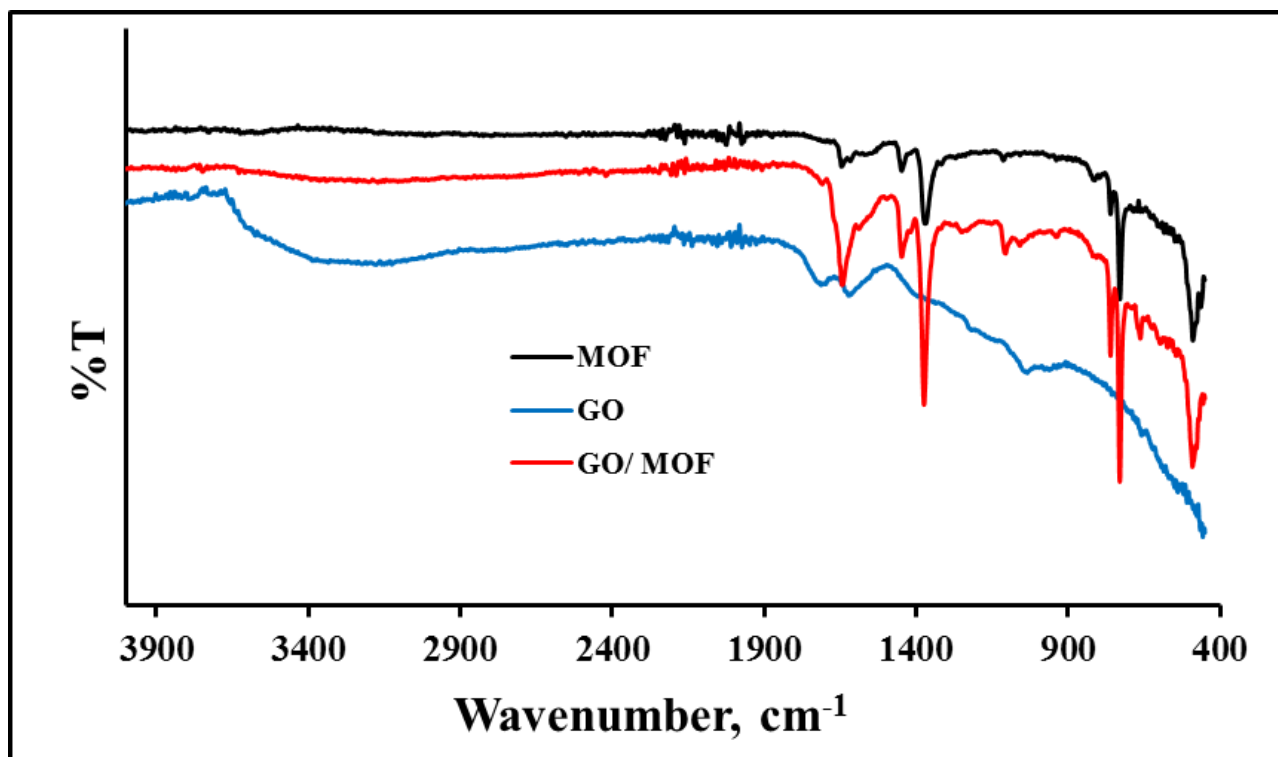


**Figure 4.2:** FTIR spectra of MOF, GO and GO/MOF

The thermal stability of the materials and their compounds is very important for composite confirmation, and might provide some structural information on molecule-based interaction and elemental composition. Hence, TGA and DSC curves of synthesised materials in this work were performed in the temperature range of  $25\text{--}500\text{ }^{\circ}\text{C}$  and presented in Figure 4.3 and 4.4, respectively. It can be seen in both TGA and DSC curves that MOF is relatively stable from the thermal perspective and that the melting point ( $370\text{ }^{\circ}\text{C}$ ) which is far above the phase transition temperature, and may be highly useful for potential practical applications [27]. As depicted in Figure 4.3, the TGA curve of MOF exhibits two clear weight loss steps. It can be seen that at around  $100\text{ }^{\circ}\text{C}$ , the weight loss may be assigned to the removal of ethanol and water

molecules per formula unit in the sample. The second step of weight loss happens between 350-370 °C, which is caused by the loss of trimesic acid per formula unit and remaining mass loss event is attributed to a CuO at temperatures between 370 °C. The TGA plot represented by blue line, indicates two degradation processes. The first degradation step is due to the loss of moisture and other solvents at low temperatures of less than 100 °C [15, 28]. The second step is the decomposition of GO, which takes place at 180 °C. This step displays that approximately 60 wt. % mass loss of GO is observed at this temperature, which is due to GO decarboxylation process [28]. As represented by red line in Figure 4.3, the composite GO/MOF shows enhancement in the thermal and moisture stability as compared to the GO and MOF, with the weight loss of about 19 wt%. It shows three degradation steps at 75, 225 and 350 °C, corresponding to ethanol/moisture, GO and BTC decomposition in MOF structure, respectively. Furthermore, DSC result correlates well to the TGA showing an exothermic peak (100–125 °C) for crystallisation transition due to the dehydration of MOF (Figure 4.4). One endothermic peak for glass transition in MOF was also observed at 375 °C. This may be due to the absorption of heat by the sample as it undergoes the endothermic phase transition from solid to liquid [28]. The DSC curve, shown in Figure 4.4 by blue line, shows an endothermic peak at around 180 °C. This peak is due to absorption of heat as GO decomposes [19]. The DSC of the composite reveals that both GO and MOF are present, showing two exothermic peaks corresponding temperatures to both GO and MOF decompositions.

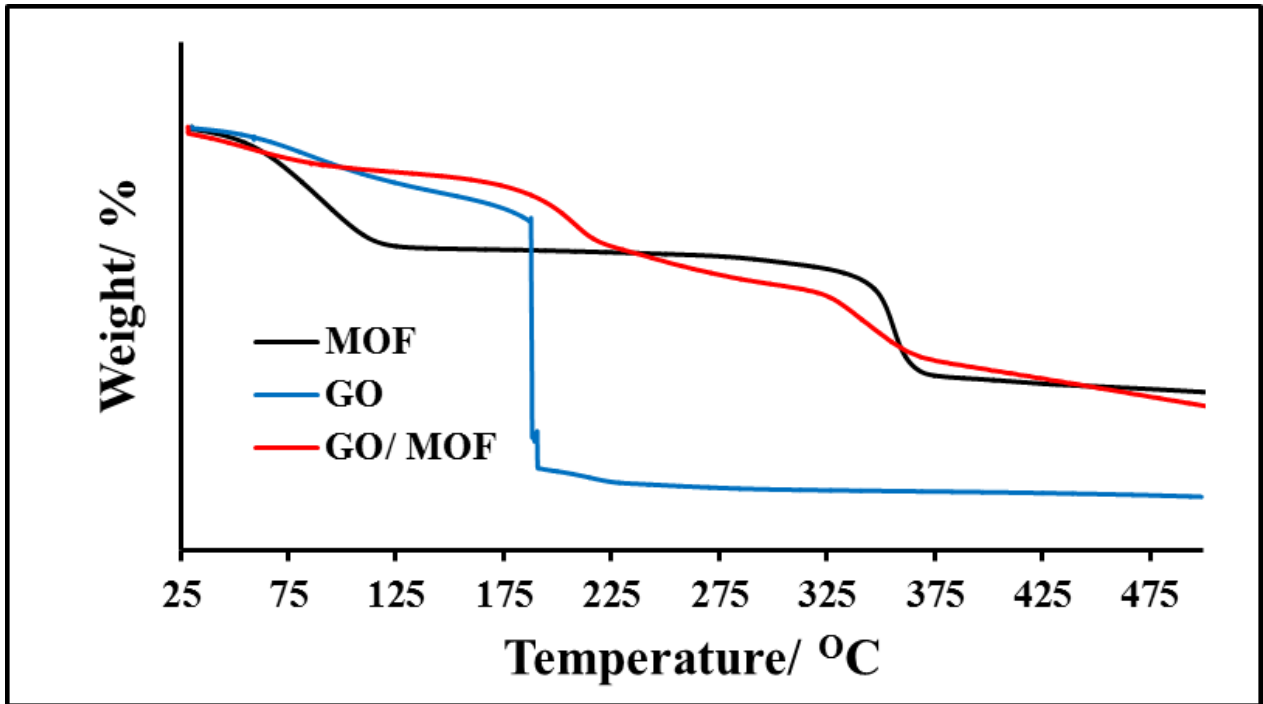


Figure 4.3: TGA analysis of MOF, GO and GO/MOF composite.

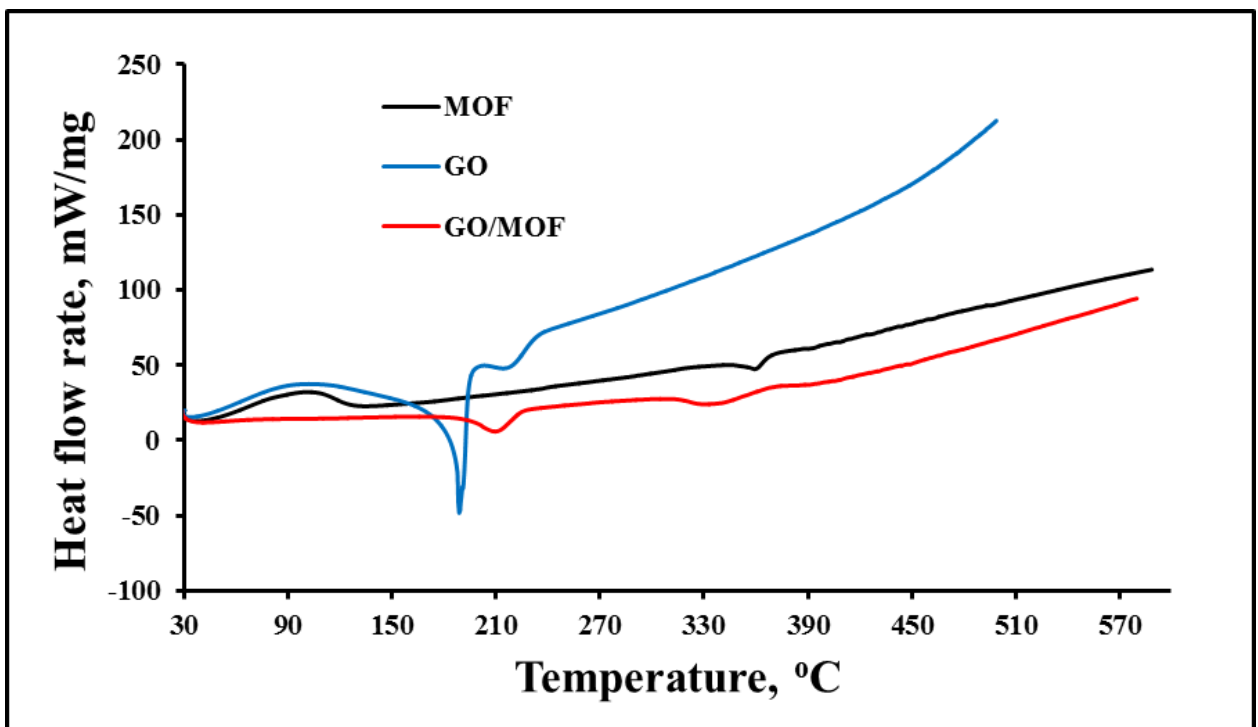
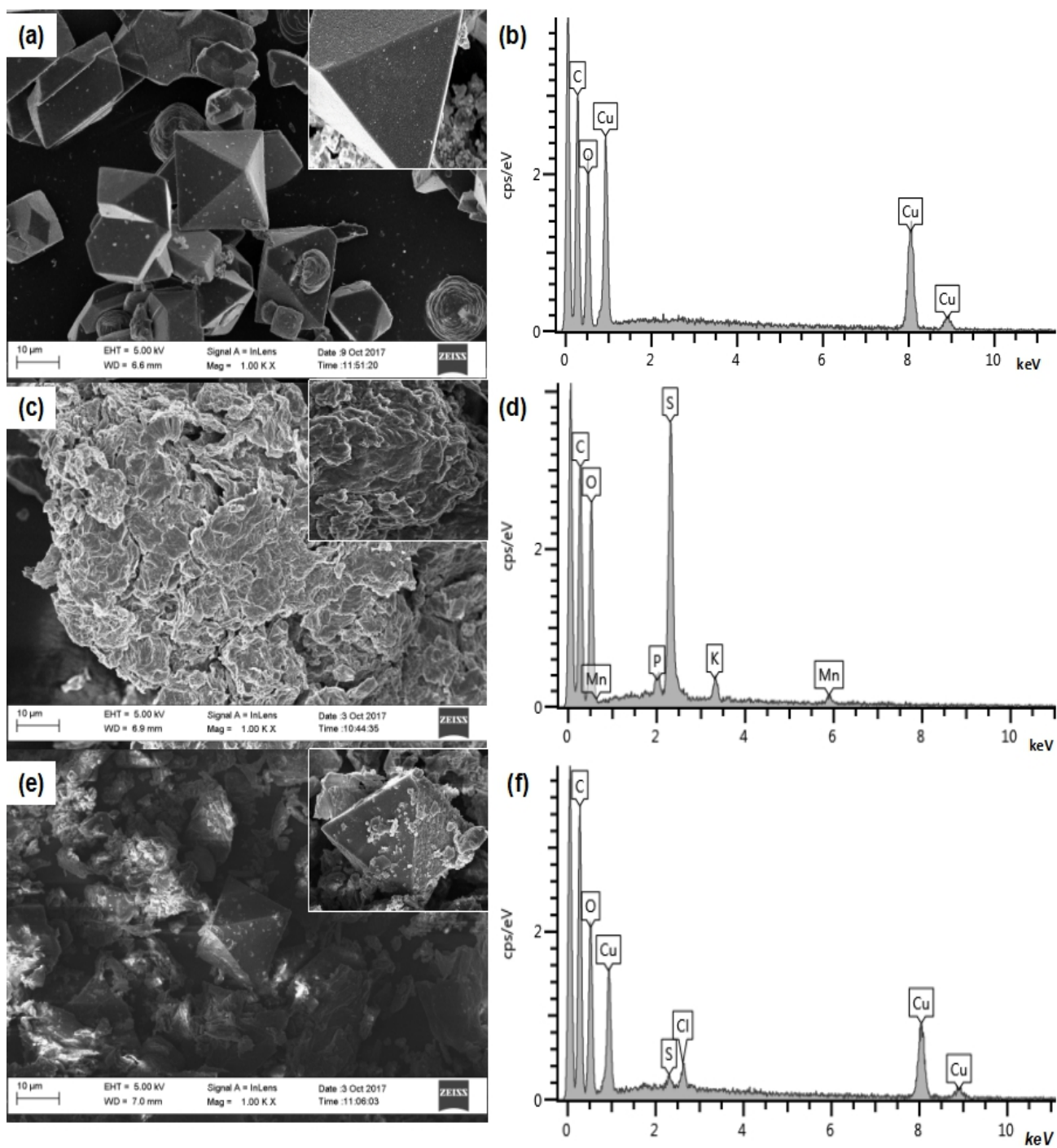


Figure 4.4: DSC analysis of MOF, GO and GO/MOF composite.

### 4.3.2. Morphological characterisation

The FE-SEM microphotographs (Figure 4.5) were used to investigate the morphologies and microstructures of MOF, GO and GO/MOF composite. As shown in Figure 4.5(a), MOF is a visible crystalline material. These MOF crystals are very clearly possessing an octahedral shape [25,29] and its corresponding EDS (Figure 4.5(b)) reveals the presences of C-, O- and Cu- atoms as the elemental composition in the MOF structure. In addition, the inset image of Figure 4.5(a) shows that MOF crystal has smooth surfaces and have an average size of 10-15  $\mu\text{m}$ . This observation confirmed that hydrothermal synthesis gives pure, highly crystalline MOF materials. The SEM image of GO in Figure 4.5(c) is seen as dense flakes of graphene sheets stacked together by dispersive forces [23]. The imaging of the composite is quite different from the parent materials as expected. Defects like fracture and corner breakage are obvious[30,31]. As seen in Figure 4.5(e) and inset image, the incorporation of GO impeded the growth of MOF crystallites, which resulted in the crystallites of the composites with small size, and coincides with the XRD results presented above. The formation of the composite is hypothesised to occur via the reaction between the copper sites of MOF and the oxygen-containing groups on GO, which has been deduced by Badosz group [31]. In addition, magnification of the octahedral crystals (inset images in Figure 4.5(e)) of GO/MOF composite showed that after introduction of GO, the surfaces of the crystals develops rough surfaces which can be due to interaction of MOF and GO through the oxygen of GO and Cu of MOF [31]. The EDS spectra (Figure 4.5(d) and (f)) show the elements present in the synthesised GO and GO/MOF materials. The GO structure consists of carbon and oxygen, and these elements are clearly observed in Figure 4.5(d). Since the elements in GO are also present in MOF, the composite GO/MOF shows an enhancement in the composition of carbon and oxygen (Figure 4.5(f)). The presence of small peaks of Mn, K, S, Cl and P are due to impurities trapped in the GO and MOF during synthesis process.



**Figure 4.5:** FE-SEM image of (a) MOF, (c) GO (e) GO/MOF composite (inset : magnification on the crystal structure to view the surface of the crystal) and EDS spectrum of (b) MOF, (d) GO, (f) GO/MOF composite.

TEM images are represented in Figure 4.6(a, c and e) for MOF, GO and GO/MOF show a clear difference among the samples' textures, respectively. The TEM image of MOF (Figure 4.6(a)) shows the well-defined octahedral shapes of this crystalline material. As seen in Figure 4.6(c), the image shows a well exfoliated graphene nanosheets and wrinkled transparent sheet-like structure. In the structure of GO/MOF composites (Figure 4.6(e)), the layers have been confirmed as the alternation between GO sheets and MOF blocks. It was seen that the functional oxygen groups from GO interact with the copper dimmers and chemical interactions are involved in the formation of composites [16]. It is interesting to observe that again in the composite, the particles preserved the shape of MOF crystals (image e) indicating the constrain effects of the GO layers resulting in preserving the shapes of the original MOF crystals in their carbonised phase [16]. The graphene phase seems to be mainly separated from the MOF phase and large aggregates can be easily distinguished. Besides this, some corrugated MOF sites are directly covered with thin graphene layers. It is known that electron beam illumination can cause the breaking down of MOF and can thus prevent any visualisation of its lattice structure [15]. Nevertheless, the pattern observed can be considered as representing the lattice image of MOF in the composite. It is likely that distorted graphene-based layers present in the composite helped the MOF to retain its crystalline structure by dissipating the electrostatic charges [15, 16]. As shown in Figure 4.6(b, d and f), the EDX spectra revealed all the elements present in GO, MOF and GO/MOF confirming the incorporation of GO onto MOF, respectively. It was observed that the presence of small peaks of K and S are due to impurities trapped in the GO and MOF during synthesis process as seen in EDS spectra above. Furthermore, Figure 4.7(a, c and e) show HRTEM images of MOF, GO and GO/MOF, respectively. It was seen in Figure 7(a) that the phase contrast of the intact crystal of MOF was barely visible, but its presence became apparent in the according SAED (Figure 4.7(b)). The measured spacings correspond to MOF in (222) orientation with d spacing of 0.857 nm (8.57 Å) and 1.00 nm (10.0 Å) in HRTEM and SAED images, respectively. In addition, the crystallinity of the MOF observed in these images show the clear diffraction spots is in agreement with XRD discussed above. The HRTEM image (Figure 4.7(c)) and its corresponding SAED

image (Figure 4.7(d)) of GO show amorphous characteristic of graphene sheet [33] with a d-spacing of 1.08 nm (10.8 Å). The GO/MOF images in Figure 4.7(e) and (f) for HRTEM and SAED show the spacing is 1.05 nm (10.5 Å) which are close to the d-spacing of (222) plane of MOF and (002) plane of GO. These results clearly suggest the formation of hybrid-structure.

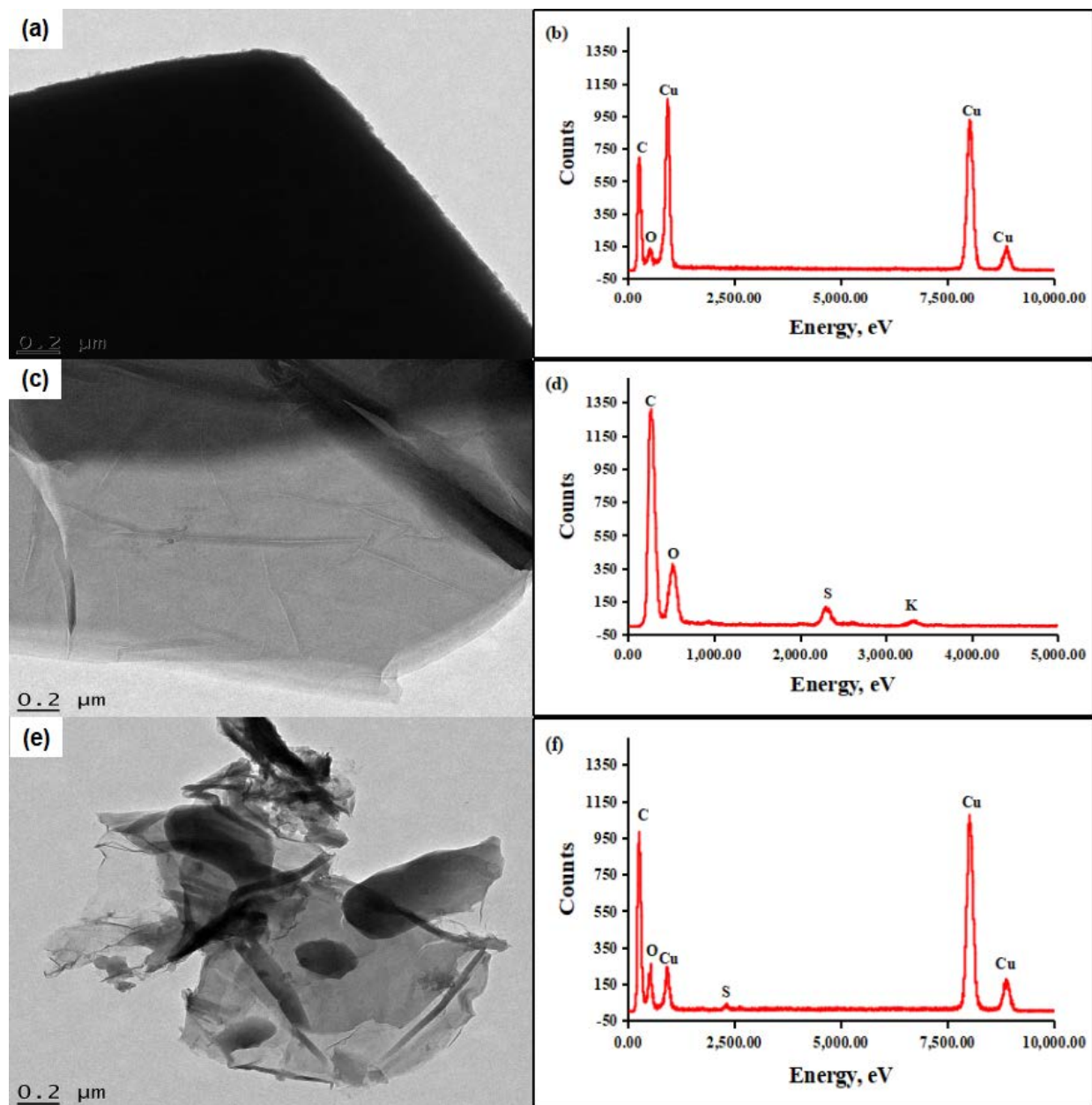


**Figure 4.6:** TEM image of (a) MOF, (c) GO and (e) GO/MOF; composite and EDX spectrum of (b) MOF, (d) GO and (f) GO/MOF composite.

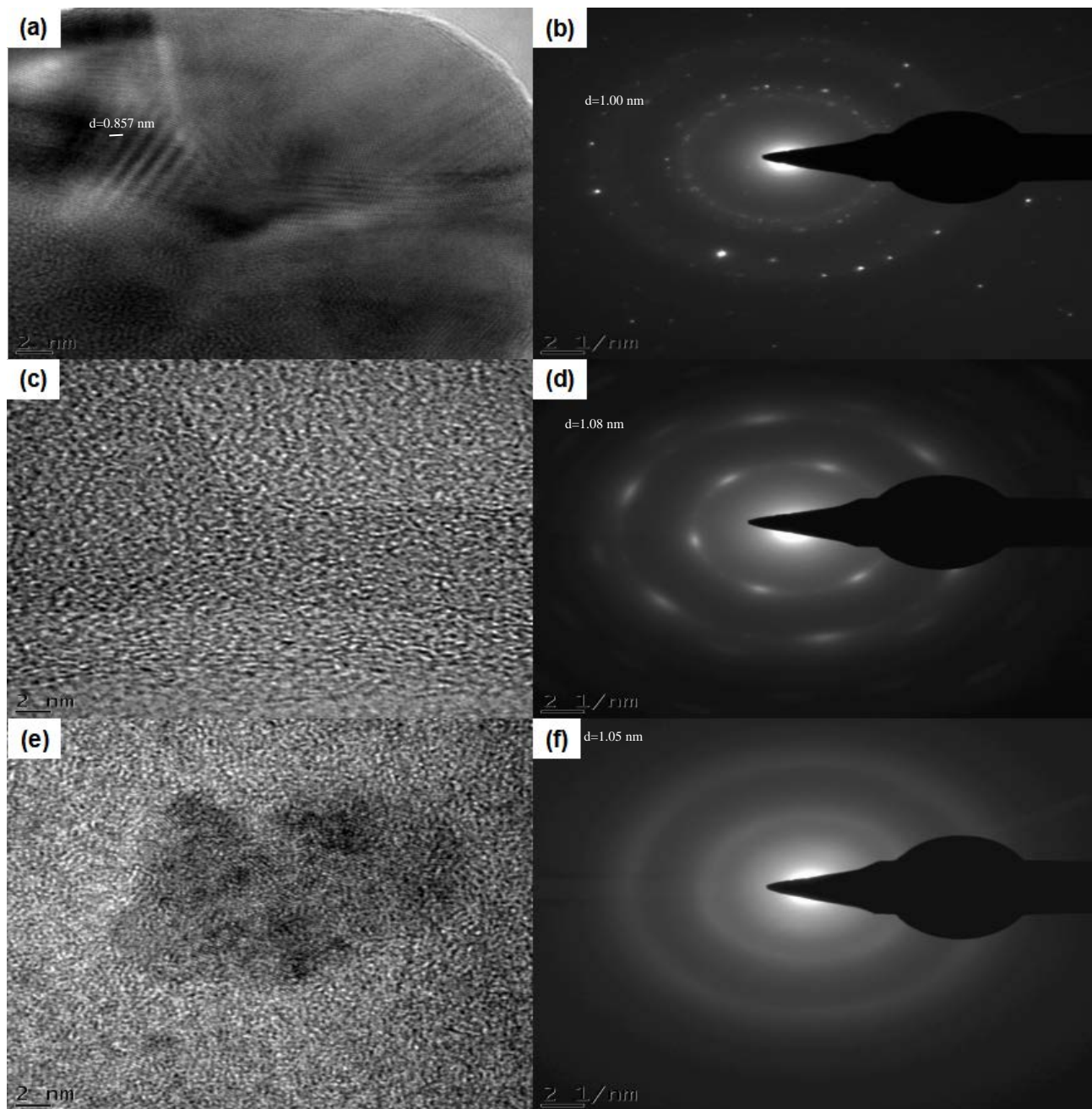


**Figure 4.7:** HRTEM images of (a) MOF, (c) GO and (e) GO/MOF composite; and SAED patterns of (b) MOF, (d) GO and (f) GO/MOF composite.

### 4.3.3. Electrochemical characterisation

Electrochemical behaviour of MOF, GO and GO/MOF composite was studied by cyclic voltammetry to understand the redox chemistry of the prepared composites. Figure 4.8(a) shows typical current-potential curves of the gold electrode in 0.1 mol.L<sup>-1</sup> TBAP/DMSO system of blank, MOF, GO and GO/MOF composite. It was noticeable that the Faradaic contributions (redox process) onto gold electrode was observed at around -0.50 V. This is a typical redox process of bare Au electrode [31,32]. However, there are three reduction processes observed in the presence of MOF electrocatalyst. The active sites on the material experiences a conversion from Cu to Cu<sup>3+</sup> and then back to Cu, respectively [32]. In the scan, the process and their inverse processes can be expressed as shown in the figure between 0 and 1 V with three anodic peaks corresponding to the conversion of Cu to +1 valency, +1 to +2 and conversion of +2 to +3 valency, respectively [33]. On the other hand, it was reported that the electrochemical reduction at cathodic region of Cu<sup>2+</sup> in solution proceeds in two successive-one electron reversible waves through a Cu<sup>+</sup> intermediate, in which the stability of the intermediate was due to the presence of ions in the solution [34]. The shift in potential was also reported by Loera-Serna et al. [28] in LiCl solution indicating that the electrochemical processes of Cu during the direct sweep took place in the MOF. However, in this study, the reduction of Cu<sup>2+</sup> to Cu<sup>+</sup> occurs to possess more negative potential, which might be due to electrochemical properties of Au electrode in TBAP/DMSO system [14]. It was seen that GO in the potential window of TBAP/DMSO electrolyte system showed a quasi-reversible processes. As clearly seen in the CV of GO/MOF on the gold electrode, still allow the diffusion of the redox mediator (Cu<sup>2+</sup>/Cu<sup>+</sup>) through their layers to the electrode surface. One of the important features observed in the CV of the composite was the enhancement of anodic peak towards potential of 0.2 V for conversion of Cu to Cu<sup>+</sup> [33].

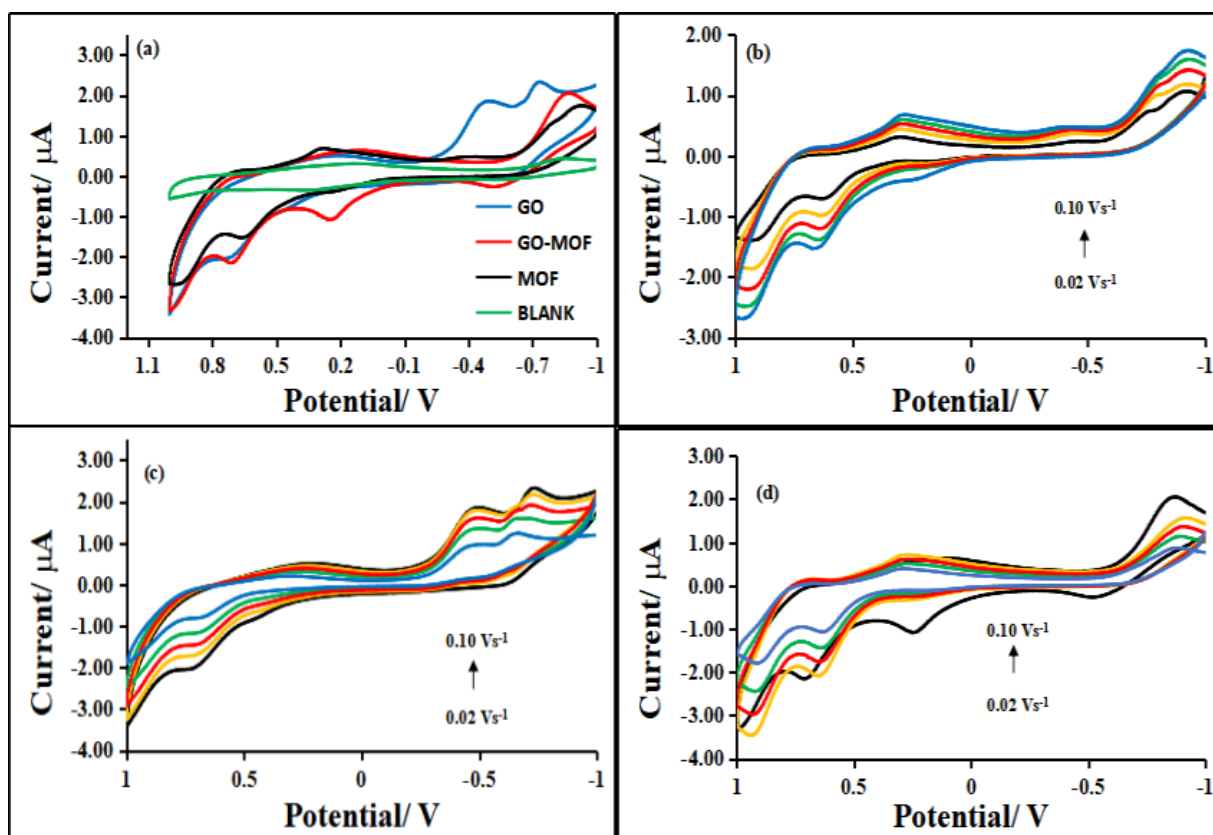


**Figure 4.8:** (a) CV curves of Blank, MOF, GO and GO/MOF composite at  $0.1 \text{ v.s}^{-1}$  in  $0.1 \text{ M TBAP/DMSO}$  electrolyte solution on Au electrode. (b-d) MOF, GO and GO/MOF at different scan rates ( $0.02\text{-}0.1 \text{ v.s}^{-1}$ ) in  $0.1 \text{ mol.L}^{-1}$  TBAP/DMSO, respectively.

The influence of scan rate on the electrochemical response of MOF, GO and GO/MOF composite was accomplished in  $0.1 \text{ mol.L}^{-1}$  TBAP/DMSO system using Au working electrode. The multiscan voltammograms of MOF, GO and GO/MOF are shown in parts b-d of Figure 4.8, respectively. As shown in Figure 4.8(b), the peak currents corresponding to three copper processes slow increase with the scan rate, whereas, the peak currents corresponding to the reverse processes increase with increase in scan rate and reach constant values. In addition, the Cu (III) formed and are used as catalysts to HER process [32,35]. It was observed that both anodic ( $I_{pa}$ ) and cathodic peak ( $I_{pc}$ ) currents increased linearly with scan rates from  $0.1$  to  $1 \text{ V.s}^{-1}$ . All redox couples showed electrochemical quasi-reversible process with respect to change in peak potential ( $\Delta E_p$ ) and the ratio of anodic and cathodic peak current ( $I_{pa}/I_{pc}$ ) values.

Unity of  $I_{pa}/I_{pc}$  ratios at all scan rates and the logarithm of the absolute value of the reductive peak current against the logarithm of the scan rate with slope of 0.5 indicates diffusion controlled characters [36,37] of the redox processes as shown in Figure 4.9(a). Furthermore, the diffusion coefficient,  $D$ , was determined for catalysts using cyclic voltammetry and following the Randles-Sevcik equation for a quasi-reversible system (Equation 4.1) [36,37].

$$I_p = (2.65 \times 10^5) n^{3/2} A C D^{1/2} (\nu)^{1/2} \quad (4.1)$$

where,  $n$  is the number of electrons transferred,  $A$  is the electrode area in  $\text{cm}^2$ ,  $D$  is the diffusion coefficient in  $\text{cm}^2 \text{s}^{-1}$ ,  $C$  is the bulk molar concentration of the electroactive species in  $\text{mol} \cdot \text{cm}^{-3}$  and  $\nu$  is scan rate in  $\text{V} \cdot \text{s}^{-1}$ . Consistent with Equation 4.1, Figure 4.9(b), showed that the current increased linearly with increasing the square root of the scan rate,  $\nu^{1/2}$ . The  $D$  values were found to be  $1.39 \times 10^{-7}$ ,  $4.15 \times 10^{-7}$  and  $3.32 \times 10^{-7} \text{ cm}^2 \cdot \text{s}^{-1}$  for MOF, GO and GO/MOF respectively. The introduction of GO on MOF surface enhanced the diffusion coefficient of the composite compared to parent MOF. Similar trend was observed in MOF based polymer composite [29, 38]. In other cases, instead of the material undergoing only diffusional process, it can also adsorb on the surface of the electrode. This observation can be obtained by directly relating the peak current with the surface coverage ( $\Gamma$ ) and the potential scan rate as given in Equation 4.2.

$$I_p = \frac{n^2 F^2 \Gamma A \nu}{4RT} \quad (4.2)$$

Figure 4.9(c) shows a linear relationship between current and scan rate (Equation 4.2). From the slope in the figure, the surface coverages for MOF, GO and GO/MOF were found to be  $1.32 \times 10^{-10}$ ,  $2.23 \times 10^{-10}$  and  $2.05 \times 10^{-10} \text{ mol} \cdot \text{cm}^{-2}$ , respectively confirming the adsorption of the material on the gold electrode.

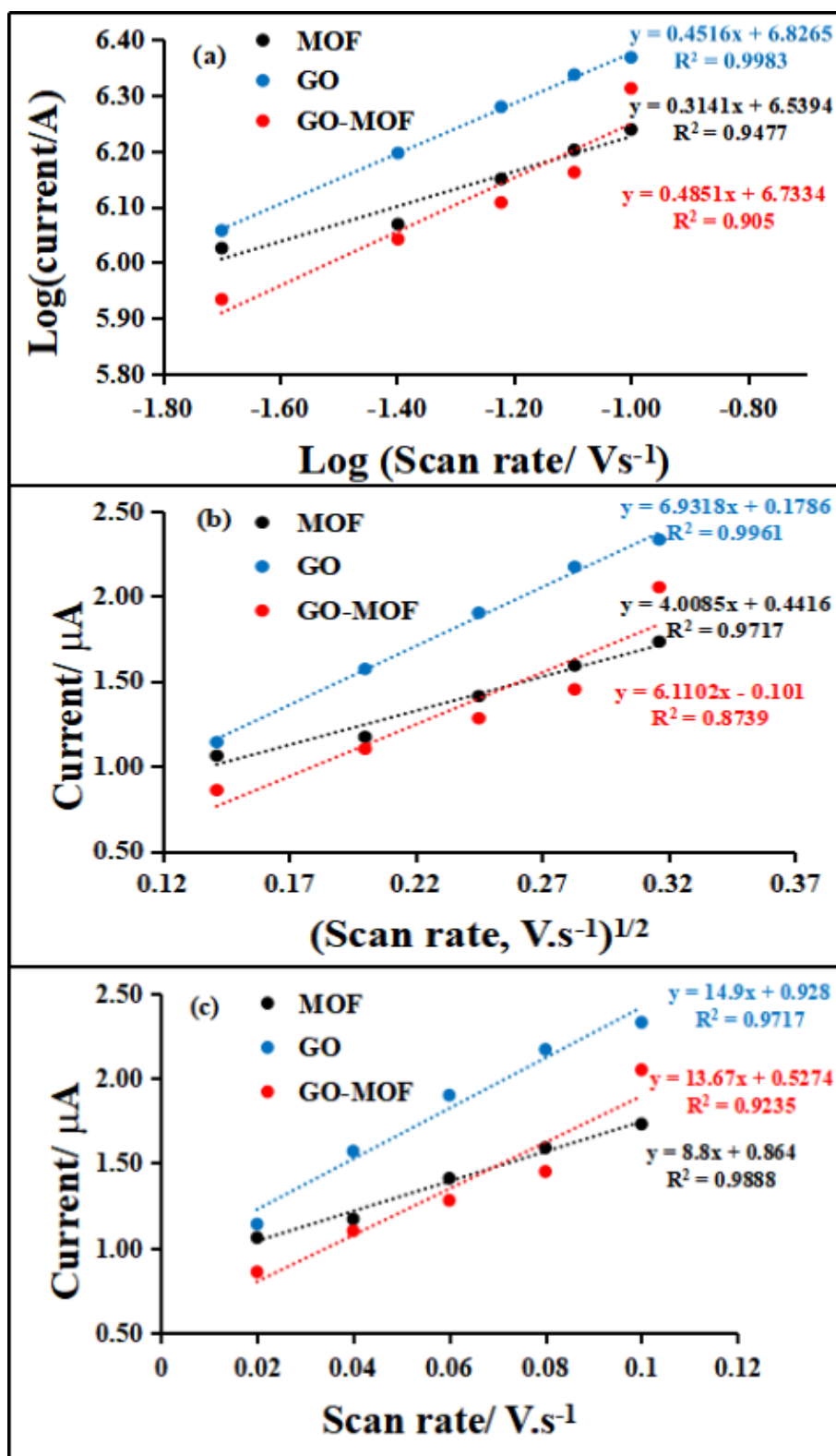


**Figure 4.9:** (a) The log-log plot of the absolute value of the peak current vs scan rate, (b) peak current as a function of square root of scan rate and (c) peak current as a

function of scan rate for MOF, GO and GO/MOF on gold in 0.1 M DMSO/TBAP electrode system at different scan rates (0.02 – 0.10 V.s<sup>-1</sup>).

#### **4.3.4. Hydrogen studies**

The HER studies of the samples was evaluated using CV in 0.1 mol.L<sup>-1</sup> TBAP/DMSO system as an electrolytic solution and H<sub>2</sub>SO<sub>4</sub> as hydrogen source and the results are presented in Figure 4.10(a-d). Upon addition of H<sub>2</sub>SO<sub>4</sub>, a wave catalytic near the reduction potential was observed, which suggested that MOF, GO and GO/MOF composite are reducing H<sub>2</sub>SO<sub>4</sub> to H<sub>2</sub> [29]. The current intensities of the samples can be related to the amount of H<sub>2</sub> produced [25,29]. Therefore, the greater the current readings will result to a large quantity of H<sub>2</sub> production. This observation confirmed that our samples possessed best electrocatalytic activity for HER [38]. Furthermore, there was an intense increase in the current intensity of GO/MOF composite at -0.7 V compared to both MOF and GO. This result indicated that the GO/MOF composite was more effective in producing maximum H<sub>2</sub> in comparison to MOF and GO. The different scan rate dependent studies were used to examine the electrochemical properties of the samples during electrocatalytic hydrogen evolution and the results showed that there is an increase in the cathodic peak current with increasing the scan rate.

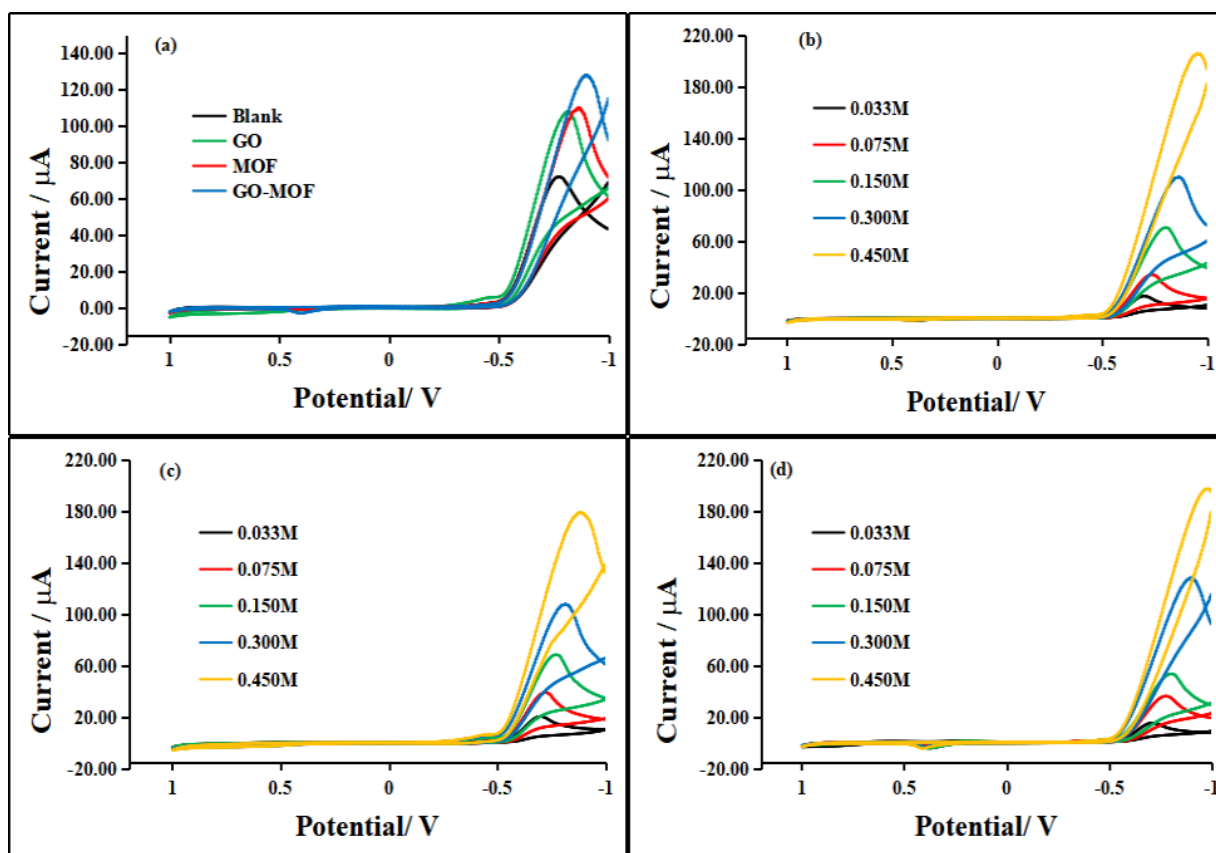
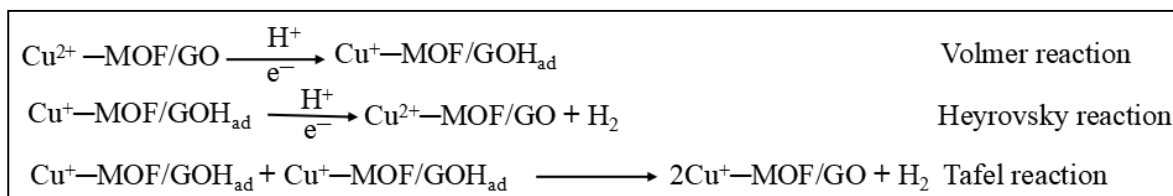


**Figure 4.10:** (a) CV curves of Blank, GO, MOF and GO/MOF composite in the presence of  $0.300 \text{ mol.L}^{-1} \text{ H}_2\text{SO}_4$  at  $0.10 \text{ V.s}^{-1}$  and CV curves of (b) MOF (c) GO and (d) GO/MOF composite in different concentration of hydrogen source ( $0.033\text{-}0.450 \text{ mol.L}^{-1} \text{ H}_2\text{SO}_4$ ) at  $0.10 \text{ V.s}^{-1}$  on Au electrode in  $0.1 \text{ mol.L}^{-1} \text{ TBAP/DMSO}$  electrode system.

The Tafel analysis is used to get a better grasp on the kinetics and activity of electrochemical reactions for HER [39]. The Tafel slope value gives important information on the rate determining step in an electrochemical reaction. It is an inherent property of the electrode material. Furthermore, the overall electrocatalytic HER in this work can also be proposed by means of mechanism. In an acid medium, the HER pathway could proceed via three main steps (Scheme 4.2): Initial reduction of Cu(II) to Cu(I) of the MOF/GO, followed by interaction of the proton with the corresponding composite and leading in to formation of the composite hydride ( $\text{MOF/GOH}_{\text{ad}}$ ) in hydrogen storage process as the most probable intermediate and

proposed to be Volmer mechanism [14,25]. After the hydride, the hydride intermediate easily undergoes a protonation or interacts with one another to form H<sub>2</sub> molecule through a Heyrovsky or Tafel reaction [14, 25, 29, 38].



**Scheme 4.2:** Proposed mechanisms involved in the HER kinetics of the composite

The Tafel plot was constructed from current density-potential data at various concentrations ranging from 0.033 to 0.450 mol.L<sup>-1</sup> H<sub>2</sub>SO<sub>4</sub>. Elucidating the mechanism of heterogeneous hydrogen evolution usually takes the form of Tafel analysis, where the steady state or quasi-steady state current, *i*, at a catalyst of a given composition is measured over a range of overpotential,  $\eta$ . Then log(*i*) can be plotted against  $\eta$  to give a linear relationship, known as a Tafel line. The intercept of the Tafel line with the current axis gives the exchange current density, *i*<sub>0</sub>, which is related to both the inherent reaction exchange rate at dynamic equilibrium and the electrochemically active surface area of the catalyst. The slope of the Tafel line is independent of surface area and takes on a limited number of values that correspond to the dominant mechanism [37]. Ramohlola *et al.* [29,38], reported that the *b* could also serve as an indicator of either Volmer, Heyrovsky and Tafel in a multi-step proton transfer process and *i*<sub>0</sub> the measure of performance of an electrocatalyst. In this study, the values of *b* and *i*<sub>0</sub> were estimated by linear polarisation curves [29,38] and the results are presented in Table 1. In addition, another important parameter that can give insight of reaction mechanism is the cathodic transfer coefficient (1- $\alpha$ ) which was calculated using high overpotential region, where Butler-Volmer equation simplifies to the Tafel equation (Equation 4.3), from the Tafel slope *b* given by the relationship:

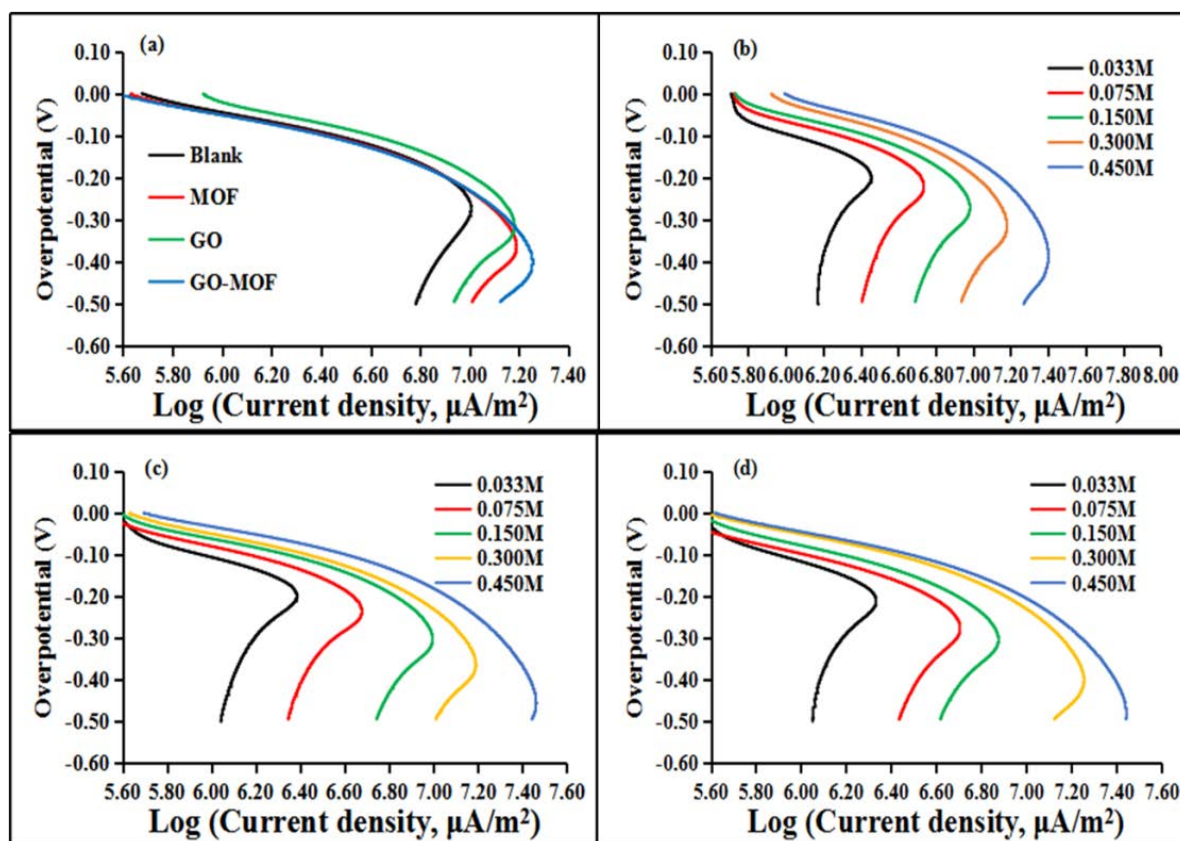
$$b = \frac{-2.303RT}{(1-\alpha)F} \quad (4.3)$$

Figure 4.11 and Table 4.1 show Tafel plots and parameters, for blank electrode, GO, MOF and GO/MOF composite. The present study exhibits that the GO gives Tafel slope of 144 mV.dec<sup>-1</sup> at 0.300 mol.L<sup>-1</sup> H<sub>2</sub>SO<sub>4</sub>. At the same acid conditions, MOF and GO/MOF composite showed lower Tafel slope values as compared to the bare GO. It was reported that Tafel slopes in the ranges of 105-150 mV.dec<sup>-1</sup> may be explained on the basis of a Volmer rate determining step for HER [40]. Nonetheless, the presence of the GO on the surface of MOF results in an increase in the Tafel slope value to 125 mV.dec<sup>-1</sup>. These results are in good consent with the work reported by Kubisztal *et al.* [41] when studying the HER behaviour of nickel-based composite coatings containing molybdenum powder. Furthermore, the charge-transfer coefficient ( $\alpha = 0.5$ ), describes a mechanism where the rate determining step is the Volmer reaction or the Volmer reaction coupled with one of the other two reactions [43]. As given in Table 4.1, the charge transfer coefficients for MOF and GO/MOF composite are close to 0.5. Thus, the rate determining step of HER on the studied MOF and the composite maybe the Volmer reaction or Volmer reaction coupled with one of the other two reactions [40,41]. Furthermore, the turnover frequency (TOF) is widely used in the molecular catalysis field to assess the efficiency of catalysts, which can also be employed for electrocatalytic reactions. The TOF is the mass of molecules reacting for a certain reaction per unit time, which can be calculated using Equation 4.4 [42]:

$$\text{TOF} = \frac{jM}{2Fm} \quad (4.4)$$

where  $j$  is the current density at a given potential,  $M$  is mass percentage of materials,  $F$  is Faraday's constant, and  $m$  is the mass of per square centimetre of MOF, GO and GO/MOF catalysts estimated from BET surface area of MOF (614.7 m<sup>2</sup>/g [25]) and GO (423 m<sup>2</sup>/g [43]). The TOF values for MOF, GO and GO/MOF are presented in the Table 4.1. It was seen the composite resulted with the enhancement of the TOF values, for example, the value was obtained to be 6.6 mol H<sub>2</sub>.s<sup>-1</sup> as compared to 4.75 mol H<sub>2</sub>.s<sup>-1</sup> of GO at 0.45 mol.L<sup>-1</sup>. In addition to the Tafel slope, the reaction order of

the HER with respect to the concentration of hydrogen ions is also a characteristic kinetic parameter that can provide additional information about the underlying mechanism. Figure 4.12(a) and (b) present the pH dependence of the current density and potential, respectively, for the experimental data obtained in the present study. The slope of the trendline in Figure 4.11(a) ( $\log(i)$  vs. pH), represents the apparent reaction order of HER which was found to be around 0.8, suggesting a mixed type mechanism [44] as observed in Tafel parameters. Furthermore, in Figure 4.12(b) which is a representation of the Pourbaix diagram and the slope was seen to be less than 0.5. The observed dependence agrees well with the proposed mechanism of the process above.



**Figure 4.11:** Tafel plots of (a) blank, GO, MOF and GO/MOF composite ( $\sim 2.0 \times 10^{-4}$  mol.L<sup>-1</sup>) in the presence 0.300 mol.L<sup>-1</sup> H<sub>2</sub>SO<sub>4</sub> at 0.10 V.s<sup>-1</sup> (b) MOF (c) GO and (d)

GO/MOF composite in different concentrations of H<sub>2</sub>SO<sub>4</sub> and 0.10 V.s<sup>-1</sup> scan rate on Au electrode in 0.1 mol.L<sup>-1</sup> TBAP/DMSO electrode system.

**Table 4. 1:** Experimental values of Tafel slope (*b*), charge transfer coefficient (1- $\alpha$ ), exchange current density (*i*<sub>0</sub>) and TOF of MOF, GO and GO/MOF composite.

Material	H <sub>2</sub> SO <sub>4</sub> (mol.L <sup>-1</sup> )	Slope ( <i>b</i> ) (V.dec <sup>-1</sup> )	- <i>b</i> (mV.dec <sup>-1</sup> )	1- $\alpha$	log <i>i</i> <sub>0</sub> ( $\mu$ A.m <sup>-2</sup> )	<i>i</i> <sub>0</sub> (A.m <sup>-2</sup> )	TOF (mol H <sub>2</sub> .s <sup>-1</sup> )
MOF	0.033	-0.1385	138	0.43	6.38	2.40	0.763
	0.075	-0.2119	212	0.28	6.65	4.47	1.421
	0.150	-0.1318	132	0.45	6.98	9.55	3.038
	0.300	-0.1058	106	0.56	7.17	14.79	4.705
	0.450	-0.1257	126	0.47	7.35	22.39	7.121
GO	0.033	-0.1391	139	0.43	6.45	2.82	0.584
	0.075	-0.1759	176	0.34	6.73	5.37	1.113
	0.150	-0.1382	138	0.43	6.98	9.55	1.979
	0.300	-0.1438	144	0.41	7.15	14.13	2.928
	0.450	-0.1887	189	0.31	7.36	22.91	4.748
GO/MOF	0.033	-0.1571	157	0.38	6.32	2.09	0.550
	0.075	-0.1529	153	0.39	6.69	4.90	1.288
	0.150	-0.1420	142	0.42	6.87	7.41	1.950
	0.300	-0.1251	125	0.47	7.24	17.38	4.571
	0.450	-0.1163	116	0.51	7.40	25.12	6.607
Pd@CuPc /MOF [31]	0.300	-0.1770	177	0.33	7.00	8.9	0.845

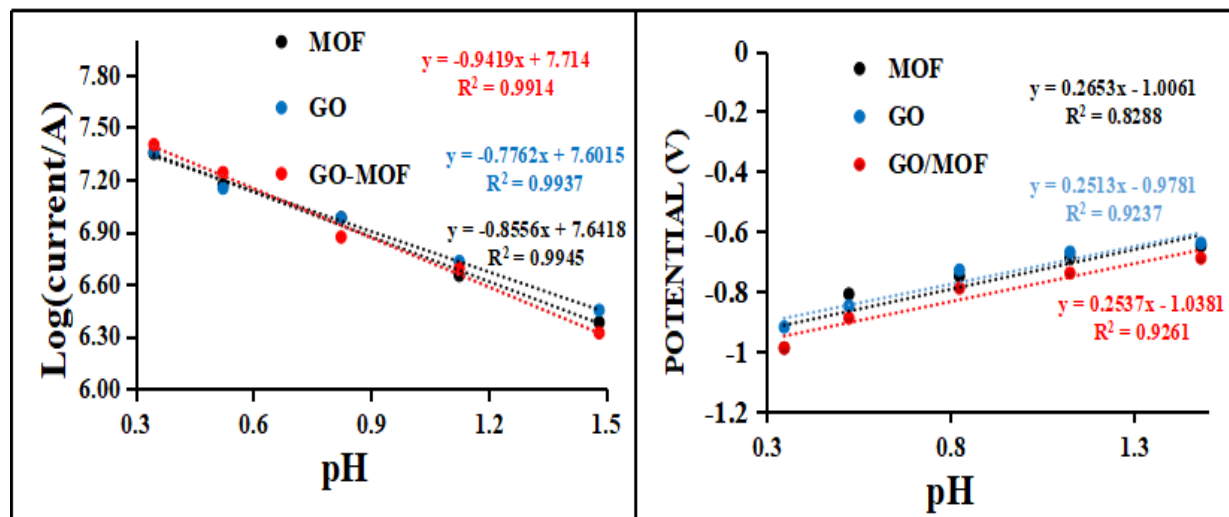


**Figure 4.12:** (a) Plot of log current as a function of pH of the solution and (b) Pourbaix diagram of hydrogen evolution reaction.

#### 4.4. CONCLUSIONS

In this work, highly active GO/MOF composite for hydrogen production and storage via HER process were prepared by impregnation method of MOF and GO. The influences of GO on the morphology and crystalline structure of MOF surface, as well as resulting electro-catalytic activity in hydrogen evolution were systematically investigated. The presence of GO on the MOF surface can significantly increase the HER exchange current density, and reduce the electrochemical reaction resistance. The electrocatalytic activity of the GO/MOF composite is higher than that of the neat MOF. The observed promotional roles of incorporated GO is ascribed to possible synergetic effects between GO crystals and the MOF matrix, leading to a facilitation of HER as part of hydrogen production with enhanced TOF values. Furthermore, the Tafel slope and charge-transfer coefficients showed that the rate determining step of HER on the studied MOF and GO/MOF composite maybe the Volmer reaction or the Volmer reaction coupled with one of other two reactions supported by slopes from the plot of log current vs pH and Pourbaix diagram. The results demonstrated that microstructured MOF based composite may be used as alternative electrocatalyst for hydrogen fuel cell applications.

#### 4.5. REFERENCES

- [1] S. Satyapal, J. Petrovic, C. Read, G. Thomas, and G. Ordaz, "The U.S. Department of Energy's National Hydrogen Storage Project: Progress towards meeting hydrogen-powered vehicle requirements," *Catal. Today*, vol. 120, pp. 246–256, 2007.
- [2] K. Zeng and D. Zhang, "Recent progress in alkaline water electrolysis for hydrogen production and applications," *Prog. Energy Combust. Sci.*, vol. 36, , pp.307–326, 2010.
- [3] J. Yang, F. Cheng, J. Liang, and J. Chen, "Hydrogen generation by hydrolysis of ammonia borane with a nanoporous cobalt-tungsten-boron-phosphorus catalyst supported on Ni foam," *Int. J. Hydrogen Energy*, vol. 36, pp. 1411–1417, 2011.
- [4] J. B. Raoof, R. Ojani, S. A. Esfeden, and S. R. Nadimi, "Fabrication of bimetallic Cu/Pt nanoparticles modified glassy carbon electrode and its catalytic activity toward hydrogen evolution reaction," *Int. J. Hydrogen Energy*, vol. 35, pp. 3937–3944, 2010.
- [5] A. Ghaffarinejad, N. Sadeghi, H. Kazemi, A. Khajehzadeh, M. Amiri, and A. Noori, "Effect of metal hexacyanoferrate films on hydrogen evolution reaction," *J. Electroanal. Chem.*, vol. 685, pp. 103–108, 2012.
- [6] D. Y. Wang, M. Gong, H.L. Chou, C.J. Pan, H.A. Chen, Y. Wu, M.C. Lin, M. Guan, J. Yang, C.W. Chen, Y.L. Wang, B.J. Hwang, C.C. Chen, and H. Dai, "Highly active and stable hybrid catalyst of cobalt-doped FeS<sub>2</sub> nanosheets-carbon nanotubes for hydrogen evolution reaction," *J. Am. Chem. Soc.*, vol. 137, pp.1587–1592, 2015.
- [7] J. Lin, J. He, F. Qi, B. Zheng, X. Wang, B. Yu, K. Zhou, W. Zhang, Y. Li, and Y. Chen, "Electrochimica Acta In-situ Selenization of Co-based Metal-Organic Frameworks as a Highly Efficient Electrocatalyst for Hydrogen Evolution Reaction," *Electrochim. Acta .*, vol. 247, pp. 258–264, 2017.
- [8] Y. Li and R. T. Yang, "Significantly Enhanced Hydrogen Storage in Metal - Organic Frameworks via Spillover," *J. Am. Chem. Soc.*, vol. 128, pp. 726–727,

- 2006.
- [9] L. Wang and R. T. Yang, "New sorbents for hydrogen storage by hydrogen spillover: A review," *Energy Environ. Sci.*, vol. 1, pp. 268–279, 2008.
- [10] R. Lin, L. Shen, Z. Ren, W. Wu, Y. Tan, H. Fu, J. Zhang, and L. Wu, "Enhanced photocatalytic hydrogen production activity via dual modification of MOF and reduced graphene oxide on CdS," *Chem. Commun.*, vol. 50, p. 8533, 2014.
- [11] J. Chen, G. Xia, P. Jiang, Y. Yang, R. Li, R. Shi, J. Su, and Q. Chen, "Active and Durable Hydrogen Evolution Reaction Catalyst Derived from Pd-Doped Metal-Organic Frameworks," *ACS Appl. Mater. Interfaces*, vol. 8, pp. 13378–13383, 2016.
- [12] C. Petit, B. Levasseur, B. Mendoza, and T. J. Bandosz, "Reactive adsorption of acidic gases on MOF/graphite oxide composites," *Microporous Mesoporous Mater.*, vol. 154, pp. 107–112, 2012.
- [13] V. Gargiulo, L. Lisi, R. Di, and M. Alf, "Synthesis and characterization of conductive copper-based metal-organic framework / graphene-like composites," *Mater. Chem. Phys.*, vol. 147, pp. 744–750, 2014.
- [14] K. E. Ramohlola, M. Masikini, S. B. Mdluli, G. R. Monama, M. J. Hato, K. M. Molapo, E. I. Iwuoha, and K. D. Modibane, "Electrocatalytic Hydrogen Production Properties of Poly(3- aminobenzoic acid) doped with Metal Organic Frameworks," *Int. J. Electrochem. Sci.*, vol. 12, pp. 4392–4405, 2017.
- [15] C. Petit, J. Burrell, and T. J. Bandosz, "The synthesis and characterization of copper-based metal-organic framework/graphite oxide composites," *Carbon N. Y.*, vol. 49, pp. 563–572, 2011.
- [16] C. Petit and T. J. Bandosz, "Engineering the surface of a new class of adsorbents: metal-organic framework/graphite oxide composites," *J. Colloid Interface Sci.*, vol. 447, pp. 139–51, 2015.
- [17] J. Song, X. Wang, and C.-T. Chang, "Preparation and Characterization of Graphene Oxide," *J. Nanomater.*, vol. 2014, pp. 1–6, 2014.
- [18] F. Ke, L. G. Qiu, Y. P. Yuan, F. M. Peng, X. Jiang, A. J. Xie, Y. H. Shen, and J. F. Zhu, "Thiol-functionalization of metal-organic framework by a facile coordination-based postsynthetic strategy and enhanced removal of Hg<sup>2+</sup> from

- water,” *J. Hazard. Mater.*, vol. 196, pp. 36–43, 2011.
- [19] J. Shen, Y. Hu, M. Shi, X. Lu, C. Qin, C. Li, and M. Ye , “Fast and Facile Preparation of Graphene Oxide and Reduced Graphene Oxide Nanoplatelets,” *Chem. Mater.* ,vol. 21, pp. 3514–3520, 2009.
- [20] S. Peng, X. Fan, S. Li, and J. Zhang, “Green synthesis and characterization of graphite oxide by orthogonal experiment,” *J. Chil. Chem. Soc.*, vol. 58, pp. 2213–2217, 2013.
- [21] J. Gascon, S. Aguado, and F. Kapteijn, “Manufacture of dense coatings of Cu<sub>3</sub>(BTC)<sub>2</sub> (HKUST-1) on  $\alpha$ -alumina,” *Microporous Mesoporous Mater.*, vol. 113, pp. 132–138, 2008.
- [22] J. Liu, H. Jeong, J. Liu, K. Lee, J.Y. Park, Y. H. Ahn, and S. Lee , “Reduction of functionalized graphite oxides by trioctylphosphine in non-polar organic solvents,” *Carbon N. Y.*, vol. 48, pp. 2282–2289, 2010.
- [23] F. Mindivan, “The synthesis and characterization of graphene oxide (GO) and reduced graphene oxide (rGO), ” *Machines , Technologies , Materials.*, vol. 6, pp. 32-35, 2017.
- [24] C. Petit, M. Seredych, and T. J. Bandoz, “Revisiting the chemistry of graphite oxides and its effect on ammonia adsorption,” *J. Mater. Chem.*, vol. 19, p. 9176, 2009.
- [25] G. R. Monama, S. B. Mdluli, G. Mashao, M. D. Makhafola, K. E. Ramohlola, K. M. Molapo, M. J. Hato, K. Makgopa, E. I. Iwuoha, and K. D. Modibane, “Palladium deposition on copper(II) phthalocyanine/metal organic framework composite and electrocatalytic activity of the modified electrode towards the hydrogen evolution reaction,” *Renew. Energy*, vol. 119, pp. 62–72, 2018.
- [26] Z. Hasan and S. H. Jhung, “Removal of hazardous organics from water using metal-organic frameworks (MOFs): Plausible mechanisms for selective adsorptions,” *J. Hazard. Mater.*, vol. 283, pp. 329–339, 2015.
- [27] X. Sun, G. Gao, D. Yan, and C. Feng., “Synthesis and electrochemical properties of Fe<sub>3</sub>O<sub>4</sub>@MOF core-shell microspheres as an anode for lithium ion battery application.” *Appl. Surf. Sci.*, vol. 405, pp. 52-59, 2017.
- [28] S. Loera-serna, M. A. Oliver-Telentino, M. L. Lopez-Nunez, A. Santana-Cruz, A.

- Guzman-Vargas, R. Cabrera-Sierra, H. I. Beltran, and J. Flores, "Electrochemical behavior of [ Cu<sub>3</sub>(BTC)<sub>2</sub> ] metal – organic framework : The effect of the method of synthesis," *J. Alloys Compd.*, vol. 540, pp. 113–120, 2012.
- [29] K. E. Ramohlola, M. Masikini, S. B. Mdluli, G. R. Monama, M. J. Hato, K. M. Molapo, E. I. Iwuoha, and K. D. Modibane , "Electrocatalytic Hydrogen Evolution Reaction of Metal Organic Frameworks decorated with poly (3-aminobenzoic acid)," *Electrochim. Acta*, vol. 246, pp. 1174–1182, 2017.
- [30] Y. Zhao, Y. Cao, and Q. Zhong, "CO<sub>2</sub> Capture on Metal-Organic Framework and Graphene Oxide Composite Using a High-Pressure Static Adsorption Apparatus," *J. of Clean Energy Technol.*, vol. 2, pp. 0–3, 2014.
- [31] L. Li, X. L. Liu, H. Y. Geng, B. Hu, G. W. Song, and Z. S. Xu, "A MOF / graphite oxide hybrid ( MOF : HKUST-1 ) material for the adsorption of methylene blue from aqueous," *J. Mater. Chem. A.*, vol 1, pp. 10292–10299, 2013.
- [32] P. Druska, "A surface analytical examination of passive layers on cu / ni alloys : part i . alkaline solution," *Corros. Sci.*, vol. 38, pp. 10292–10299, 1996.
- [33] L. Zhang *et al.*, "A CuNi/C Nanosheet Array Based on a Metal–Organic Framework Derivate as a Supersensitive Non-Enzymatic Glucose Sensor," *Nano-Micro Lett.*, vol. 28, pp. 1-10, 2018.
- [34] C. Nila and I. Gonzilez, "Thermodynamics of Cu-H , SO , -Cl-H , 0 and Cu-NH & I-H<sub>2</sub>O based on predominance-existence diagrams and Pourbaix-type diagrams," *Hydrometallurg.*, vol. 42, pp. 63–82, 1995.
- [35] M. Jafarian, F. Forouzandeh, I. Danaee, and F. Gobal, "Electrocatalytic oxidation of glucose on Ni and NiCu alloy modified glassy carbon electrode," *J. Solid State Electrochem.*, vol. 13, pp. 1171–1179, 2009.
- [36] D. N. Li, A. J. Wang, J. Wei, Q. L. Zhang, and J. J. Feng, "Facile synthesis of flower-like Au@AuPd nanocrystals with highly electrocatalytic activity for formic acid oxidation and hydrogen evolution reactions," *Int. J. Hydrogen Energy*, vol. 42, pp. 19894–19902, 2017.
- [37] B. E. Conway, "Electrochemical proton transfer and cathodic hydrogen evolution," *Sci. Rev.*, vol. 71, pp. 479–509, 2017.

- [38] K. E. Ramohlola, G. R. Monama, M. J. Hato, K. D. Modibane, K. M. Molapo, M. Masikini, S. B. Mdluli, and E. I. Iwuoha, "Polyaniline-metal organic framework nanocomposite as an efficient electrocatalyst for hydrogen evolution reaction," *Compos. Part B Eng.*, vol. 137, pp. 129–139, 2018.
- [39] C. F. Leung, Y. Z. Chen, H. Q. Yu, S. M. Yiu, C. C. Ko, and T. C. Lau, "Electro- and photocatalytic hydrogen generation in acetonitrile and aqueous solutions by a cobalt macrocyclic Schiff-base complex," *Int. J. Hydrogen Energy*, vol. 36, pp. 11640–11645, 2011.
- [40] M. R. Gao, J. X. Liang, Y. R. Zheng, Y. F. Xu, J. Jiang, Q. Gao, J. Li, and S. H. Yu, "An efficient molybdenum disulfide/cobalt diselenide hybrid catalyst for electrochemical hydrogen generation," *Nat. Commun.*, vol. 6, pp. 1–7, 2015.
- [41] J. Kubisztal, A. Budniok, and A. Lasia, "Study of the hydrogen evolution reaction on nickel-based composite coatings containing molybdenum powder," *Int. J. Hydrogen Energy*, vol. 32, pp. 1211–1218, 2007.
- [42] W. Shen, B. Wu, F. Liao, B. Jiang, and M. Shao, "Optimizing the hydrogen evolution reaction by shrinking Pt amount in Pt-Ag/SiNW nanocomposites," *Int. J. Hydrogen Energy*, vol. 42, pp. 15024–15030, 2017.
- [43] Y. Gao, D. Ma, C. Wang, J. Guan, and X. Bao, "Reduced graphene oxide as catalyst for hydrogenation of nitrobenzene," *Structure*, vol. 47, pp. 2432–2434, 2011.
- [44] L. Giordano, B. Han, M. Risch, W. T. Hong, R. R. Rao, K. A. Stoerzinger, y. Shao-Horn, "pH dependence of OER activity of oxides: Current and future perspectives," *Catal. Today*, vol. 262, pp. 2-10, 2016.

## CHAPTER FIVE

### PALLADIUM SUPPORTED GRAPHENE OXIDE BASED METAL ORGANIC FRAMEWORK NANOCOMPOSITE WITH IMPROVED ELECTROCATALYTIC EFFICIENCY FOR HYDROGEN EVOLUTION REACTION

---

*This chapter is pending submission for publication in a peer review journal:*

#### CHAPTER SUMMARY

Limited reserve in earth and high cost of Pt based materials restrict their wide application in industry, which is a major challenge for commercialisation of the hydrogen fuel cell devices. In this study, a composite of palladium supported graphene oxide (GO) based metal organic framework (MOF) was synthesised using electrodeposition of Pd on GO followed by impregnation method. The prepared materials were characterised with various analytical techniques and their applications as HER electrocatalysts were evaluated using cyclic voltammetry (CV), Tafel plots and turn over frequencies (TOFs). The XRD analyses showed the incorporation between MOF and Pd@GO, wherein the pattern of the composite contains the characteristic peaks of the two parent materials, showing that the incorporation did not dismantle the framework and structure of the MOF and Pd@GO respectively. This is in agreement with FTIR, whereby the functional groups of MOF and GO were observed in the nanocomposite. TGA/DCS curves revealed the improvement of thermal and moisture stability of the nanocomposite with respect to parent MOF, The scanning electron microscopy/Energy dispersive spectroscopy (SEM/EDS) and high resolution transmission electron microscopy/Energy dispersive x-ray spectroscopy/selected area electron diffraction (HRTEM/EDX/SAED) confirmed the presence of octahedral structure of MOF in the Pd@GO sheet-like structure, elemental composition and crystallinity of the synthesised materials. The performance of the proposed electrolytic system for electrochemical HER by Tafel parameters and turn over frequencies

(TOFs). The HER results showed a drastic increase in catalytic H<sub>2</sub> production in the composite through the Volmer reaction coupled with one of the mechanisms. This disclosed that the addition of Pd@GO/MOF in the electrolytic system possessed better catalytic characteristics with enhanced current density which may open a new way for hydrogen production and storage via HER and spillover mechanisms.

**Keywords:** Electrocatalysts, Hydrogen evolution reaction, Metal organic framework, Palladium, Graphene oxide

## 5.1. INTRODUCTION

The extreme dependence of fossil fuels are escalating the global environmental pollution and the energy crisis [1]. Currently, there is an increasing courtesy on the development of sustainable and clean energy sources [2–4]. Hydrogen from water splitting electrolysis, is universally recognised as a candidate for future energy technology [5–7]. This is due to advantages such as recyclability, free pollution and high energy efficiency as compared to gasoline based fuels[5,7] . However, electrochemical water splitting hydrogen generation mainly depends on the cathode material used hydrogen evolution reaction (HER) occurs at the cathode half reaction of the electrolytic cell [6,8,9]. Although Pt and Pt-based materials have shown to be the efficient electrocatalysts for HER, high cost and low earth-abundance restrict their widespread applications [10]. Thus, replacement of this expensive and precious metal with cost-effective and earth-abundant materials is a matter of utmost urgency [11]. Non-noble catalysts such as transition metal dichalcogenides have attracted research interest as alternatives to Pt-based electrocatalysts due to their excellent electrical conductivity and outstanding durability [12–14] However , their limited active sites limit their HER performance [6,15]. Metal-organic frameworks (MOFs) with large surface, low density and controllable 3D structure, which can provide abundant controllable nanoscaled cavities and offer congenital channels for small molecules and ions [16,17], have been identified as promising catalysts for HER. A few reports showed the use of these materials as electro/photocatalyst in water splitting[14,18,19].

Nevertheless, MOFs showed low electrochemical hydrogen production due to poor conductivity caused by its organic linker [14]. Therefore, there is a need to improve the physical and electrochemical properties of MOFs. Recently, Ramohlola *et al.* [20–22] presented polymer based metal organic framework composites with a drastic increase in catalytic H<sub>2</sub> evolution and higher Tafel slope in H<sub>2</sub>SO<sub>4</sub> due increase in electron density of the polymer by introduction of MOF. Herein, we modified the MOF surface with a carbon based material, graphene oxide (GO). GO has attracted much attention in the field of gas adsorption owing to its dense array of atoms and rich functional oxygen groups that enhance the dispersive forces and increase the porosity of materials by incorporating into composites [23,24]. For example, Petit and Badosz [25,26] have reported the formation of GO/MOF composites via interactions between oxygen groups of GO and metallic centers of MOF, where the synergetic effect between MOF units and GO layers was responsible for enhanced adsorption amounts compared to the parent material [26,27]. In relation to this, Monama *et al.* [28] introduced a porphyrin (phthalocyanine) on MOF using impregnation method, followed by Pd electrodeposition and the resultant composite showed an improved HER catalytic efficiency. In this work, we present the dispersion of the palladium onto the GO surface and then later incorporate with MOF, as to increase the dissociation ability of the metal and the quantity of hydrogen to be adsorbed in hydrogen evolution reaction. Palladium, as compared to platinum, is of very low cost and has high affinity to hydrogen [29]. Structure and morphology of the composite were characterised by various analytical techniques, and its electrochemical hydrogen production and storage performance was compared with blank electrode and MOF and investigated through HER studies.

## 5.2. EXPERIMENTAL

### 5.2.1. Materials

Copper nitrate trihydrate (Cu(NO<sub>3</sub>)<sub>2</sub>·3H<sub>2</sub>O), trimesic acid (H<sub>3</sub>BTC), graphite powder, tetrabutylammonium percholate (TBAP) and Sodium nitrate (NaNO<sub>3</sub>) were purchased from Sigma Aldrich, South Africa., dimethylformamide (DMF), palladium chloride

(PdCl<sub>2</sub>), ammonium solution (NH<sub>4</sub>OH), ammonium chloride (NH<sub>4</sub>Cl), dimethylsulfoxide (DMSO), phosphoric acid (H<sub>3</sub>PO<sub>4</sub>) and sulphuric acid (H<sub>2</sub>SO<sub>4</sub>) were purchased from Rochelle chemicals. Potassium permanganate (KMnO<sub>4</sub>) and hydrochloric acid (HCl) were purchased from SAARCHEM. Hydrogen peroxide (H<sub>2</sub>O<sub>2</sub>) from Moncon. H<sub>2</sub>SO<sub>4</sub> standard solutions were made in DMSO solution with 0.1 mol.L<sup>-1</sup> TBAP as a supporting electrolyte system unless otherwise stated. Electrochemical measurements were carried out at 22±2 °C.

### 5.2.2. Synthesis of MOF and Pd@GO/MOF composite

MOF was synthesised by the following hydrothermal procedure [30]. Briefly, 4.5 mmol (1.087 g) of Cu(NO<sub>3</sub>)<sub>2</sub>.3H<sub>2</sub>O was dissolved in 10 mL of distilled water and then mixed with 2.5 mmol (0.525 g) of H<sub>3</sub>BTC dissolved in 10 mL of ethanol. The mixture was stirred for 30 minutes and then transferred to a 23 mL Teflon stainless-steel autoclave and sealed to react for 36 hours at 120 °C in thermostatic drying oven. After cooling to room temperature, the product was filtered, washed with ethanol repeatedly, and then dried at 50 °C for overnight.

Pd@GO/MOF composite was synthesised through impregnation method of directly mixing of Pd@GO (see supporting information for preparation of Pd@GO) and MOF). Approximately, 0.1 g of as-synthesised MOF sample was dehydrated at 150 °C for 1 hour. It was then suspended in 10 mL DMF. In a separate beaker, 0.1 g of Pd-supported graphene oxide (50 wt.% of Pd@GO loading in the composite) was dispersed in 1.4 mL DMF, and then the two mixtures were mixed together and stirred magnetically for 24 hours at 50 °C. The resulting product was recovered by filtration and washed with ethanol and then dried overnight at 50 °C.

### 5.2.3. Materials characterisation

The FTIR spectra were recorded on Spectrum II spectrometer (PerkinElmer) in the wavenumber range between 400 and 4500 cm<sup>-1</sup> at room temperature and X-ray diffraction (XRD Phillips PW 1830, CuKα radiation, λ = 1.5406 Å). The thermal stability

was studied by a thermogravimetric analyser (STA Perkin-Elmer 4000). Samples ranging between 1 to 4 mg were heated from 30-500 °C at a heating rate of 20 °C.min<sup>-1</sup> under N<sub>2</sub> environment. Morphological characterisations were performed using Auriga Field Emission Scanning Electron Microscope (FESEM) coupled with EDS detector for elemental analysis. The internal morphology was carried out using a FEI Tecnai G2 20 transmission electron microscope (TEM) coupled with EDX and SAED, operated at an accelerating voltage of 200 kV and 100 mm camera length. Electrochemical measurements were performed using EPSILON electrochemical workstation. The data were collected using gold (3 mm diameter, 0.071 cm<sup>2</sup> area), Pt and Ag/AgCl electrode as working electrode, counter electrode and reference electrode, respectively. Repetitive scanning of the solutions of MOF, Pd@MOF, Pd@GO, and Pd@GO/MOF composite ( $\sim 2.0 \times 10^{-4}$  mol.L<sup>-1</sup>) was from -1 to 1 V at scan rate of 0.02 - 0.10 V.s<sup>-1</sup>. Electrochemical experiments were performed in 25 mL of 0.1 mol.L<sup>-1</sup> TBAP/DMSO electrolytic system. HER studies were done using different concentrations of 0.03 - 0.45 mol.L<sup>-1</sup> H<sub>2</sub>SO<sub>4</sub> as H<sub>2</sub> source in 0.1 mol.L<sup>-1</sup> TBAP/DMSO system and  $\sim 2.0 \times 10^{-4}$  mol.L<sup>-1</sup> of MOF, Pd@MOF and Pd@GO/MOF composites as electrocatalysts.

## 5.3. RESULTS AND DISCUSSION

### 5.3.1. Structural Characterisation

Figure 5.1 shows X-ray diffraction (XRD) patterns of MOF CSID, MOF, Pd@GO and Pd@GO/MOF composite. The XRD pattern of MOF (Figure 5.1) is characterised by an intense peak at  $2\theta=12^\circ$ , which is indexed as the (222) lattice plane with interplanar d spacing of 7.68 Å (estimated using Bragg's equation:  $n\lambda=2d\sin\theta$ , where  $n$ =positive integer,  $\lambda$ =wavelength,  $d$ = interplanar spacing and  $\theta$ =scattering angle), typical for HKUST-1 type of MOF and is in agreement MOF crystal structure information data (CSID) [30]. It was seen in Figure S1(a) that the pattern of Pd@MOF shows the appearance of peaks as a result of Pd interaction with the MOF, and the intensities of the weak peaks are related to Pd doping [31]. Furthermore, palladium coated materials

showed two reflection indexes of (111) and (200) at  $2\theta$  values of 39 and 45°, respectively, and this is an indication of cubic phase of Pd [31]. On the other hand, there was reduction and shift of peak intensity of MOF phases with introduction of Pd and the hkl (222) lattice plane with interplanar d spacing of 7.64 Å. The XRD pattern of GO (Figure S1(a)) is observed to have one broad peak at  $2\theta=10.5^\circ$  ( $d = 6.70 \text{ \AA}$ ), corresponding to GO (002) crystal face [32] and is due to the presence of oxygen-containing groups [32]. However, it is observed that after introduction of palladium, there is a shift of this mentioned peak to the right of the pattern, indicating the change in environment of the oxygen containing groups as palladium is incorporated on GO (Figure 5.1). Characteristic peaks of palladium in Pd@GO are observed at  $2\theta$  of 38 and 45° similar to the one observed on Pd@MOF (Figure S1(a)) [31]. The final composite Pd@GO/MOF consists of phases from both GO and MOF but with decreased and shifted intensities. The hkl indexes (002) and (222), of GO and MOF phases were calculated to have the interplanar d spacing of 8.73 and 7.64 Å, respectively. The palladium peaks in the composite are observed at very low intensities, indicating the presence of palladium in the composite.

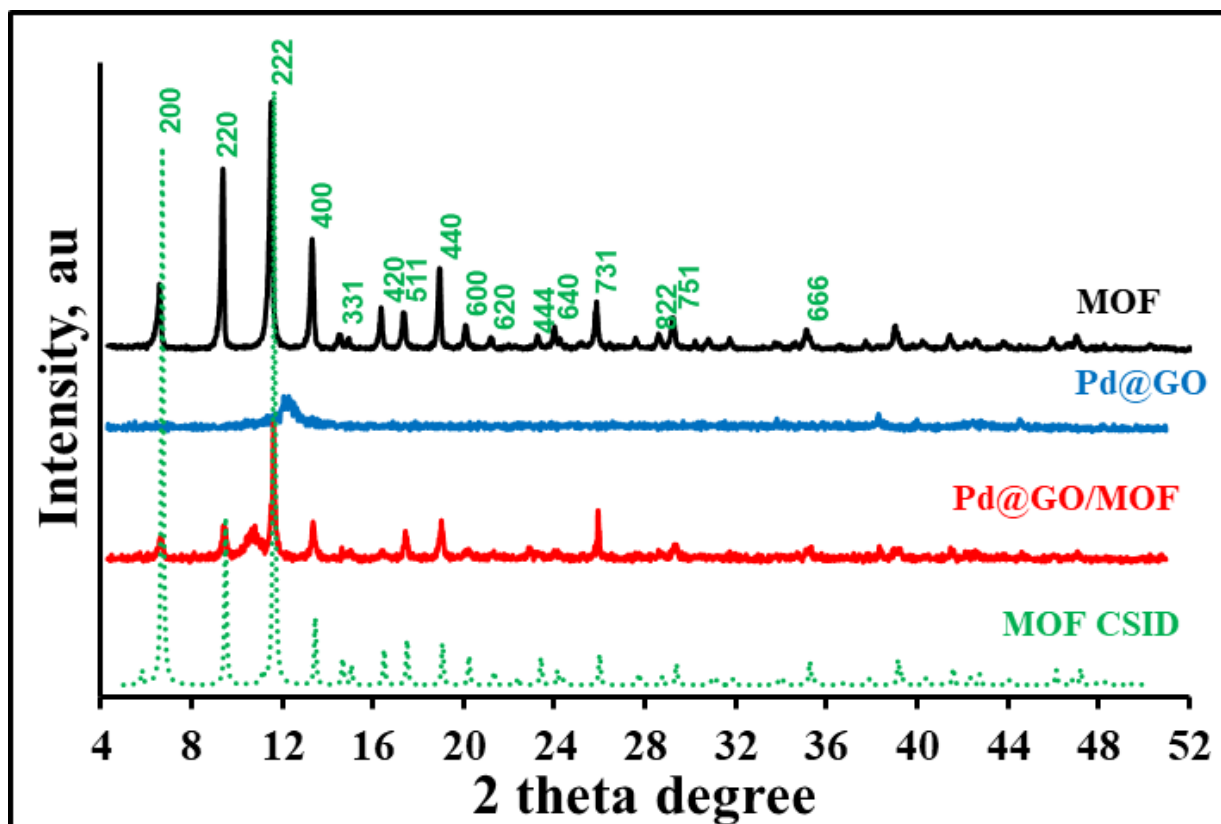


**Figure 5.1:** XRD patterns of MOF, Pd@GO and Pd@GO/MOF with reference to MOF CSID.

The FTIR spectra of MOF, Pd@GO and Pd@GO/MOF are described in Figure 5.2 below. The lattice vibrations of as-prepared MOF are in agreement with literature [33]. In the spectrum, the region below  $1300\text{ cm}^{-1}$ , shows various bands assigned to a bridging bidentate coordination of the carboxylate group in the organic linker; and between  $1300\text{-}1700\text{ cm}^{-1}$  with the bands at  $1645$  and  $1590\text{ cm}^{-1}$  correspond to the asymmetric and at  $1450$  and  $1370\text{ cm}^{-1}$  for the symmetric stretching vibrations of the C=O groups in BTC [28,33]. Lastly in the spectrum of MOF, the band centred at  $530\text{ cm}^{-1}$  is assigned to a vibrational mode directly involving the Cu centre and the organic ligand (Cu-O) [20]. The spectrum of GO (Figure S1(b)) was reported elsewhere [34] and possessed vibration of C–O at around  $1060\text{ cm}^{-1}$  and the vibration of O–H bond in water and/or oxygen surface groups at  $1450\text{ cm}^{-1}$  and C=O vibration from carboxyl and/or carbonyl groups is detected at  $1735\text{ cm}^{-1}$ . Notably, the introduction of palladium

on to both parent materials (GO and MOF) reveals different interactions. The presence of Pd in Pd@GO is seen by the reduction in band intensities as compared to GO spectrum (Figure S1(b)). Whereas in Pd@MOF, there is an appearance of a new band at wavenumber of  $1200\text{ cm}^{-1}$ . Since this band is not observed in the parent MOF, it implies that the incorporation of palladium is on the surface of MOF through an electrostatic interaction between Pd and oxygen group in the carboxylate ligands. The spectrum of Pd@GO/MOF shows the presence of MOF and Pd@GO functional group as indicative of the Pd supported composite formation.

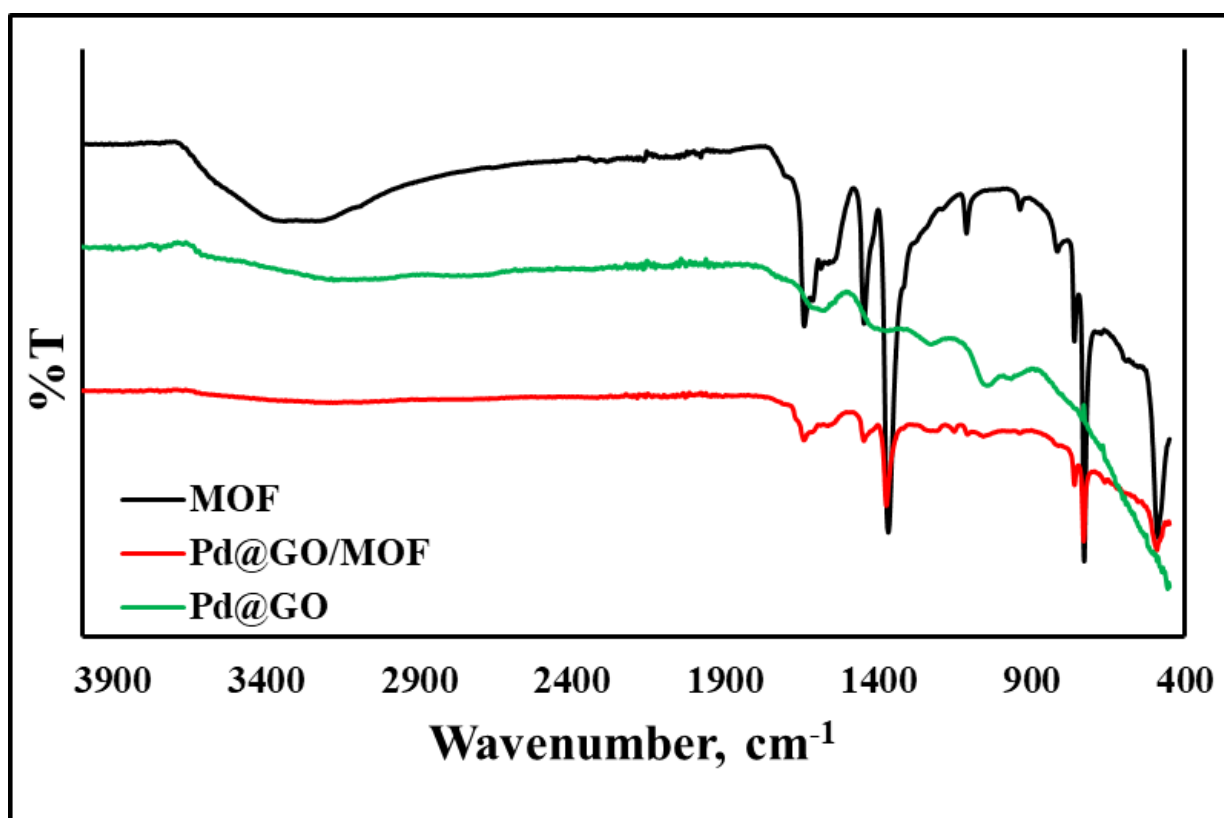


**Figure 5.2:** FTIR spectra of MOF, Pd@GO and Pd@GO/MOF.

TGA analysis was used to determine the thermal stability of the synthesised materials. In addition, by comparing the TGA curve of each component separately to its curve in a composition material, we can also learn about the degree of interaction between the reacting species. The thermal analysis of the prepared materials are shown in Figure 5.3., MOF is thermally stable up to  $370\text{ }^{\circ}\text{C}$ . The dehydration of MOF occurs at  $100-$

125 °C and the frameworks collapses at 350-370 °C [22]. Graphene oxide (Figure S1(c)) was reported to be thermally stable up to 180 °C, this collapse is attributed to the loss of oxygen containing functional groups [35]. After the addition of Pd, the stability was enhanced as presented in Figure 5.3. This is due to the palladium occupying most of the oxygen containing groups, and hence limiting/reducing the loss in those functional groups. The introduction of Pd@GO on the MOF surface showed improvement of stability as compared to MOF, Pd@MOF (Figure S1(c)) and Pd@GO. Interestingly, this composite is now found to be moisture stable losing about 10% of water as compared to the parent MOF (losing 30% water). Furthermore, the transitions of both MOF and GO are observed in the final composite, which confirms the incorporation between the two materials.

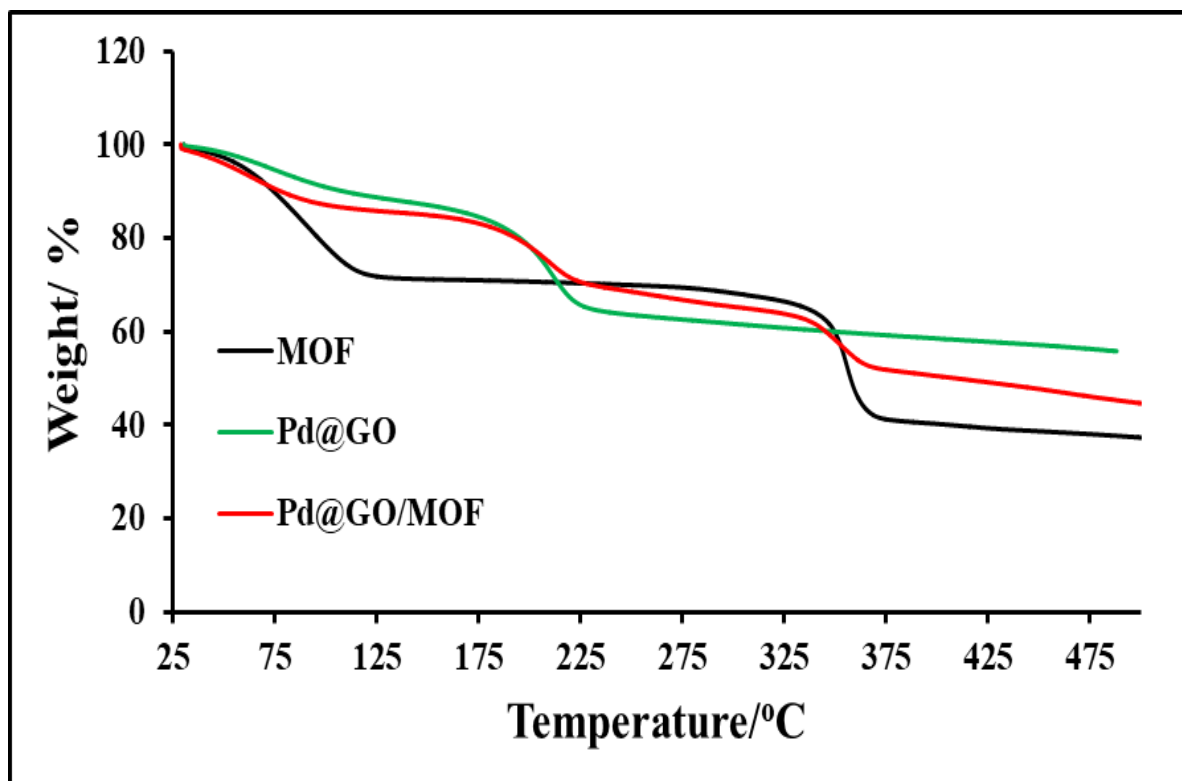


**Figure 5.3:** TGA analysis of MOF, Pd@GO and Pd@GO/MOF composite.

The DSC results correlates well with the TGA analysis. There is an exothermic peak at 100-125 °C in MOF, which is due to the heat released when the dehydration process

occurs [22]. Moreover, an endothermic peak at 350-370 °C is due to absorption of heat as the frameworks of the MOF material collapses. With the introduction of palladium onto the MOF materials (Figure S1(d)), there is an enhancement in moisture stability and also the stability of the frameworks[28]. The Pd@GO shows an endothermic peak at 210 °C which is similar to the one of GO (Figure S1(d), due to the absorption of heat as material loses all the functional groups [35]. The final composite shows peaks corresponding to the loss of the two parent materials (GO and MOF). This also confirms the formation of the composite Pd@GO/MOF

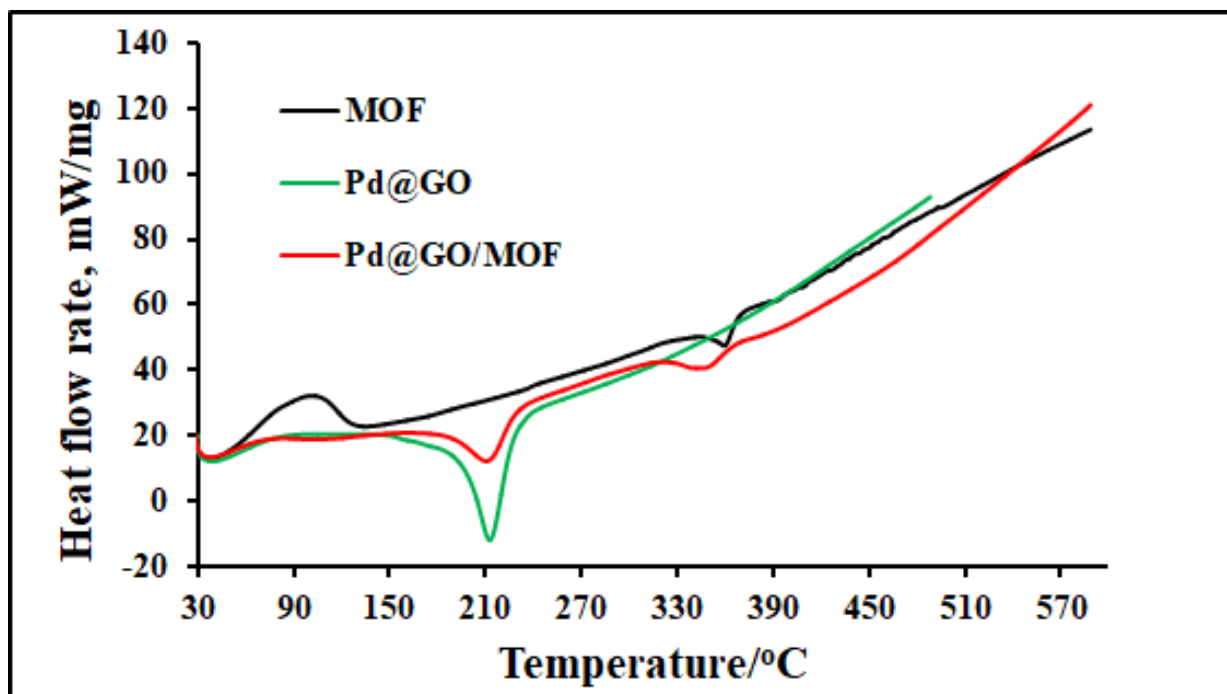


**Figure 5.4:** DSC analysis of MOF, Pd@GO and Pd@GO/MOF composite.

### 5.3.2. Morphological characterisation

The SEM images (Figure 5.5) were used to further provide the structural morphology and microstructure of MOF, Pd@GO, and Pd@GO/MOF composite. As shown in Figure 5.5(a), MOF demonstrates typical irregular crystals with octahedral shapes confirming a low control on the crystal growth parameters [22,28] and its corresponding EDS (Figure 5.5(b)) reveals the presence of C-, O- and Cu- atoms in the MOF structure. The inset image of Figure 5(a) shows that MOF crystals have

smooth surfaces. This observation confirmed that hydrothermal synthesis gives pure, highly crystalline MOF materials. On the SEM image of Pd@GO crystals, it is clear to see that the Pd nanoparticles are well-dispersed on the GO surface as compared to SEM image of GO (Figure S2(a)) and no apparent aggregation can be observed. Element mapping image and EDS spectrum of Pd@GO also confirmed the presence of Pd distributed through the GO sheets (Figure 5.5(d)).

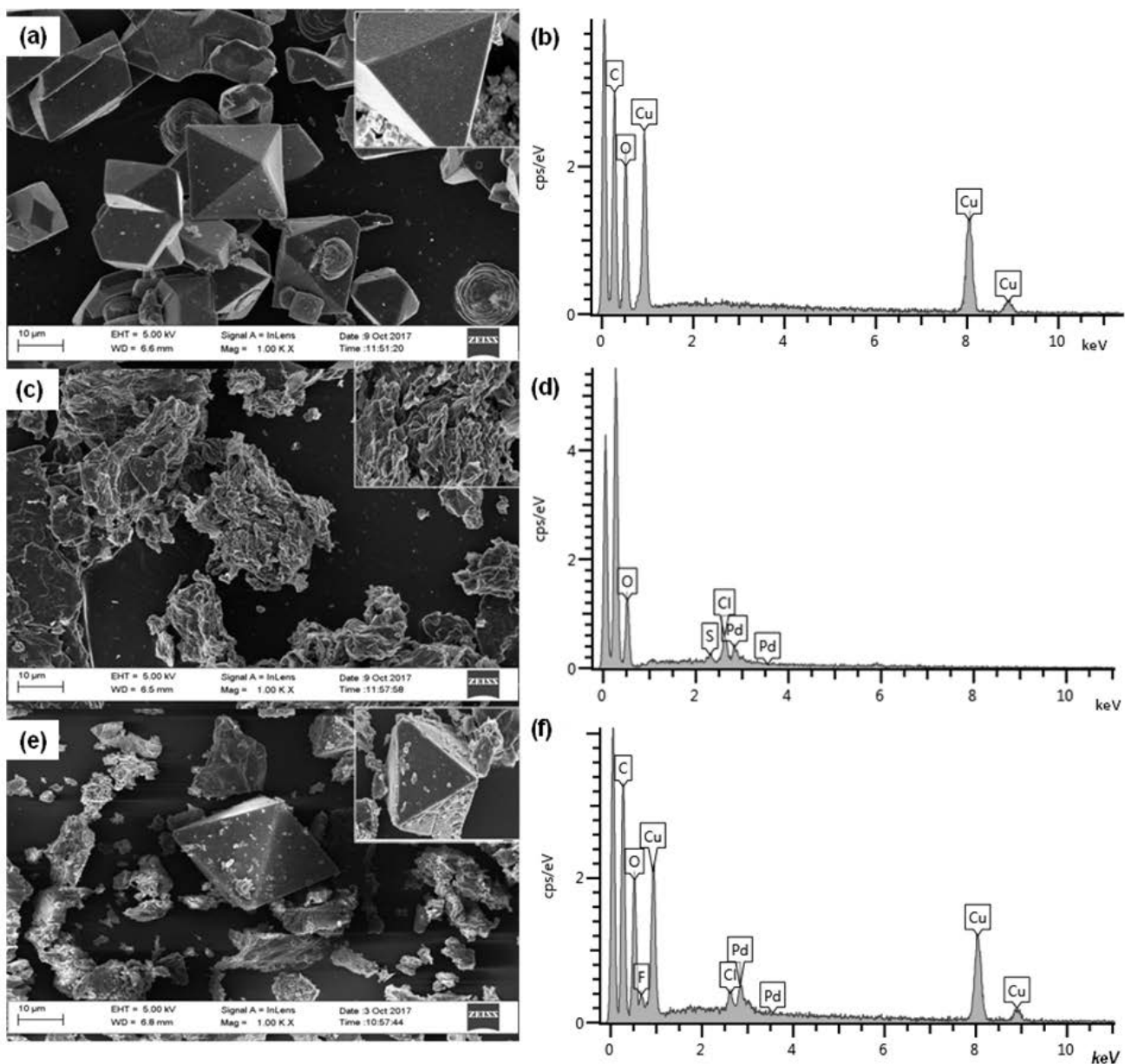


**Figure 5.5:** FE-SEM image of (a) MOF, (c) Pd@GO (e) Pd@GO/MOF composite (inset : magnification on the crystal structure to view the surface of the crystal) and EDS spectrum of (b) MOF, (d) Pd@GO, (f) Pd@GO/MOF composite.

In addition, the presence of characteristic peaks of oxygen element indicated that functional oxygen groups were still reserved on GO layers after doping Pd metals. On the SEM image of Pd@GO/MOF composite, there is a clear demonstration of rough surfaces observed when the Pd@GO is introduced on MOF, in which the inset image (Figure 5.5(e)) shows the interconnecting structures of nanoparticles on the surfaces of MOF composite. This observation can be attributed to the morphology of Pd@GO on the MOF structure as compared to neat MOF. EDS (Figure 5.5(f)) showed the presence of Pd nanoparticles in the composite at low weight percent. The change in morphology played a significant role in improving the thermal stability of the composite as observed in the TGA results.

TEM images are represented in Figure 5.6(a, c and e) for MOF, Pd@GO and Pd@GO/MOF show a clear difference among the samples' textures, respectively. The image of MOF (Figure 5.6(a)) shows the well-defined octahedral shapes of this crystalline material. As seen in Figure 5.6(c) for Pd@GO with respect to TEM image of GO (Figure S2(c)), the image shows a well exfoliated graphene nanosheets and wrinkled transparent sheet-like structure. In the structure of Pd@GO/MOF composites (Figure 5.6(e)), the layers have been confirmed as the alternation between Pd@GO sheets and MOF blocks. It was seen that the functional oxygen groups from Pd@GO interact with the copper dimers and chemical interactions are involved in the formation of composites [26] with reference to the neat MOF (Figure 5.6(a)) and Pd@MOF (Figure S2(d)). It is interesting to observe that again in the composite, the particles preserved the shape of MOF crystals (image e) indicating the constrain effects of the Pd@GO layers resulting in preserving the shapes of the original MOF crystals in their carbonised phase [26]. Nevertheless, the pattern observed can be considered as representing the lattice image of MOF in the composite. It is likely that distorted graphene-based layers present in the composite helped the MOF to retain

its crystalline structure by dissipating the electrostatic charges [25,26]. As shown in Figure 5.6(b, d and f), the EDX spectra revealed all the elements present in MOF, Pd@GO and Pd@GO/MOF confirming the incorporation of Pd@GO onto MOF, respectively. It was observed that the presence of small peaks of Na, Mn and S are due to impurities trapped in the GO and Pd@GO/MOF during synthesis process as seen in EDX spectra below.

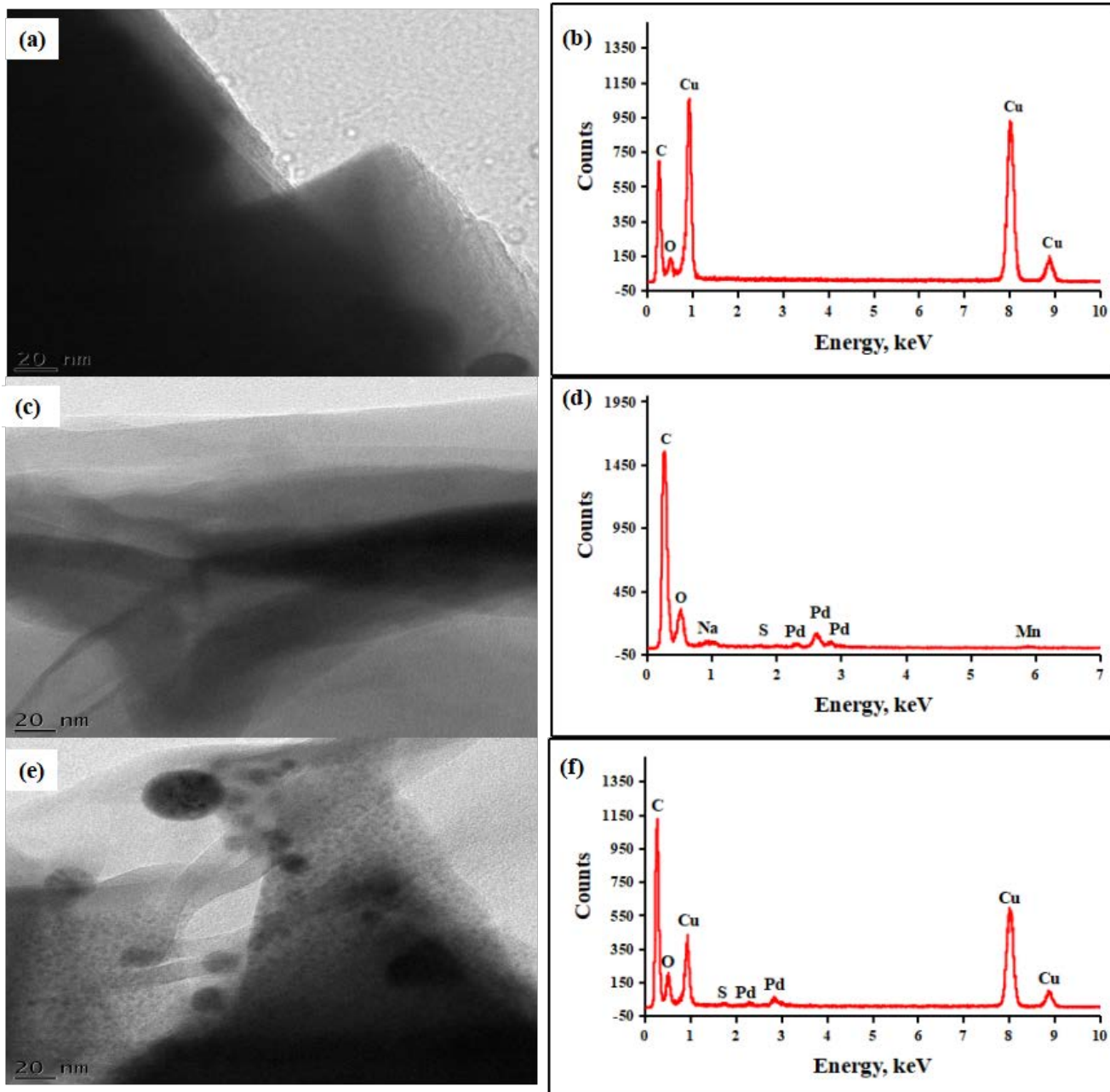


**Figure 5.6:** TEM image of (a) MOF, (c) Pd@GO (e) Pd@GO/MOF composite (inset : magnification on the crystal structure to view the surface of the crystal) and EDX spectrum of (b) MOF, (d) Pd@GO, (f) Pd@GO/MOF composite.

In addition, Figure 5.7(a) demonstrates the phase contrast of the intact crystal of MOF was barely visible, and its presence became apparent in the according SAED (Figure 5.7(b)). The measured interplanar d spacings of 0.857 nm (8.57 Å, estimated from scale bar measurement) and 1.00 nm (10.0 Å, estimated using Bragg's law:  $Rd = \lambda L$ , where R=radius, d= interplanar spacing,  $\lambda$ =wavelength, and L=camera length) correspond to MOF in (222) orientation in HRTEM and SAED images, respectively. In addition, the crystallinity of the MOF observed in these images show the clear diffraction spots is in agreement with XRD discussed above. The HRTEM image (Figure 5.7(c)) and its corresponding SAED image (Figure 5.7(d)) of Pd@GO show amorphous characteristic of graphene sheet [24] with a d-spacing of 1.10 nm (11.0 Å) which was similar to GO images (Figure S3(c)). The Pd@GO/MOF images in Figure 5.7(e) and (f) for HRTEM and SAED show the spacing is 1.00 nm (10.0 Å) which is close to the d-spacing of (222) plane of MOF and (002) plane of GO. These results clearly suggest the formation of hybrid-structure of Pd@GO/MOF as compared to neat MOF (Figure 5.7(a) and (b)) and Pd@MOF (Figure S3(c) and (d)).

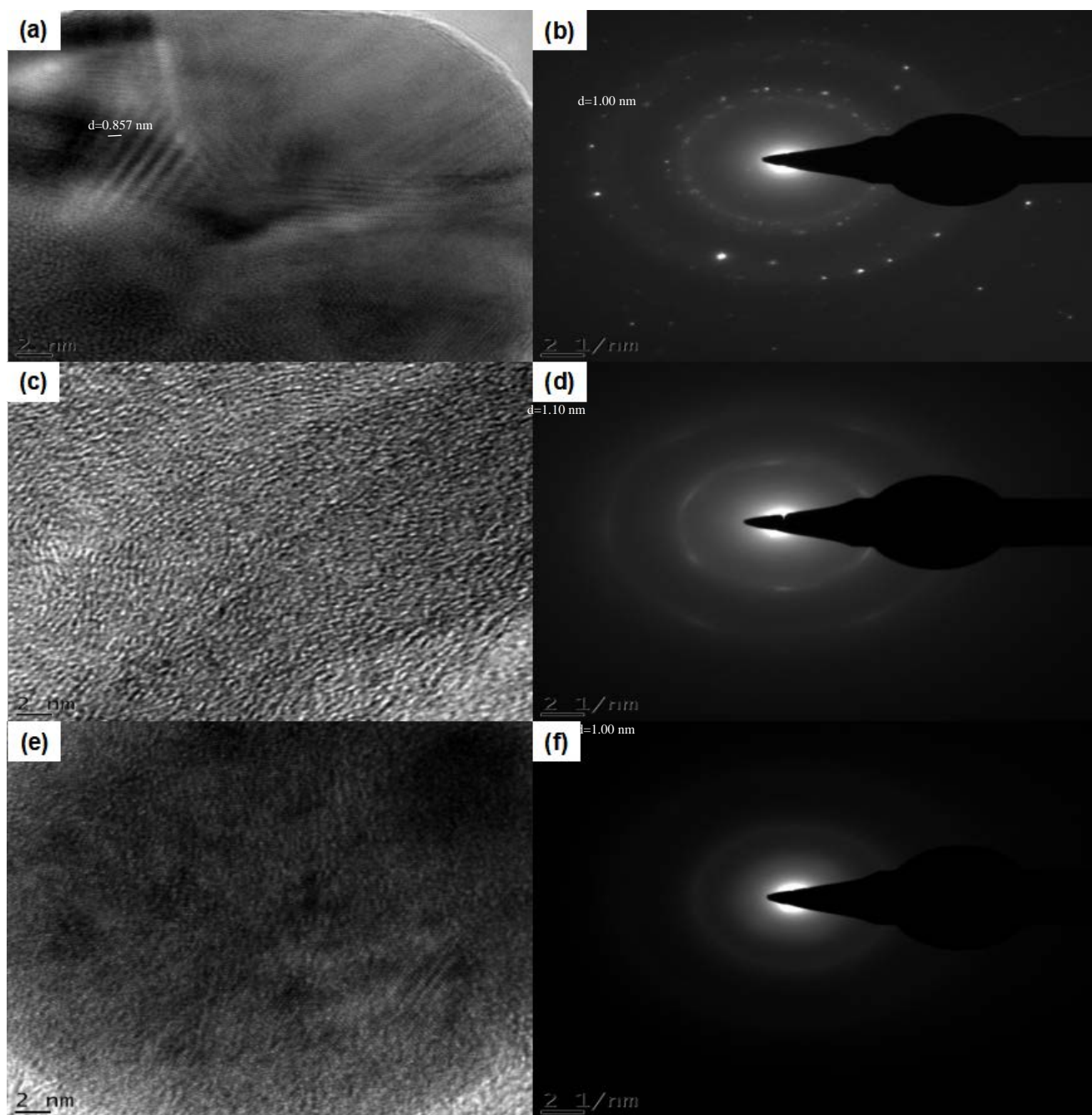


**Figure 5.7:** HRTEM images of (a) MOF, (c) Pd@GO (e) Pd@GO/MOF composite and SAED patterns of (b) MOF, (d) Pd@GO, (f) Pd@GO/MOF composite.

### 5.3.3. Electrochemical characterisation

Electrochemical behaviour of MOF, Pd@MOF, Pd@GO and Pd@GO/MOF composite was studied by cyclic voltammetry to understand the redox chemistry of the prepared materials and their voltammograms are represented in Figure 5.8(a). It was noticeable that the Faradaic contributions (redox process) onto gold electrode was observed at around -0.50 V due to redox process of bare Au electrode [36]. MOF displayed three oxidation processes attributed to the conversion from Cu/Cu<sup>1+</sup>, Cu<sup>1+</sup>/Cu<sup>2+</sup> and Cu<sup>2+</sup>/Cu<sup>3+</sup> between 0 and 1 V [37,38]. Furthermore, the reduction of Cu<sup>2+</sup> to Cu<sup>+</sup> occurs to possess more negative potential, which might be due to electrochemical properties of Au electrode in TBAP/DMSO system [21]. However, Nila and Gonzales [39] reported that the electrochemical reduction of Cu<sup>2+</sup> in solution proceeds in two successive-one electron reversible waves through a Cu<sup>+</sup> intermediate, in which the stability of the intermediate was due to the presence of ions in the solution [39]. The similar behaviour was also observed by Loera-Serna *et al.* [33] in LiCl solution indicating that the electrochemical processes of Cu during the direct sweep took place in the MOF. On the other hand, the CV of Pd@MOF in the same condition shows enhancement of both cathodic and reduction peaks as compared to alone MOF as a clear indicative of Pd introduction on MOF surface. It was seen that Pd@GO in the potential window of TBAP/DMSO electrolyte system showed a quasi-reversible processes corresponding with the electroactive species of GO [40] and Pd metal [40] which is clearly seen in Figure 5.8(c). The CV of Pd@GO/MOF on the gold electrode, still allows the diffusion of the redox mediator (Cu<sup>2+</sup>/Cu<sup>+</sup>) through their layers to the electrode surface [28]. One of the important features observed in the CV of the composite was the enhancement of anodic and cathodic peak towards potential of 0.3 V for conversion of Cu/Cu<sup>+</sup> and at Cu<sup>3+</sup>/Cu<sup>2+</sup>, respectively .

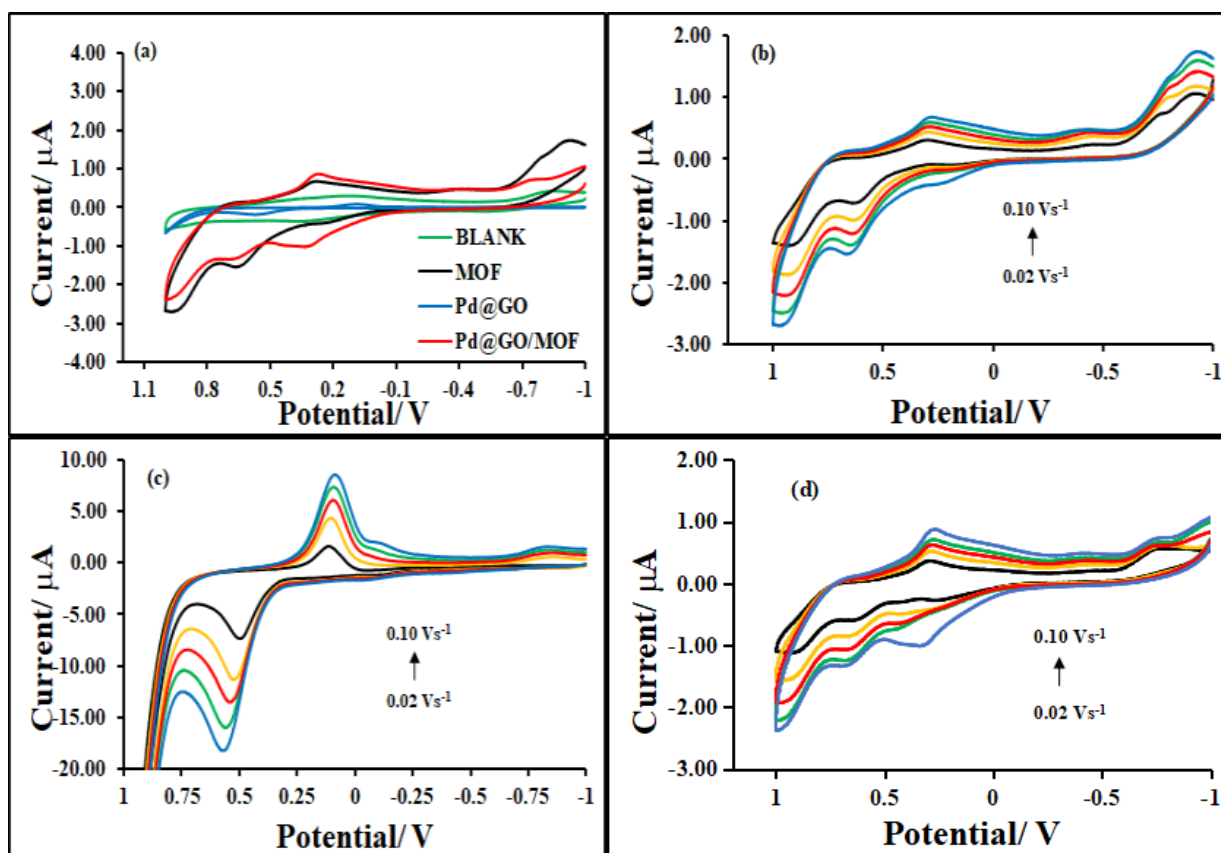


**Figure 5.8:** (a). CV curves of Blank, MOF, Pd@GO, Pd@MOF and Pd@GO/MOF composite at 0.1 v.s<sup>-1</sup> in 0.1 mol.L<sup>-1</sup> TBAP/DMSO electrolyte solution on Au electrode. (b-d). MOF, Pd@GO and Pd@GO/MOF at different scan rates (0.02-0.1 v.s<sup>-1</sup>) in 0.1 mol.L<sup>-1</sup> TBAP/DMSO, respectively.

The scan rate studies of MOF, Pd@GO and Pd@GO/MOF composite was accomplished in 0.1 mol.L<sup>-1</sup> TBAP/DMSO system using Au working electrode. The multiscan voltammograms of MOF, Pd@GO and Pd@GO/MOF composite are shown in parts b-d of Figure 5.8, respectively. As shown in Figure 5.8(b) and (d) and Figure S4(a) for MOF, Pd@GO/MOF and Pd@MOF, the peak currents corresponding to process 1 to 3 decrease with the scan rate and finally disappear, while the peak currents corresponding to the reverse processes increase with increase in scan rate and reach constant values. In addition, the Cu ions generated during electrochemical processes are used as catalysts to HER mechanism [37,41]. Figure 5.8(c) demonstrates an increase reversible peaks with the increase in scan rate. From the

voltammograms, it was observed that both anodic ( $I_{pa}$ ) and cathodic peak ( $I_{pc}$ ) currents increased linearly with scan rates from 0.1 to 1  $V.s^{-1}$ . All redox couples showed electrochemical quasi-reversible process with respect to change in peak potential ( $\Delta E_p$ ) and the ratio of anodic and cathodic peak current ( $I_{pa}/I_{pc}$ ) values. Unity of  $I_{pa}/I_{pc}$  ratios with respect to  $Cu^{1+}/Cu^{2+}$  and its reverse couple at all scan rates for MOF and Pd@GO/MOF and the logarithm of the absolute value of the reductive peak current against the logarithm of the scan rate with slope of 0.5 indicate diffusion controlled characters [42,43] of the redox processes as shown in Figure 5.9(a) and Table 5.1.

In addition, the diffusion coefficient,  $D$ , was determined for electrocatalysts using cyclic voltammetry and following the Randles-Sevcik equation for a quasi-reversible system (Equation 5.1) [42,43].

$$I_p = (2.65 \times 10^5) n^{3/2} A C D^{1/2} (\nu)^{1/2} \quad (5.1)$$

where,  $n$  is the number of electrons transferred,  $A$  is the electrode area in  $cm^2$ ,  $D$  is the diffusion coefficient in  $cm^2.s^{-1}$ ,  $C$  is the bulk molar concentration of the electroactive species in  $mol.cm^{-3}$  and  $\nu$  is scan rate in  $V.s^{-1}$ . Figure 5.9(b) showed that the current increased linearly with increasing the square root of the scan rate,  $\nu^{1/2}$  which is consistent with Equation 1. The  $D$  values as presented in Table 5.1, were found to be  $1.39 \times 10^{-7}$ ,  $1.08 \times 10^{-4}$  and  $7.79 \times 10^{-7} cm^2.s^{-1}$  for MOF, Pd@GO, Pd@MOF and Pd@GO/MOF respectively. The introduction of Pd@GO on MOF surface enhanced the diffusion coefficient of the composite compared to parent MOF. Similar trend was observed in MOF based polymer composite [21,22].

Furthermore, it was seen that instead of the material undergoing only diffusional process, it can also adsorb on the surface of the electrode [44]. This behaviour can be obtained by directly relating the peak current with the surface coverage ( $\Gamma$ ) and the scan rate as presented in Equation 5.2.

$$I_p = \frac{n^2 F^2 \Gamma A \nu}{4RT} \quad (5.2)$$

Figure 5.9(c) shows a linear relationship between current and scan rate where regression line equation and  $R^2$  are presented to determine the surface coverages (Table 5.1) for MOF, Pd@GO, Pd@MOF and Pd@GO/MOF were found to be  $1.32 \times 10^{-10}$ ,  $1.27 \times 10^{-9}$ ,  $1.69 \times 10^{-10}$  and  $1.09 \times 10^{-10}$  mol.cm<sup>-2</sup>, respectively, confirming the adsorption of the material on the gold electrode.

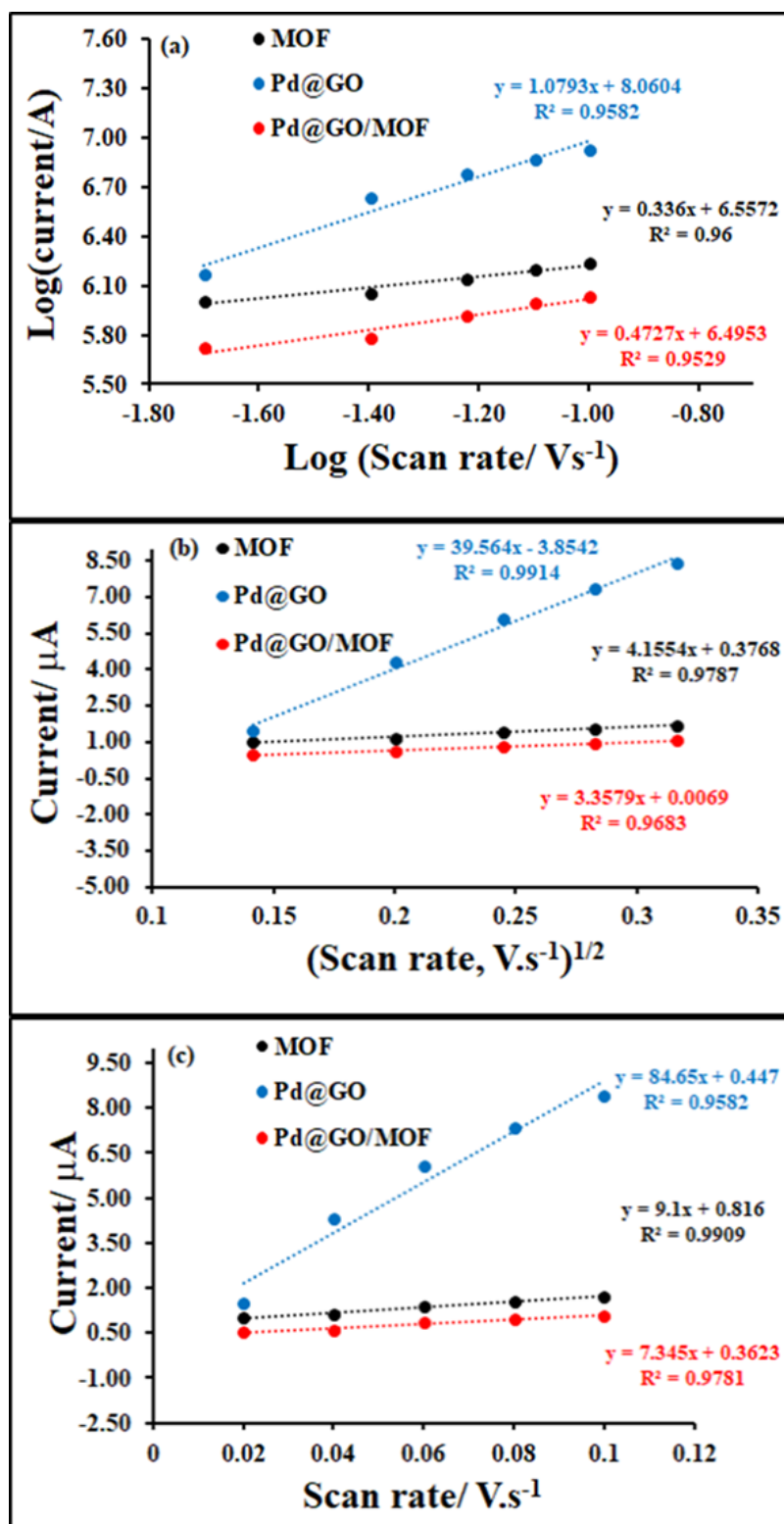


**Figure 5.9:** (a) The log-log plot of the absolute value of the peak current vs scan rate, (b) peak current as a function of square root of scan rate and (c) peak current as a

function of scan rate for MOF, Pd@GO and Pd@GO/MOF on gold in 0.1 mol.L<sup>-1</sup> DMSO/TBAP electrode system at different scan rates (0.02 – 0.10 V.s<sup>-1</sup>).

**Table 5.1:** Electrochemical parameters of MOF, Pd@GO, Pd@MOF and Pd@GO/MOF composite.

Material	$i_{pa}/i_{pc}$	Log(I vs $v^{1/2}$ ) Slope	D (cm <sup>2</sup> . s <sup>-1</sup> )	$\Gamma$ (mol.cm <sup>-2</sup> )
MOF	2.39	0.34	$1.39 \times 10^{-7}$	$1.32 \times 10^{-10}$
Pd@GO	5.73	1.08	$1.08 \times 10^{-4}$	$1.27 \times 10^{-9}$
Pd@MOF	1.65	0.33	$1.90 \times 10^{-6}$	$1.69 \times 10^{-10}$
Pd@GO/MOF	1.20	0.47	$7.79 \times 10^{-7}$	$1.09 \times 10^{-10}$

#### 5.3.4. Hydrogen studies

The electrochemical hydrogen activities of all prepared samples were measured in 0.1 M TBAP/ DMSO electrolyte in the presence of H<sub>2</sub>SO<sub>4</sub> as a proton source using a three-electrode set-up system. Figure 5.10(a) present the plot of current vs potential of the blank gold electrode, MOF, Pd@GO and Pd@GO/MOF. As compared to CV plots in Figure 5.8(a) in absence of proton source, upon addition of H<sub>2</sub>SO<sub>4</sub>, a new cathodic wave on MOF and Pd@GO/MOF appeared at onset potential of -0.5 V with increase cathodic current. However, this behaviour was not observed in the case of Pd@GO, which designates that there was no hydrogen evolution. From this observation, it can be deduced that the MOF and Pd@GO/MOF have the ability to reduce hydrogen protons (H<sup>+</sup>) to form molecular hydrogen (H<sub>2</sub>) at lower potentials [22]. In order to substantiate that the current obtained is a source of the cathodic wave, the concentration-dependant studies were carried out and results are shown in Figure 5.10(b-d). Moreover, it can be observed that an increase in H<sub>2</sub>SO<sub>4</sub> concentration results in a further increase in current reading at lower onset potential, thus the new catalytic wave is due to the proton source. Furthermore, small anodic peak in Figure 5.10(d) and Figure S4(b) relate to different hydrogen sorption processes in the MOF

material as observed by Monama *et al.* [28]. This was attributed to the presence of Pd nano- particles as an indication of hydrogen spillover mechanism [28]. It is known that hydrogen usually combines with Pd to form Pd hydride instead of physically adsorbing on Pd surfaces [42,45].

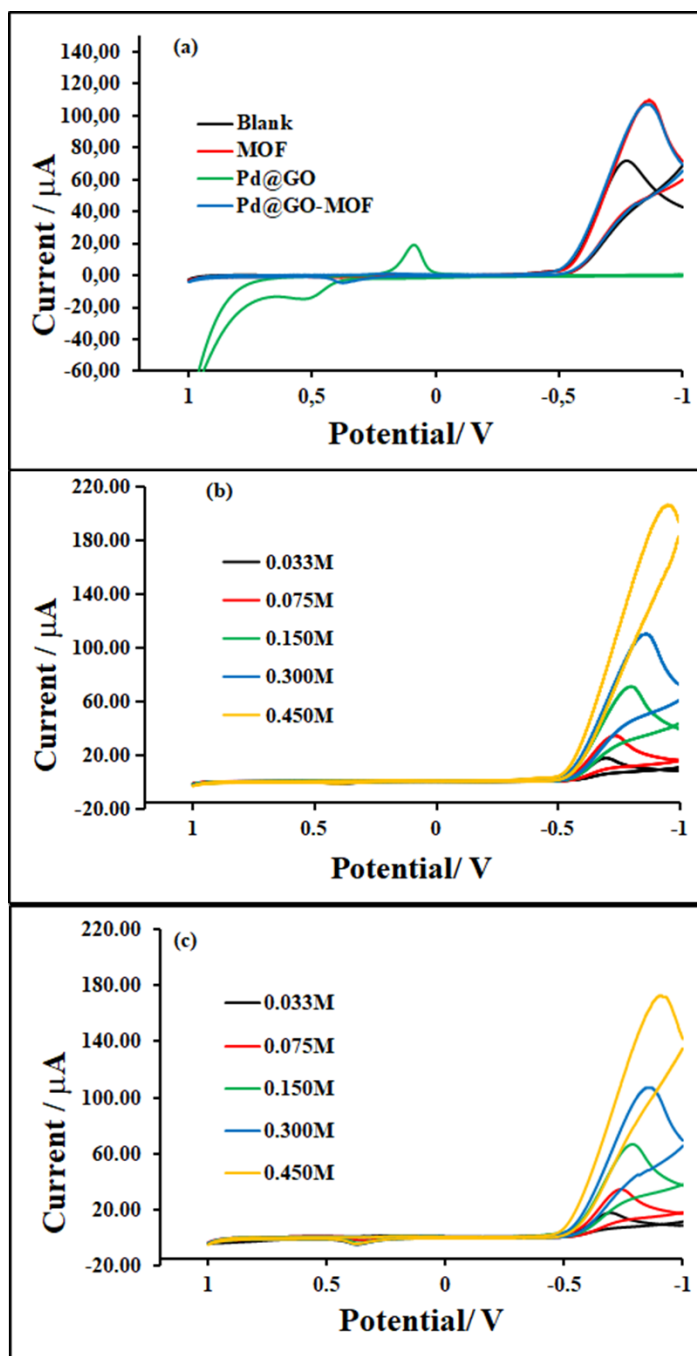
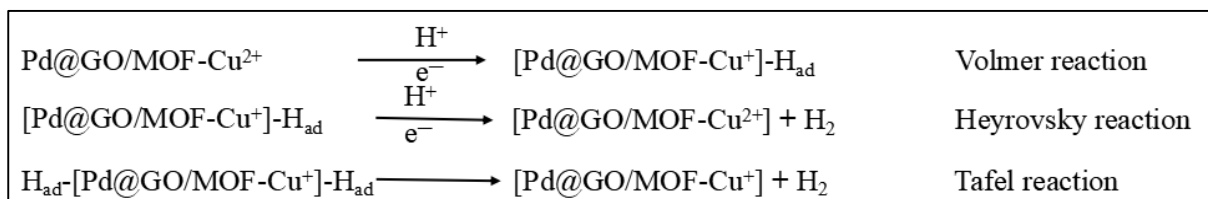


**Figure 5.10:** (a) CV curves of Blank, MOF, Pd@GO and Pd@GO/MOF composite in the presence of 0.300 mol.L<sup>-1</sup> H<sub>2</sub>SO<sub>4</sub> at 0.10 V.s<sup>-1</sup> and CV curves of (b) MOF and (c) Pd@GO/MOF composite in different concentration of hydrogen source (0.033-0.450 mol.L<sup>-1</sup> H<sub>2</sub>SO<sub>4</sub>) at 0.10 V.s<sup>-1</sup> on Au electrode in 0.1 mol.L<sup>-1</sup> TBAP/DMSO electrode system.

The Tafel analysis is used to get a better grasp on the kinetics and activity of electrochemical reactions for HER [46]. The Tafel slope value gives important information on the rate determining step in an electrochemical reaction. It is an inherent property of the electrode material. Furthermore, the overall electrocatalytic HER in this work can also be proposed by means of mechanism. In an acid medium, the HER pathway could proceed via three main steps (Scheme 5.1): Initial reduction of Cu(II) to Cu(I) of the Pd@GO/MOF, followed by interaction of the proton with the corresponding composite and leading in to formation of the composite hydride (Pd@GO/MOF)H<sub>ad</sub> in hydrogen storage process as the most propable intermediate and proposed to be Volmer mechanism[20,28,47]. After the hydride, the hydride intermediate easily undergoes a protonation or interacts with one another to form H<sub>2</sub> molecule through a Heyrovsky or Tafel reaction [20,28,47].



**Scheme 5.1:** Proposed mechanisms involved in the HER kinetics of the composite.

The Tafel plot was constructed from current density-potential data at various concentrations ranging from 0.033 to 0.450 mol.L<sup>-1</sup> H<sub>2</sub>SO<sub>4</sub> for MOF, Pd@GO and Pd@GO/MOF composite. Elucidating the mechanism of heterogeneous hydrogen evolution usually takes the form of Tafel analysis, where the steady state or quasi-steady state current, *i*, at a catalyst of a given composition is measured over a range of overpotential, *η*, then log(*i*) can be plotted against *η* to give a linear relationship,

known as a Tafel line. The intercept of the Tafel line with the current axis gives the exchange current density,  $i_0$ , which is related to both the inherent reaction exchange rate at dynamic equilibrium and the electrochemically active surface area of the catalyst. The slope of the Tafel line is independent of surface area and takes on a limited number of values that correspond to the dominant mechanism [6]. Ramohlola *et al.* [20,22], reported that the  $b$  could also serve as an indicator of either Volmer, Heyrovsky and Tafel in a multi-step proton transfer process and  $i_0$  the measure of performance of an electrocatalyst. In this study, the values of  $b$  and  $i_0$  were estimated by linear polarization curves and the results are presented in Table 5.2.

In addition, another important parameter that can give insight of reaction mechanism is the cathodic transfer coefficient ( $1-\alpha$ ) which was calculated using high overpotential region, where Butler-Volmer equation simplifies to the Tafel equation (Equation 4.3), from the Tafel slope  $b$  given by the relationship:

$$b = \frac{-2.303RT}{(1-\alpha)F} \quad (4.3)$$

Figure 5.11 and Table 5.2 show Tafel plots and parameters, for blank electrode, MOF, Pd@GO and Pd@GO/MOF composite. The present study exhibits that the Pd@GO gives Tafel slope of  $149 \text{ mV.dec}^{-1}$  at  $0.450 \text{ mol.L}^{-1} \text{ H}_2\text{SO}_4$ . At the same acid conditions, MOF and Pd@GO/MOF composite showed lower Tafel slope values as compared to the Pd@GO and Pd@MOF (Figure S4(c)). It was reported that Tafel slopes in the ranges of  $105\text{-}150 \text{ mV.dec}^{-1}$  may be explained on the basis of a Volmer rate determining step for HER [8]. The Tafel slopes obtained in the present study suggests that the HER on the prepared electrocatalysts proceeds via Volmer-Heyrovsky or Volmer-Tafel mechanisms, with the adsorption of proton on the electrocatalyst surface (Volmer step) as the rate determining step. These results are in good consent with the work reported by Kubisztal *et al.* [47] when studying the HER behaviour of nickel-based composite coatings containing molybdenum powder. Furthermore, the charge-transfer coefficient ( $\alpha = 0.5$ ), describes a mechanism where the rate determining step

is the Volmer reaction or the Volmer reaction coupled with one of the other two reactions [8]. As given in Table 5.2, the charge transfer coefficients for MOF and Pd@GO/MOF composite are all close to 0.5. Thus, the rate determining step of HER on the studied MOF and the composite maybe the Volmer reaction or Volmer reaction coupled with one of the other two reactions [8, 47]. To further estimate the intrinsic activity of the electrocatalyst, the exchange current density ( $j_0$ ) was determined by extrapolation of the Tafel plots [20,21]. For  $\eta = b \log j + a$ , the constant terms  $a$  and  $b$  are known from the Tafel plot,  $n$  is zero, and then  $j_0$  is received. The exchange current densities obtained for different electrocatalysts are recorded in Table 5.2 and the values increase with increase in  $H_2SO_4$  concentration. The obtained exchange current densities are higher compared to those reported in other studies [8,17,47,48]. From this, it can be concluded that the prepared electrocatalyst possess large surface area, fast electron transfer and favourable HER kinetics [9].

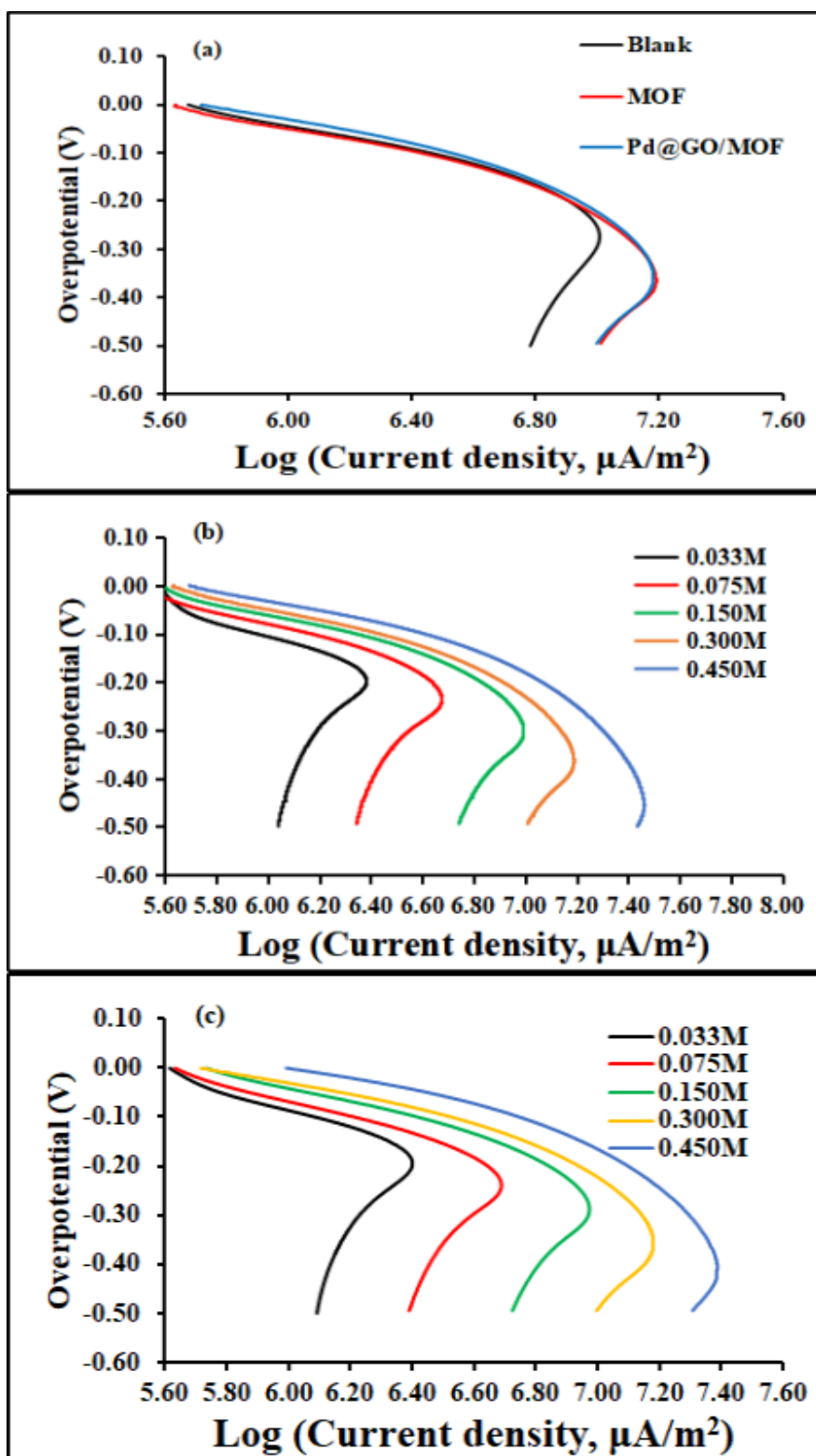


**Figure 5.11:** Tafel plots of (a) blank, MOF and Pd@GO/MOF composite ( $\sim 2.0 \times 10^{-4}$  mol.L $^{-1}$ ) in the presence 0.300 mol.L $^{-1}$  H $_2$ SO $_4$  at 0.10 V.s $^{-1}$  (b) MOF and (c)

Pd@GO/MOF composite in different concentrations of H<sub>2</sub>SO<sub>4</sub> and 0.10 V.s<sup>-1</sup> scan rate on Au electrode in 0.1 mol.L<sup>-1</sup> TBAP/DMSO electrode system.

**Table 5.2:** Experimental values of tafel slope (*b*), charge transfer coefficient (1- $\alpha$ ), exchange current density (*i*<sub>0</sub>) and TOF of MOF and Pd@GO/MOF composite.

Material	H <sub>2</sub> SO <sub>4</sub> (mol.L <sup>-1</sup> )	Slope ( <i>b</i> ) (V.dec <sup>-1</sup> )	- <i>b</i> (mV.dec <sup>-1</sup> )	1- $\alpha$	log <i>i</i> <sub>0</sub> ( $\mu$ A.m <sup>-2</sup> )	<i>i</i> <sub>0</sub> (A.m <sup>-2</sup> )	TOF (mol H <sub>2</sub> .s <sup>-1</sup> )
MOF	0.033	-0.138	138	0.43	6.38	2.4	0.76
	0.075	-0.212	212	0.28	6.65	4.5	1.42
	0.150	-0.132	132	0.45	6.98	9.5	3.04
	0.300	-0.106	106	0.56	7.17	14.8	4.71
	0.450	-0.126	126	0.47	7.35	22.4	7.12
Pd@GO/M	0.033	-0.159	159	0.37	6.39	2.5	0.78
OF	0.075	-0.163	163	0.36	6.66	4.6	1.45
	0.150	-0.161	161	0.37	6.97	9.3	2.97
	0.300	-0.138	138	0.43	7.17	14.8	4.71
	0.450	-0.123	123	0.48	7.39	24.5	7.81
	Pd@MOF	0.300	-0.193	193	0.31	6.9	7.1
[28]							
Pd@CuPc/	0300	-0.177	177	0.33	7	8.9	2.83
MOF [28]							

The turnover frequency (TOF) is widely used in the molecular catalysis field to assess the efficiency of catalysts, which can also be employed for electrocatalytic reactions. The TOF is the mass of molecules reacting for a certain reaction per unit time, which can be calculated using Equation 5.4 [49]:

$$\text{TOF} = \frac{jM}{2Fm} \quad (5.4)$$

where  $j$  is the current density at a given potential,  $M$  is mass percentage of materials,  $F$  is Faraday's constant, and  $m$  is the mass of per square centimeter of catalysts estimated from BET surface area of MOF (614.7 m<sup>2</sup>/g [28]) and GO (423 m<sup>2</sup>/g [50]). The TOF values for MOF and Pd@GO/MOF composite are presented in the Table 5.2. It was seen that Pd@GO/MOF synthesised materials resulted with the enhancement of the TOF values as the concentration of H<sub>2</sub>SO<sub>4</sub> increases, for example, the values were obtained to be 7.8 mol H<sub>2</sub> .s<sup>-1</sup> at the highest H<sub>2</sub>SO<sub>4</sub> concentration (0.450 mol.L<sup>-1</sup>). In addition to the Tafel slope, the reaction order of the HER with respect to the concentration of hydrogen ions is also a characteristic kinetic parameter that can provide additional information about the underlying mechanism. Figure 5.12(a) and (b) present the pH dependence of the current density and potential, respectively, for the experimental data obtained in the present study. The slope of the trendline in Figure 5.11(a) (log( $i$ ) vs. pH), represents the apparent reaction order of HER which was found to be around 0.8, suggesting a mixed type mechanism [51] as observed in Tafel parameters. Furthermore, in Figure 5.12(b) which is a representation of the Pourbaix diagram and the slope was seen to be less than 0.5. The observed dependence agrees well with the proposed mechanism of the process above.

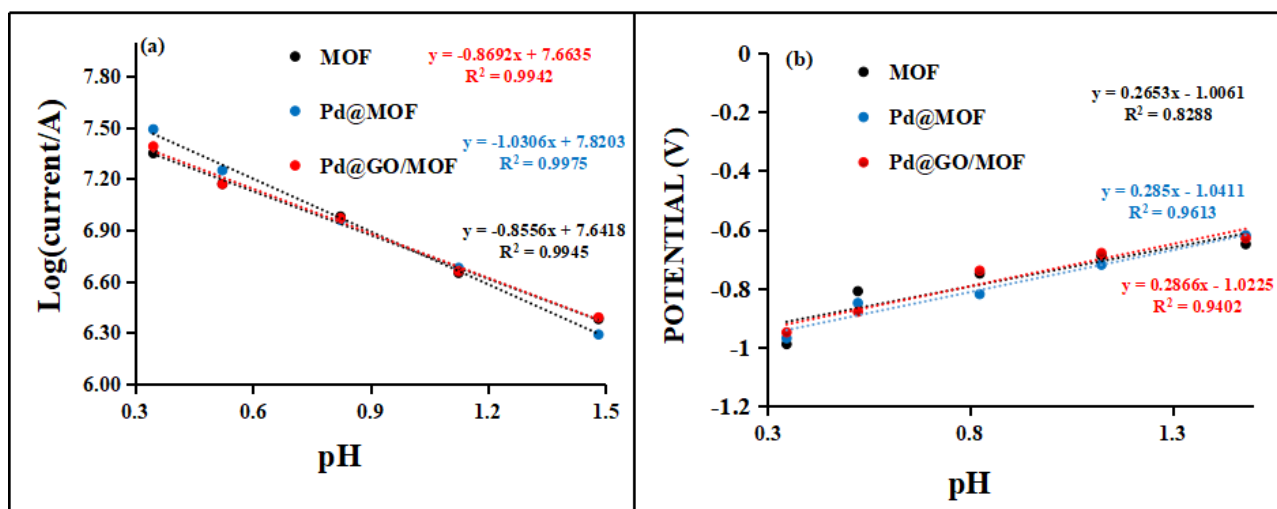


**Figure 5.12:** (a) Plot of log current as a function of pH of the solution and (b) Pourbaix diagram of hydrogen evolution reaction

## 5.4. CONCLUSIONS

In summary, an efficient electrocatalyst (Pd@GO/MOF) derived from MOF and Pd@GO was successfully synthesised through electroless Pd deposition followed by impregnation procedure. The presence of GO was a crucial step for both the diffusion process of Pd atoms to form Pd@GO/MOF and the introduction of defects into GO to expose catalytic sites. The influences of Pd@GO on the morphology and crystalline structure of MOF surface, as well as resulting electro-catalytic activity in hydrogen evolution were systematically investigated. The observed promotional roles of incorporated Pd@GO on MOF surface is ascribed to possible synergetic effects between Pd, GO crystals and the MOF matrix, leading to a facilitation of HER as part of hydrogen production with enhanced TOF values. Furthermore, the Tafel slope and charge-transfer coefficients showed that the rate determining step of HER on the studied MOF and Pd@GO/MOF composite maybe the Volmer reaction or the Volmer reaction coupled with one of other two reactions supported by slopes from the plot of log current vs pH and Pourbaix diagram. Herein, the reported strategy of Pd@GO/MOF expose active sites of the MOF core, meanwhile, maintaining the porous carbon skeleton of Pd@GO, which holds a great potential for more applications in the electrocatalytic HER and hydrogen storage.

## 5.5. REFERENCES

- [1] J. A. Turner, "Sustainable hydrogen production," *Sci.*, vol. 305, pp. 972–974, 2004.
- [2] H. Lund, "Renewable energy strategies for sustainable development," *Energy.*, vol. 32, pp. 912–919, 2007.
- [3] O. Ellabban, H. Abu-Rub, and F. Blaabjerg, "Renewable energy resources: Current status, future prospects and their enabling technology," *Renew. Sustain. Energy Rev.*, vol. 39, pp. 748–764, 2014.
- [4] I. Dincer, "Renewable energy and sustainable development: a crucial review," *Renew. Sustain. Energy Rev.*, vol. 4, pp. 157–175, 2000.

- [5] C. Y. Chiang, K. Aroh, and S. H. Ehrman, "Copper oxide nanoparticle made by flame spray pyrolysis for photoelectrochemical water splitting – Part I. CuO nanoparticle preparation," *Int. J. Hydrogen Energy*, vol. 37, pp. 4871–4879, 2012.
- [6] Y. Yan, Y. Xia, and X. Wang, "A review on noble-metal-free bifunctional heterogeneous catalysts for overall electrochemical water splitting," *J. Mater. Chem. A Mater. energy Sustain.*, vol. 4, pp. 17587–17603, 2016.
- [7] K. Zeng and D. Zhang, "Recent progress in alkaline water electrolysis for hydrogen production and applications," *Prog. Energy Combust. Sci.*, vol. 36, pp. 307–326, 2010.
- [8] M. R. Gao, J. X. Liang, Y. R. Zheng, Y. F. Xu, J. Jiang, Q. Gao, J. Li, and S. H. Yu., "An efficient molybdenum disulfide/cobalt diselenide hybrid catalyst for electrochemical hydrogen generation," *Nat. Commun.*, vol. 6, pp. 1–7, 2015.
- [9] W. Zhou, J. Jia, J. Lu, L. Yang, D. Hou, G. Li, and S. Chen., "Recent developments of carbon-based electrocatalysts for hydrogen evolution reaction," *Nano Energy*, vol. 28, pp. 29–43, 2016.
- [10] J. B. Raoof, R. Ojani, S. A. Eshfedan, and S. R. Nadimi, "Fabrication of bimetallic Cu/Pt nanoparticles modified glassy carbon electrode and its catalytic activity toward hydrogen evolution reaction," *Int. J. Hydrogen Energy*, vol. 35, pp. 3937–3944, 2010.
- [11] A. Ghaffarinejad, N. Sadeghi, H. Kazemi, A. Khajehzadeh, M. Amiri, and A. Noori, "Effect of metal hexacyanoferrate films on hydrogen evolution reaction," *J. Electroanal. Chem.*, vol. 685, pp. 103–108, 2012.
- [12] D. D. Konieczna, H. Biller, M. Witte, W. G. Schmidt, A. Neuba, and R. Wilhelm, "New pyridinium based ionic dyes for the hydrogen evolution reaction," *Tetrahedron*, 2017.
- [13] Z. Sun, W. Fan, and T. Liu, "Graphene/graphene nanoribbon aerogels as tunable three-dimensional framework for efficient hydrogen evolution reaction," *Electrochim. Acta.*, vol. 250, pp. 91–98, 2017.
- [14] J. Lin, J. He, F. Qi, B. Zheng, X. Wang, B. Yu, K. Zhou, W. Zhang, Y. Li, and Y. Chen, "Electrochimica Acta In-situ Selenization of Co-based Metal-Organic

- Frameworks as a Highly Efficient Electrocatalyst for Hydrogen Evolution Reaction,” *Electrochim. Acta.*, vol. 247, pp. 258–264, 2017.
- [15] Z. S. Wu, G. Zhou, L. C. Yin, W. Ren, F. Li, and H. M. Cheng, “Graphene/metal oxide composite electrode materials for energy storage,” *Nano Energy*, vol. 1, pp. 107–131, 2012.
- [16] B. Valizadeh, T. N. Nguyen, and K. C. Stylianou, “Shape engineering of metal–organic frameworks,” *Polyhedron*, vol. 145, pp. 1–15, 2018.
- [17] Y. Z. Chen, R. Zhang, L. Jiao, and H. L. Jiang, “Metal–organic framework-derived porous materials for catalysis,” *Coord. Chem. Rev.*, vol. 362, pp. 1–23, 2018.
- [18] N. M. Musyoka, J. Ren, H. W. Langmi, B. C. North, M. Mathe, and D. Bessarabov, “Synthesis of rGO / Zr-MOF composite for hydrogen storage application,” *J. Alloys Compd.*, vol. 724, pp. 450–455, 2017.
- [19] R. Lin, L. Shen, Z. Ren, W. Wu, Y. Tan, H. Fu, J. Zhang, and L. Wu, “Enhanced photocatalytic hydrogen production activity via dual modification of MOF and reduced graphene oxide on CdS,” *Chem. Commun.*, vol. 50, p. 8533, 2014.
- [20] K. E. Ramohlola, M. Masikini, S. B. Mdluli, G. R. Monama, M. J. Hato, K. M. Molapo, E. I. Iwuoha, and K. D. Modibane, “Electrocatalytic Hydrogen Production Properties of Poly(3-aminobenzoic acid) doped with Metal Organic Frameworks,” *Int. J. Electrochem. Sci.*, vol. 12, pp. 4392–4405, 2017.
- [21] K. E. Ramohlola, G. R. Monama, M. J. Hato, K. D. Modibane, K. M. Molapo, M. Masikini, S. B. Mdluli, and E. I. Iwuoha, “Polyaniline-metal organic framework nanocomposite as an efficient electrocatalyst for hydrogen evolution reaction,” *Compos. Part B Eng.*, vol. 137, pp. 129–139, 2018.
- [22] K. E. Ramohlola, M. Masikini, S. B. Mdluli, G. R. Monama, M. J. Hato, K. M. Molapo, E. I. Iwuoha, and K. D. Modibane, “Electrocatalytic Hydrogen Evolution Reaction of Metal Organic Frameworks decorated with poly (3-aminobenzoic acid),” *Electrochim. Acta*, vol. 246, pp. 1174–1182, 2017.
- [23] D. R. Dreyer, S. Park, W. Bielawski, and R. S. Ruoff, “The chemistry of graphene oxide,” *Chem.Soc.Rev.*, vol. 39, pp. 228–240, 2010.
- [24] R. M. N. M. Rathnayake, H. W. M. A. C. Wijayasinghe, H. M. T. G. A. Pitawala,

- M. Yoshimura, and H. H. Huang, "Synthesis of graphene oxide and reduced graphene oxide by needle platy natural vein graphite," *Appl. Surf. Sci.*, vol. 393, pp. 309–315, 2017.
- [25] C. Petit, J. Burrell, and T. J. Bandosz, "The synthesis and characterization of copper-based metal-organic framework/graphite oxide composites," *Carbon N. Y.*, vol. 49, pp. 563–572, 2011.
- [26] C. Petit and T. J. Bandosz, "Engineering the surface of a new class of adsorbents: metal-organic framework/graphite oxide composites.," *J. Colloid Interface Sci.*, vol. 447, pp. 139–51, 2015.
- [27] C. Petit, B. Levasseur, B. Mendoza, and T. J. Bandosz, "Reactive adsorption of acidic gases on MOF/graphite oxide composites," *Microporous Mesoporous Mater.*, vol. 154, pp. 107–112, 2012.
- [28] G. R. Monama, S. B. Mdluli, G. Mashao, M. D. Makhafola, K. E. Ramohlola, K. M. Molapo, M. J. Hato, K. Makgopa, E. I. Iwuoha, and K. D. Modibane, "Palladium deposition on copper(II) phthalocyanine/metal organic framework composite and electrocatalytic activity of the modified electrode towards the hydrogen evolution reaction," *Renew. Energy*, vol. 119, pp. 62–72, 2018.
- [29] S. K. Konda and A. Chen, "Palladium based nanomaterials for enhanced hydrogen spillover and storage," *Biochem. Pharmacol.*, vol. 19, no. 2, pp. 100–108, 2016.
- [30] F. Ke, L. G. Qiu, Y. P. Yuan, F. M. Peng, X. Jiang, A. J. Xie, Y. H. Shen, and J. F. Zhu, "Thiol-functionalization of metal-organic framework by a facile coordination-based postsynthetic strategy and enhanced removal of Hg<sup>2+</sup> from water," *J. Hazard. Mater.*, vol. 196, pp. 36–43, 2011.
- [31] H. Zhou, J. Zhang, J. Zhang, X. Yan, X. Shen, and A. Yuan, "High-capacity room-temperature hydrogen storage of zeolitic imidazolate framework/graphene oxide promoted by platinum metal catalyst," *Int. J. Hydrogen Energy*, vol. 40, no. 36, pp. 12275–12285, 2015.
- [32] J. Liu, H. Jeong, J. Liu, K. Lee, J.Y. Park, Y. H. Ahn, and S. Lee, "Reduction of functionalized graphite oxides by trioctylphosphine in non-polar organic solvents," *Carbon N. Y.*, vol. 48, pp. 2282–2289, 2010.

- [33] S. Loera-serna, M. A. Oliver-Telentino, M. L. Lopez-Nunez, A. Santana-Cruz, A. Guzman-Vargas, R. Cabrera-Sierra, H. I. Beltran, and J. Flores, "Electrochemical behavior of [ Cu<sub>3</sub> ( BTC )<sub>2</sub> ] metal – organic framework : The effect of the method of synthesis," *J. Alloys Compd.*, vol. 540, pp. 113–120, 2012.
- [34] J. Shen, Y. Hu, M. Shi, X. Lu, C. Qin, C. Li, and M. Ye , "Fast and Facile Preparation of Graphene Oxide and Reduced Graphene Oxide Nanoplatelets," *Chem. Mater.* ,vol. 21, pp. 3514–3520, 2009.
- [35] F. Mindivan, "The synthesis and characterization of graphene oxide ( GO ) and reduced graphene oxide ( rGO )," *Machines , Technologies , Materials.*, vol. 6, pp. 32-35, 2017.
- [36] H. Guo, Y. Zhang, Z. Zheng, H. Lin, and Y. Zhang, "Facile one-pot fabrication of Ag@MOF(Ag) nanocomposites for highly selective detection of 2,4,6-trinitrophenol in aqueous phase," *Talanta*, vol. 170, pp. 146–151, 2017.
- [37] P. Druska, "A surface analytical examination of passive layers on cu / ni alloys : part i . alkaline solution," *Corros. Sci.*, vol. 38, pp. 10292–10299, 1996.
- [38] L. Zhang, C. Ye, X. Li, Y. Ding, H. Liang, G. Zhao, and Y. Wang, "A CuNi / C Nanosheet Array Based on a Metal – Organic Framework Derivate as a Supersensitive Non-Enzymatic Glucose Sensor," *Nano-Micro Lett.*, vol. 28, pp. 1-10, 2018.
- [39] C. Nila and I. Gonzilez, "Thermodynamics of Cu-H , SO , -Cl--H , 0 and Cu-NH & I-H 2O based on predominance-existence diagrams and Pourbaix-type diagrams," *Hydrometallurg .*, vol. 42, pp. 63–82, 1995.
- [40] T. Kokulnathan, T. S. K. Sharma, S. M. Chen, T. W. Chen, and B. Dinesh, "Ex-situ decoration of graphene oxide with palladium nanoparticles for the highly sensitive and selective electrochemical determination of chloramphenicol in food and biological samples," *J. Taiwan Inst. Chem. Eng.*, vol. 0, pp. 1–13, 2018.
- [41] M. Jafarian, F. Forouzandeh, I. Danaee, and F. Gobal, "Electrocatalytic oxidation of glucose on Ni and NiCu alloy modified glassy carbon electrode," *J. Solid State Electrochem.*, vol. 13, pp. 1171–1179, 2009.
- [42] D. N. Li, A. J. Wang, J. Wei, Q. L. Zhang, and J. J. Feng, "Facile synthesis of

- flower-like Au@AuPd nanocrystals with highly electrocatalytic activity for formic acid oxidation and hydrogen evolution reactions,” *Int. J. Hydrogen Energy*, vol. 42, pp. 19894–19902, 2017.
- [43] B. E. Conway, “Electrochemical proton transfer and cathodic hydrogen evolution,” *Sci. Rev.*, vol. 71, pp. 479–509, 2017.
- [44] F. Safizadeh, E. Ghali, and G. Houlachi, “ScienceDirect Electrocatalysis developments for hydrogen evolution reaction in alkaline solutions : A Review,” *Int. J. Hydrogen Energy*, vol. 40, pp. 256–274, 2014.
- [45] J. Chen, G. Xia, P. Jiang, Y. Yang, R. Li, R. Shi, J. Su, and Q. Chen, “Active and Durable Hydrogen Evolution Reaction Catalyst Derived from Pd-Doped Metal-Organic Frameworks,” *ACS Appl. Mater. Interfaces*, vol. 8, pp. 13378–13383, 2016.
- [46] C. F. Leung, Y. Z. Chen, H. Q. Yu, S. M. Yiu, C. C. Ko, and T. C. Lau, “Electro- and photocatalytic hydrogen generation in acetonitrile and aqueous solutions by a cobalt macrocyclic Schiff-base complex,” *Int. J. Hydrogen Energy*, vol. 36, pp. 11640–11645, 2011.
- [47] J. Kubisztal, A. Budniok, and A. Lasia, “Study of the hydrogen evolution reaction on nickel-based composite coatings containing molybdenum powder,” *Int. J. Hydrogen Energy*, vol. 32, pp. 1211–1218, 2007.
- [48] R. Nivetha, S. Chella, P. Kollu, S. K. Jeong, A. Bhatnagar, and N. G. Andrews, “Cobalt and nickel ferrites based graphene nanocomposites for electrochemical hydrogen evolution,” *J. Magn. Magn. Mater.*, vol. 448, pp. 165–171, 2018.
- [49] W. Shen, B. Wu, F. Liao, B. Jiang, and M. Shao, “ScienceDirect Optimizing the hydrogen evolution reaction by shrinking Pt amount in Pt-Ag / SiNW nanocomposites,” *Int. J. Hydrogen Energy*, vol. 42, pp. 15024–15030, 2017.
- [50] Y. Gao, D. Ma, C. Wang, J. Guan, and X. Bao, “Reduced Graphene Oxide as Catalyst for Hydrogenation of Nitrobenzene,” *Structure*, vol. 47, pp. 2432–2434, 2011.
- [51] L. Giordano, B. Han, M. Risch, W. T. Hong, R. R. Rao, K. A. Stoerzinger, y. Shao-Horn, “pH dependence of OER activity of oxides: Current and future perspectives,” *Catal. Today*, vol. 262, pp. 2-10, 2016.

## CHAPTER SIX

### GENERAL DISCUSSION, CONCLUSIONS AND RECOMMENDATIONS

---

#### 6.1. GENERAL DISCUSSION AND CONCLUSIONS

This chapter deals with general discussion and conclusions of the results presented in the study and make further recommendations for future electrocatalysts in hydrogen absorption and storage through hydrogen evolution reaction, electrochemical charging/discharge and gas phase storage. This study has been directed towards the development of hybrid materials based on palladium supported graphene oxide/metal organic framework prepared using electroless palladium deposition on GO followed by impregnation method of Pd@GO and MOF. The overall goal of this dissertation was to develop the most optimal, efficient and viable novel electrocatalyst composite in order to increase the scope of these MOF composite chemistry for application in different areas such as; electrocatalysis, hydrogen evolution reaction and in the development of hydrogen fuel cell devices in the future. The electrocatalyst based on MOF materials studied in this work were identified and chosen on the basis of their excellent properties. For example, graphene oxide and its derivative composites exhibit thermal, optical and electrical properties of semiconductors, whilst retaining attractive adsorption properties and processing advantages of rich carbon based compound. Furthermore, carboxylate, epoxide and 6-carbon rings play important role in efficiency of the GO for many applications. They also exhibit favourable electrochemical redox properties such as being able to undergo electron transfer reactions at potentials that are accessible. On the other hand, MOFs hold a greater promise as potential material due to their large surface area, highly porous structure and H<sub>2</sub> binding dominated by van der Waals interactions. MOFs are 2D-, 3D dimensional inorganic-organic hybrid compounds built from metal ions and organic ligands by coordination bonds and are class of crystalline porous solids. MOFs possess high surface area and high pore volumes in uniformly sized pores as well as high metal content. Based on these properties, MOFs have been used in various

applications such as energy storage, CO<sub>2</sub> adsorption, hydrocarbon adsorption/separation, catalysis and sensors.

The dissertation was outlined into six chapters. Chapter one (introduction) was based on the background of renewable energy in general. Especially on aspects that play vital important role in hindering commercialisation of hydrogen as an energy carrier in fuel cell technology. The problem statement and hypothesis were derived in order to place hydrogen energy into practical applications where MOF was identified as an alternative electrocatalyst. This was supported by well organised aim and objectives to develop a palladium supported graphene oxide/metal organic framework composites for hydrogen fuel cell applications (hydrogen production and storage) through electrochemical HER studies. In depth literature survey was outlined in Chapter two based on graphene oxide and metal organic framework nanocomposite for hydrogen technology: a review. Hydrogen technology concepts were thoroughly reviewed, studying the traditional hydrogen production and storage mechanisms. In addition, materials of interest in this study (graphene oxide and metal organic framework) were extensively discussed to fully understand their physical and chemical properties. Furthermore, graphene oxide and metal organic framework composite for hydrogen evolution reaction were reviewed in detail. The analytical techniques were presented in Chapter three where the short background and objectives of using the in this study.

The first approach taken in Chapter four involves preparation of graphene oxide/metal organic framework nanocomposites with improved electrocatalytic efficiency for hydrogen production and storage. GO was synthesised using modified Hummer's method whereby black product was obtained as an indicative of typical GO material. On the other hand, MOF was synthesised using hydrothermal method which allows precise control over the size, shape distribution, highly crystalline solid on the nano-/microscale, and controlled morphology. The formation of composite was deduced by the appearance of new bands or disappearance of peaks in the FTIR spectra. It was seen in the spectrum of the composite that the peaks at around 1583 and 1336 cm<sup>-1</sup>

of the GO/MOF composite can be assigned to the presence GO and MOF, respectively. Furthermore, the influences of GO on the crystalline structure and thermal of MOF surface, were systematically investigated using XRD and TGA/DSC, respectively. The scanning electron microscopy/Energy dispersive spectroscopy (SEM/EDS) and high resolution transmission electron microscopy/Energy dispersive x-ray spectroscopy (HRTEM/EDX) confirmed the presence of octahedral structure of MOF in the GO sheet-like structure and elemental composition of the synthesised materials. The presence of GO on the MOF surface enhanced the HER performance whereby the electrocatalytic activity of the GO/MOF composite is higher than that of the neat MOF. Furthermore, the HER properties were based on the evaluation of Tafel slope, charge-transfer coefficients and TOFs. The performance of the proposed electrolytic system for electrochemical HER by Tafel parameters and TOFs showed a drastic increase in catalytic H<sub>2</sub> production in the composite through the Volmer reaction coupled with one of the mechanisms.

Final approach was taken in Chapter five whereby a novel Pd-supported graphene oxide/metal organic frameworks (Pd@GO/MOF) composite was synthesised by first electroless Pd deposition on GO followed by impregnation method of directly mixing of Pd@GO and MOF. The influences of Pd and GO on the morphology and crystalline structure of MOF surface, as well as resulting electro-catalytic activity in hydrogen evolution and TOFs were systematically investigated and discussed. The presence of Pd on the MOF surface can significantly increase the HER exchange current density, and reduce the electrochemical reaction resistance. The presence GO as a support observed to enhance the HER properties in the Pd@GO/MOF as compared to neat MOF. The observed promotional role of incorporated Pd is ascribed to possible synergetic effects between the GO particles and MOF matrix, leading to a facilitation of H<sub>ads</sub> migration. Furthermore, the Tafel slope, TOFs and charge-transfer coefficients showed that the rate determining step of HER on the studied MOF, and Pd@GO/MOF composite may be also the Volmer reaction or the Volmer reaction coupled with one of other two reactions as supported by logarithm of current vs pH and Pourbaix diagram. The presence of Pd showed the enhancement of hydrogen spillover for

hydrogen absorption and desorption and also leading to high TOF value of 7.8 molecule of hydrogen produced per second. These demonstrated that the Pd@GO/MOF nanocomposites are suitable materials for electrocatalytic hydrogen production and storage for hydrogen fuel applications. Since, there is involvement of hydrogen evolution reaction which undergoes in the different HER mechanisms, Volmer reaction or the Volmer reaction coupled with one of other two reactions. These mechanisms illustrate that the hydrogen gas may be produced in acidic condition followed by adsorption of hydrogen atoms by the composite material as part of hydrogen storage.

## **6.2. RECOMMENDATIONS FOR FUTURE WORK**

Further improvement of the electrocatalyst materials will aid towards an increase of hydrogen productivity and efficiency. An important milestone in the work was to develop other alternative electrocatalyst which are to MOF material as HER material. X-ray photon spectroscopy will be of a good handy to veal the interaction mechanism of GO and Pd@GO on the MOF and also the reveal the electrochemical hydrogen evolution on the electrocatalyst before and after HER studies. The CV voltammograms revealed good electrochemical properties and the HER studies however it will of a good idea to support with linear square wave voltammograms. It was clear from the work that the HER responses obtained in neat MOF and GO were significantly low when compared to the lead GO/MOF and Pd@GO/MOF composites. Furthermore, since the GO/MOF and Pd@GO/MOF in the conventional solvents such DMSO or DMF showed to be insoluble and partially soluble, respectively and completely decomposed in concentrated acid. However, it would be useful to consider other solvents that can be used for homogeneous HER applications.

Moreover, low HER responses of neat MOF and GO have also been attributed to instability of the radical cations produced during HER experiment in acidic condition, two alternatives can potentially be explored in the future to improve the HER response.

The first is to consider alkaline solution as the alternative solvents for HER studies for practical application of water electrolysis. The second strategy is to investigate the HER of GO/MOF, and Pd@GO/MOF composites films on interdigitated electrodes in the future through electrochemical polymerisation as heterogeneous HER studies. This is because the results showed that the cross reaction between the GO/MOF and Pd@GO/MOF composites radicals and the electrolytic solution is an important contributing process which influences the HER performance as reflected in the scan rate dependent studies. In-depth studies of the effect of increased amount of MOF in the composite up until they have the same proportion on the catalytic activity of the material will also help in understand the role of MOF on the matrix. Even though the materials showed good catalytic activities, stability and durability of the materials during HER studies are very important for practical application of these materials.

The GO/MOF and Pd@GO/MOF composites showed good HER performance however quantification of the amount of hydrogen produced will be important. This can be achieved by coupling CV experiments with gas chromatography or mass spectroscopy to form a hyphenated instrument that can reveal the amount of gases in the HER. Furthermore, the effect of varying the amount of GO and Pd@GO from 5 to 50 loading weight percentage while MOF remains fixed on the catalytic performance of the material will be of a good use to reveal the role of GO and Pd@GO on the MOF surface. The Photo-catalytic hydrogen evolution reaction studies of these materials are an alternative route to be employed in future study the HER. Furthermore, it will be noteworthy to consider coupling photo-and-electro-catalytic hydrogen evolution studies in future. The in-depth electrochemical hydrogen absorption and desorption (charge and discharge) to evaluate the hydrogen storage capacity in terms of weight percentage. Furthermore, the gas phase hydrogen absorption by these materials will be of a good idea to correlate the relationship between electrochemical and gas phase hydrogen storage.

In general, most of the HER electrocatalysts function only under alkaline conditions. Therefore, HER catalysts that can efficiently work a tall pH values are highly desirable.

The HER mechanism for some of the materials are well known but there are majority of materials whose mechanism are still not fully understandable, and it is more than ideal to know the mechanism of all these materials in order to improve their activity. Opportunities come with challenges and we believe that HER will play a very important role to solve the problem of energy. As for the process and application, the sustainable energy utilisation in HER is vital for the practical units and devices. Specifically, using cost-effective triboelectric nano-generator, which can utilise and convert the sustainable mechanical energy (such as blue energy, wind, and rain) to electricity, as self-powered unit is a very perspective approach to obtain the sustainably self-powered HER system in the near future. In addition, clearly, great progress is being made in the nonprecious metal HER field recently. Much help has come from the computational tools available today, and there is hope that we may find a material that essentially matches platinum as an HER catalyst. This indicates that the future research focus will shift toward achieving year-long catalyst stability, scalable synthesis techniques, and tolerance toward a real-world electrolyte (unclean electrolyte!) in the years to come.

## SUPPORTING INFORMATION

### PALLADIUM SUPPORTED GRAPHENE OXIDE BASED METAL ORGANIC FRAMEWORK NANOCOMPOSITE WITH IMPROVED ELECTROCATALYTIC EFFICIENCY FOR HYDROGEN EVOLUTION REACTION

---

#### S1: EXPERIMENTAL SECTION

Pd@MOF and Pd@GO were prepared by electroless Pd plating method [1-3]. Briefly, the plating solution was prepared by initially dissolving 1 g of PdCl<sub>2</sub> in 2.0 mL of 32% HCl and 10 mL of ultra-pure water, then heated at 50 °C for 30 min with constant stirring at 300 rpm. After complete dissolution of PdCl<sub>2</sub>, 80 mL of 28% NH<sub>4</sub>OH and 27 g of NH<sub>4</sub>Cl were added respectively. The mixture was then transferred to 500 mL volumetric flask and made up to the mark with ultra-pure water. The electroless plating bath, containing 25 mL of 5 g.L<sup>-1</sup> of sodium hypophosphite as reducing agent to initiate the reaction and 2.5 g batch of MOF or GO was subjected to constant agitation (300 rpm) for 30 min at 50 °C in a separate bath to avoid decomposition during storage of the bath. Finally, the 25 mL of plating solution was added into the bath solution and the mixture was agitated for 30 min to allow the plating of Pd to the surface of the composite. The mixture was filtered, washed with ultra-purewater and dried for overnight at 80 °C.

## S2: RESULTS

### S2.1: Structural characterisation

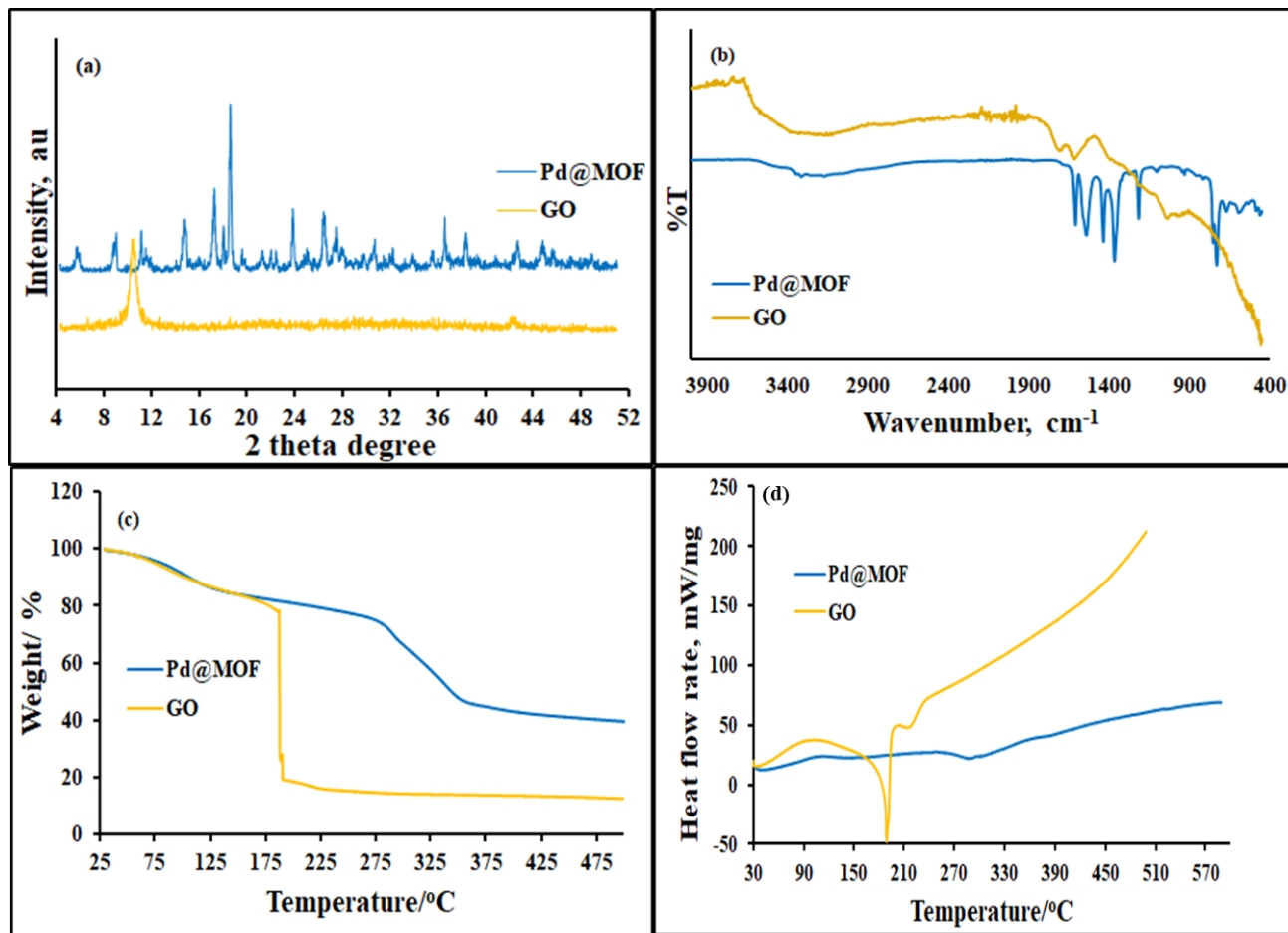


**Figure S1:** (a). XRD patterns, (b). FTIR spectra, (c). TGA and (d). DSC curves of GO and Pd@MOF.

## S2.2: Morphological characterisation

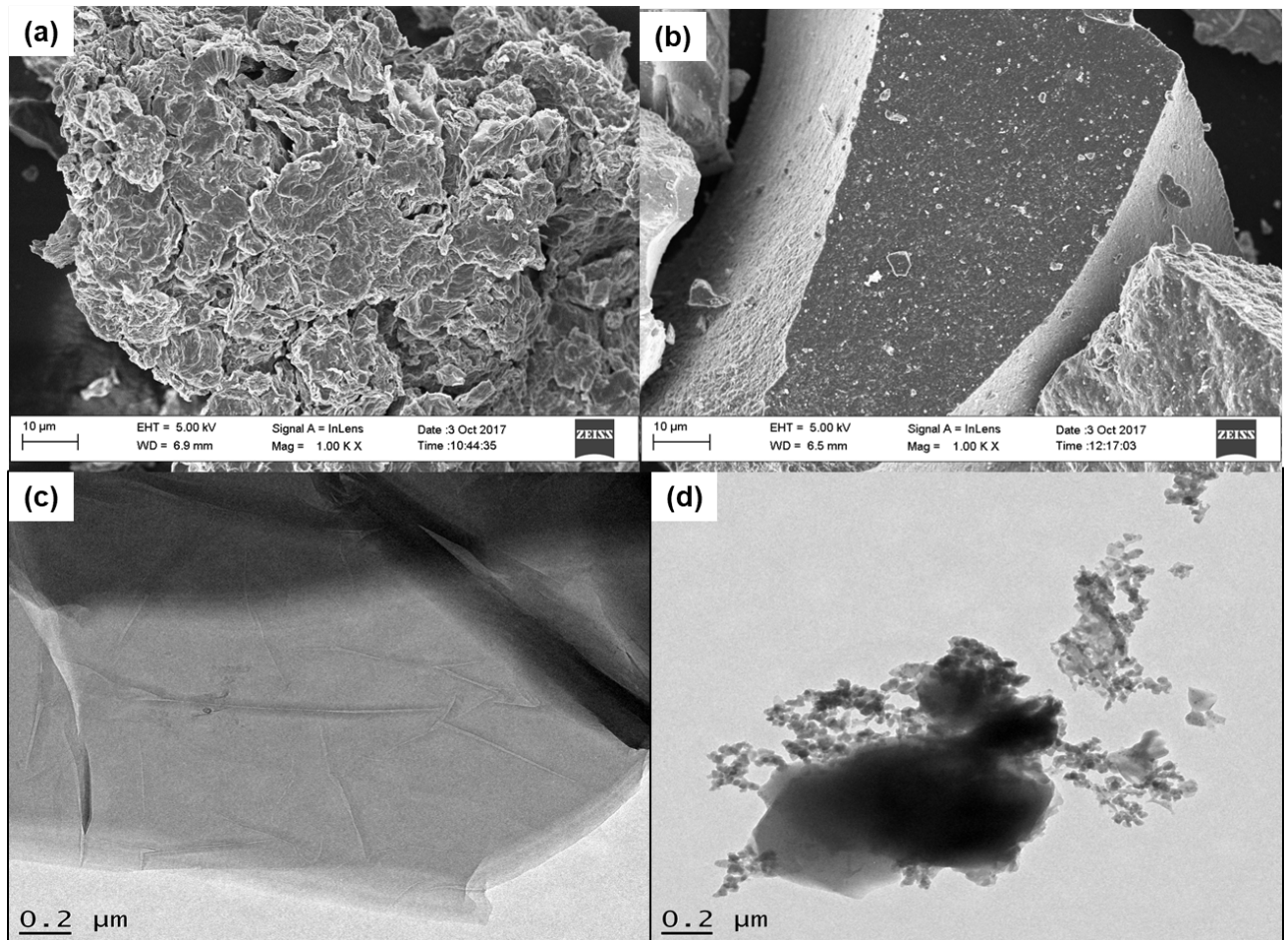


**Figure S2:** FE-SEM images of (a).GO and (b).Pd@MOF and TEM images of (c).GO and (d) [Pd@MOF](#)

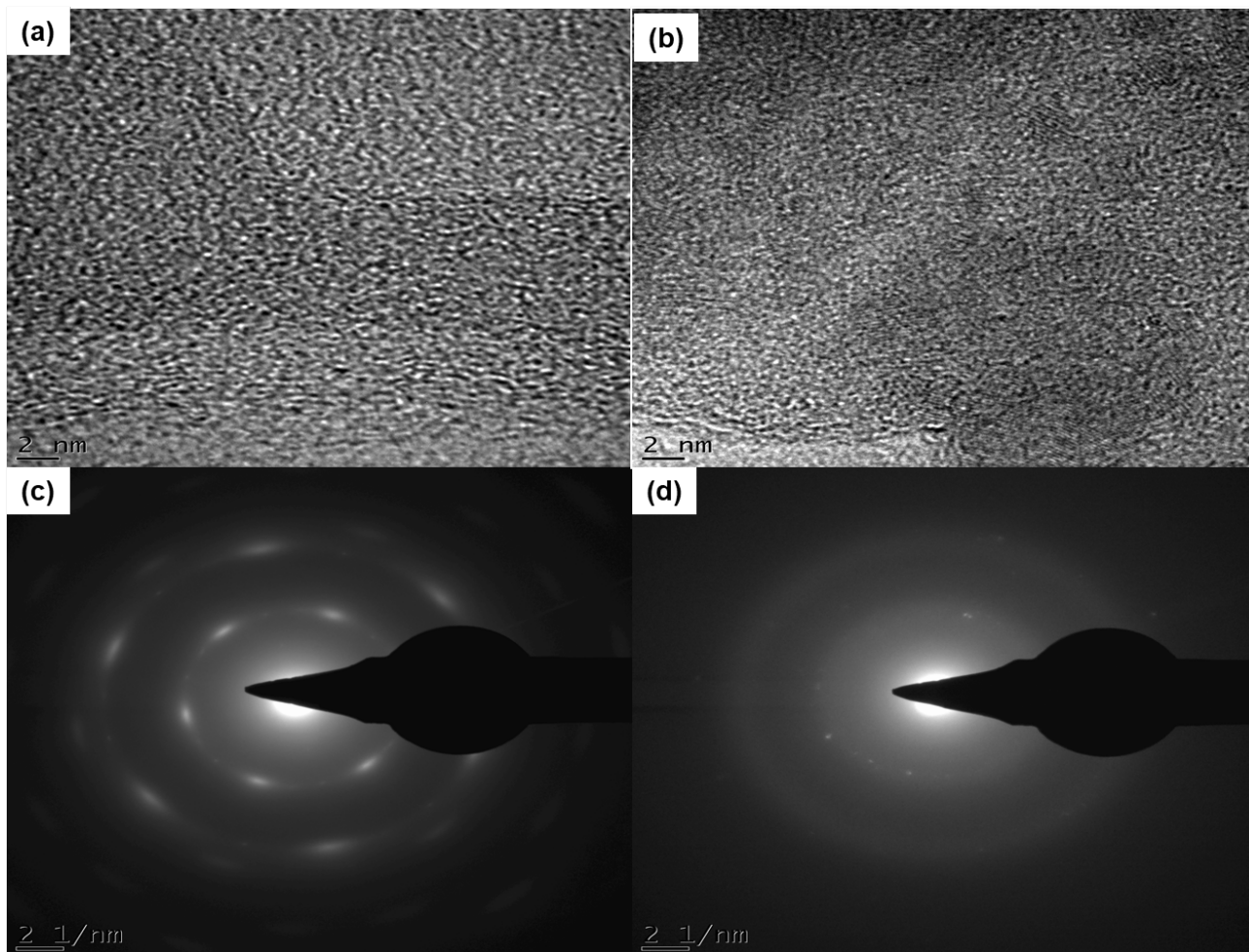


**Figure S3:** HR-TEM images of (a).GO and (b).Pd@MOF and SAED images of (c).GO and (d).Pd@MOF

### S2.3: Electrochemical characterisation

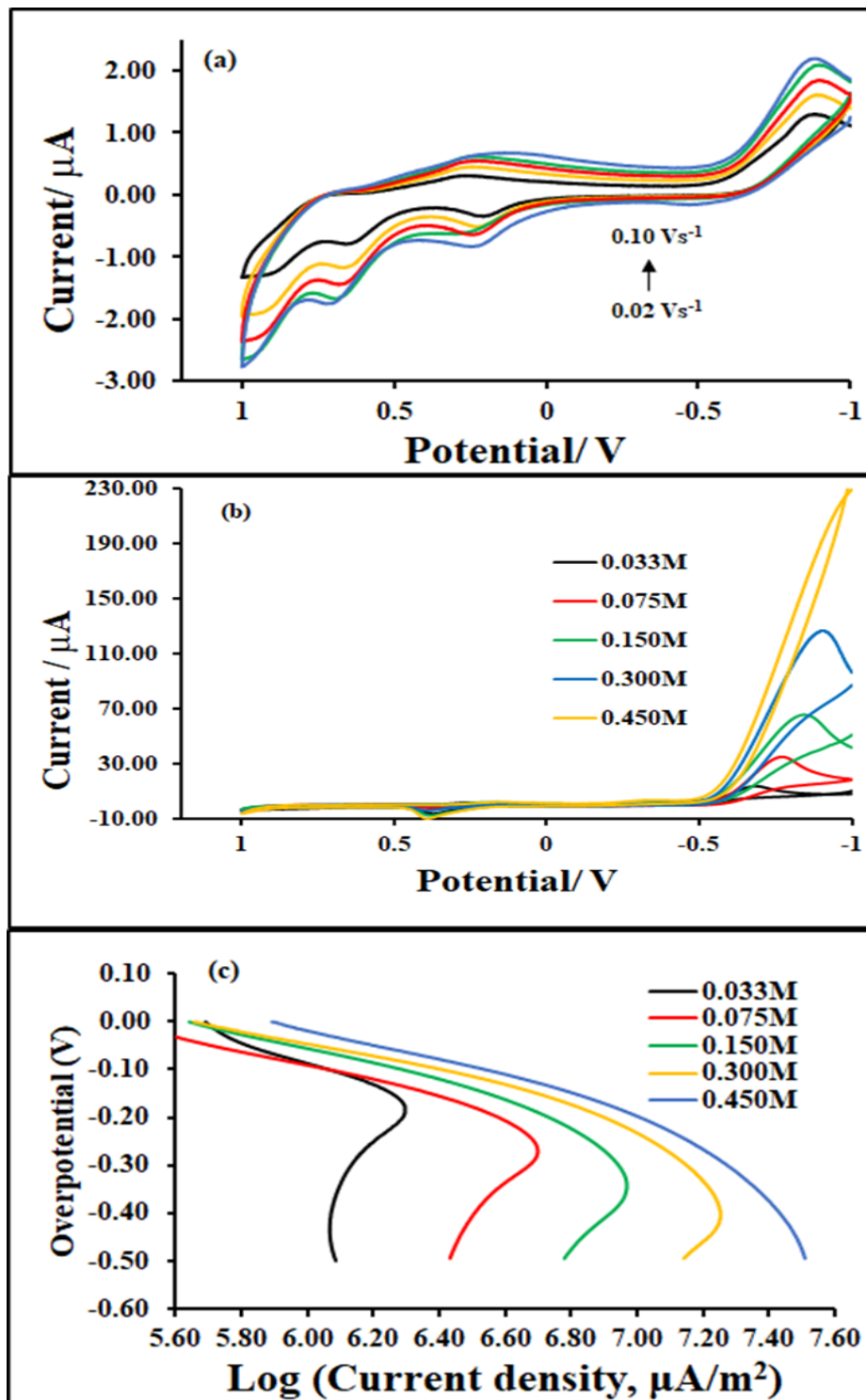


**Figure S4:** (a). CV curves at different scan rates (0.02-0.1  $\text{v.s}^{-1}$ ), (b). CV curves in different concentration of hydrogen source (0.033-0.450  $\text{mol.L}^{-1}$   $\text{H}_2\text{SO}_4$ ) at 0.10  $\text{Vs}^{-1}$

and (c). Tafel plots in different concentrations of H<sub>2</sub>SO<sub>4</sub> for Pd@MOF on Au electrode in 0.1 mol.L<sup>-1</sup> TBAP/DMSO electrode system.

### S3. REFERENCES

1. G. R. Monama, S. B. Mdluli, G. Mashao, M. D. Makhafola, K. E. Ramohlola, K. M. Molapo, M. J. Hato, K. Makgopa, E. I. Iwuoha, and K. D. Modibane, "Palladium deposition on copper(II) phthalocyanine/metal organic framework composite and electrocatalytic activity of the modified electrode towards the hydrogen evolution reaction," *Renew. Energy*, vol. 119, pp. 62–72, 2018.
2. M. Lototsky, K.D. Modibane, M. Williams, Ye Klochko, V. Linkov, B.G. Pollet, "Application of surface-modified metal hydrides for hydrogen separation from gas mixtures containing carbon dioxide and monoxide" *J. Alloys Compd.*, vol. 580, pp. S382-S385, 2013.
3. K.D. Modibane, M. Williams, M. Lototsky, M.W. Davids, Ye Klochko, B.G. Pollet, "Poisoning-tolerant metal hydride materials and their application for hydrogen separation from CO<sub>2</sub>/CO containing gas mixtures" *Int. J. Hydrogen Energy*, vol. 38, pp. 9800-9810, 2013.

## APPENDIX 1



Modibane, Kwena <kwena.modibane@ul.ac.za>

---

### IntechOpen - Minor Review Requested - MOFs

---

Dolores Kuzelj <kuzelj@intechopen.com>

Mon, May 28, 2018 at 2:17 PM

To: Kwena Desmond Modibane <kwena.modibane@ul.ac.za>

Dear Dr. Modibane,

I am pleased to inform you that your chapter titled "Graphene oxide/Metal Organic Frameworks (CuPc/MOF) Nanocomposite with Improved Electrocatalytic Efficiency for Hydrogen Production and Storage," submitted to the book under the working title "MOFs," has been reviewed. The Editor has accepted your full chapter but requested that you implement some minor changes outlined in the review comments.

In the attachment you will find recommendations/suggestions for changes from the Editor(s) that would improve the overall quality of your chapter.

Current Step: Upload Revision

Upload your revised chapter on your Author Panel incorporating the review comments within the next 3 days.

Next Step:

Language Copyediting and Typeset Proof. Once your revision is uploaded, your paper will undergo specialized proofreading and editing to improve grammar, spelling, style, and accuracy at no additional charge, while our Technical Editors prepare your chapter for online publication.

Upcoming Promotion!

I would also like to take this opportunity to inform you of an upcoming promotion. When your full chapter is accepted for publication you can pre-order your book and get one print copy for free on the first order you place. All contributing authors can benefit from this exclusive promotion available only through your Author Panel.

If you have any additional questions or concerns, do not hesitate to contact me.

Cordially,

Dolores Kuzelj  
Author Service Manager

---

IntechOpen  
The Shard, 32 London Bridge Street, London SE1 9SG, United Kingdom  
+38551688994  
[www.intechopen.com](http://www.intechopen.com)

INTECHOPEN LIMITED, Registered in England and Wales No. 11086078

We are IntechOpen, the first native scientific publisher of Open Access books

---

## APPENDIX 2

3<sup>rd</sup> International Hydrogen Technologies Congress (IHTEC-2018), March 15-18, 2018, Alanya/Antalya, Turkey

---

### Fabrication of graphene oxide/metal organic framework nanocomposite with improved electrocatalytic activity for hydrogen evolution reaction

Emmanuel I. Iwuoha<sup>2</sup>, Mogwasha Daphney Makhafole<sup>1</sup>, Kabelo Edmond Ramohlola<sup>1</sup>, Thabang Ronny Somo<sup>1</sup>, Gobeng Release Monama<sup>1</sup>, Mpitloane Joseph Hato<sup>1</sup>, Kerileng M. Molapo<sup>2</sup>, Kwena Desmond Modibane<sup>1,\*</sup>

<sup>1</sup>University of Limpopo, Private Bag X1106, Sovenga, 0727, South Africa,

<sup>2</sup>University of the Western Cape, Private Bag X17, Bellville, 7535, South Africa

\*E-mail addresses: [kwena.modibane@ul.ac.za](mailto:kwena.modibane@ul.ac.za)

#### Abstract

In this study, a composite of graphene oxide (GO) and HKUST-1 type of metal organic framework (MOF) was synthesized by impregnation method, and its application as electrocatalyst for hydrogen production via hydrogen evolution reaction (HER) was studied. X-ray diffraction (XRD), Fourier Transform Infrared spectroscopy (FTIR), Scanning electron microscopy (SEM) and Transmission electron microscopy (TEM) were used to characterize GO, MOF, and GO/MOF catalysts. The XRD and FTIR results of the composite showed the phases and characteristic bands for both parent materials as indicative of the composite. The SEM and TEM images revealed the presence of octahedral structure of MOF in the GO sheet-like structure. The performance of the proposed electrolytic system for electrochemical HER was studied by cyclic voltammetry and Tafel plots. The results showed that the addition of GO/MOF in the electrolytic system reveals better catalytic characteristics such as highest catalytic activity and lowest onset potential.

**Keywords:** Hydrogen evolution reaction, Metal organic framework, Graphene oxide

#### I. Introduction

In developing countries, energy supplies are mainly based on combustion of fossil fuels accompanied by a number of environmental problems such as green house emission. In order to overcome those challenges, renewable energies are needed, since the supply of non-renewable energy sources is finite. Owing to its excellent properties (i.e. light weight and high energy density), hydrogen has been designated as the best energy carrier. However, there are significant challenges hindering the large scale applications and commercialization of hydrogen fuel especially in mobile transportation. These problems include the lack of safe handling and effective methods for hydrogen production and storage (Salehabadi, Salavati-Niasari and Gholami, 2017). With this being noted, electrochemical reduction of water is considered as one of the promising route for hydrogen production due to its simplicity and economical way to produce hydrogen with large and quantity high purity. Even though in the electrochemical studies platinum (Pt) is known as an excellent electrode for hydrogen generation, it is limited by its high cost and low abundance (Satyapal *et al.*, 2007). MOFs have shown to be very promising HER electrocatalysts mainly due their extremely large surface area, high porosity, adjustable pore sizes as well as defined hydrogen occupation sites (Ramohlola *et al.*, 2017). Unfortunately, these MOF materials have been reported to exhibit several weak points such as the relative low stability in solution and conductivity hampering their realistic applications. Combining MOF materials with other substrates has been proposed in order to mitigate the above-mentioned drawbacks (Zhou *et al.*, 2013). Graphene oxide (GO) with rich functional groups is very suitable to construct graphene-based hybrid composites (Zhou *et al.*, 2015). Petit and Badosz (2015) have reported the formation of GO/MOF composites using hydrothermal method, where the synergetic effect between MOF units and GO layers was responsible for enhanced adsorption amounts compared to the parent material. To the best of our knowledge, there are no studies reported on HER using composite of GO/MOF prepared by impregnation procedure. Hence in this study, a composite of MOF with GO (GO/MOF) was prepared through impregnation method and applied for electrochemical hydrogen generation.

#### II. Experimental Set-up and Procedure

GO/MOF composite (Scheme 1) was prepared through impregnation method of directly mixing of GO and MOF. Briefly, 0.1 g of as-synthesized MOF sample was dehydrated at 150 °C for 1 hour. It was then suspended in 10 mL DMF. In a separate beaker, 0.1 g of graphene oxide was dispersed in 1.4 mL DMF, and then the two mixtures were mixed together and stirred magnetically for 24 hours at 50 °C. Electrochemical measurements were carried out using EPSILON electrochemical workstation. The data was collected using a conventional three-electrode set-up with gold electrode (3 mm diameter, 0.071 cm<sup>2</sup> area) as a working electrode, Pt wire as a counter electrode and Ag/AgCl wire as a reference electrode. Repetitive scanning of the solutions of MOF, GO and MOF composite (~2.0x10<sup>-3</sup> mol.L<sup>-1</sup>) was measured from -1.0 to 1 V at the scan rate of 0.02 - 0.10 Vs<sup>-1</sup>. Electrochemical experiments were performed in 10 ml of 0.1 M TBAP/DMSO electrolytic system. HER studies were done using different concentrations of 0.03 - 0.45 M H<sub>2</sub>SO<sub>4</sub> as H<sub>2</sub> source in 0.1 M TBAP/DMSO system and ~2.0x10<sup>-4</sup> mol.L<sup>-1</sup> of MOF, GO and MOF composite composite as electrocatalysts.

## APPENDIX 3

3<sup>rd</sup> International Hydrogen Technologies Congress (IHTEC-2018), March 15-18, 2018, Alanya/Antalya, Turkey

### Copper(II)phthalocyanine/metal organic frameworks (CuPc/MOF) composite with improved electrocatalytic efficiency for hydrogen production

Emmanuel I. Iwuoha<sup>2</sup>, Gobeng Release Monama<sup>1</sup>, Kwena Desmond Modibane<sup>1,\*</sup>, Kabelo Edmond Ramohlola<sup>1</sup>, Kerileng Mildred Molapo<sup>2</sup>, Mpitloane Joseph Hato<sup>1</sup>, Mogwasha Daphney Makhafola<sup>1</sup>, Gloria Mashao<sup>1</sup>, Siyabonga Beizel Mdluli<sup>2</sup>,

<sup>1</sup>University of Limpopo, Private Bag X1106, Sovenga, 0727, South Africa,

<sup>2</sup>University of the Western Cape, Private Bag X17, Bellville, 7535, South Africa

\* E-mail: [kwena.modibane@ul.ac.za](mailto:kwena.modibane@ul.ac.za)

#### Abstract

The hydrogen evolution reaction (HER) of CuPc/MOF composite was investigated for hydrogen production. The SEM and EDS analyses showed that CuPc was incorporated into MOF through impregnation method. The electrochemical measurements were studied using cyclic voltammetry (CV) and it was found that CuPc/MOF composite exhibited favourable catalytic activity for HER. The Tafel slope value of the CuPc/MOF composite was found to be 185.3 mV.dec<sup>-1</sup> and noticeably lower than that of the bare MOF (236.7 mV.dec<sup>-1</sup>) at 0.30 M of the acid, and the charge transfer coefficients are all close to 0.5, suggesting the Volmer reaction coupled with either Heyrovsky or Tafel reaction for hydrogen production. The exchange current density, ( $i_0$ ) of all the samples increased with increasing the concentration of the hydrogen source. Nonetheless, the CuPc/MOF composite showed a higher  $i_0$  as compared to bare MOF. These observations provide a platform to synthesize promising low-cost CuPc/MOF electrocatalyst with high efficiency and excellent electrocatalytic performance for HER.

**Keywords:** Metal organic frameworks; Phthalocyanine; Hydrogen evolution reaction

#### I. Introduction

In recent years, fossil fuels are considered as the main energy resources. Nonetheless, they possess some disadvantages such as limited resources, global warming and environmental pollution. A numerous efforts have been considered to use alternative energy sources instead of fossil fuels to circumvent these problems. In this context, hydrogen fuel cell technology is one of the promising technology for sustainable energy applications owing to its various advantages such as recyclability, pollution-free and fuel efficiency Ren et al (2013). In addition, H<sub>2</sub> gas yields more energy, which is about 2.75 times greater as compared to traditional gasoline based energy resources. However, the problem for practical usage of H<sub>2</sub> gas as an energy carrier lies in the production and storage technology Ehsan and Wahid (2016). Up to this stage, electrochemical reduction of water is preferred as an effective and alternative route to produce hydrogen with high purity and in large quantity because of its simplicity and economical way Ren et al (2013). A number of porous materials such as carbon nanotubes, metal organic frameworks (MOFs), graphite nanofibers, zeolites and activated carbon were proposed as candidates for HER Ren et al. (2013) and Benck (2014). Among these materials, MOFs hold a greater promise as potential candidates in the design of advanced multifunctional materials due to their unique structures Zheng and Jiao (2017). MOFs are inorganic-organic hybrid compounds built from metal ions or clusters and organic ligands by coordination bonds, providing highly crystalline porous structures with large surface area, high pore volume as well as uniform nanoscale cavities Ramohlola et al. (2017). Thus, MOFs have been used in various applications such as energy storage, CO<sub>2</sub> adsorption, hydrocarbon adsorption/separation, catalysis, advanced sorbents for solids extraction and sensors. However, MOFs possess some drawbacks as HER material because of H<sub>2</sub> embrittlement, moisture instability and poor H<sub>2</sub> adsorption and desorption at ambient conditions Ramohlola et al. (2017). To the best of our knowledge, there are no studies reported on the formation and observation of HER using CuPc incorporated on the MOF surface to prepare an effective electrocatalyst. Therefore, this study reports on the synthesis, characterization and application of the hybrid-hybrid CuPc/MOF composite as a suitable electrocatalyst for HER.

#### II. Experimental Set-up and Procedure

MOF was synthesized following our recent published work Ramohlola et al (2017). In brief, 4.5 mmol of Cu(NO<sub>3</sub>)<sub>2</sub>·3H<sub>2</sub>O was dissolved in 10 ml of distilled water and then mixed with 0.525 g (2.5 mmol) of H<sub>3</sub>BTC dissolved in 10 ml of ethanol. The mixture was stirred for 30 min and then transferred into a 23 ml Teflon stainless-steel autoclave and sealed to react for 36 hours at 120 °C in thermostatic drying oven. Copper phthalocyanine (CuPc) was synthesised from phthalimide according to previous method reported elsewhere Chiang et al. (2012). Typically, a mixture of phthalimide (3.00 g, 0.0200 mol) in the presence of excess urea (3.00 g, 0.0500 mol), ammonium heptamolybdate (0.0800g, 0.0600 mmol) and copper nitrate (1.40 g, 0.0058 mol) in nitrobenzene (15.00 mL) was refluxed for 5 hours at 180 °C to give a target compound. CuPc/MOF composite (Scheme 1) was prepared by

## APPENDIX 4

---



Modibane, Kwena <kwena.modibane@ul.ac.za>

---

### **IntechOpen - Thank you for Submitting your Full Chapter - Polyaniline - From Synthesis to Practical Applications**

---

Ms. Sara Debeuc <debeuc@intechopen.com>

Mon, Jun 18, 2018 at 8:07 PM

To: Mpitloane Joseph Hato <mpitloane.hato@ul.ac.za>

Cc: Kwena Desmond Modibane <kwena.modibane@ul.ac.za>, Gobeng Release Monama <release.monama@ul.ac.za>, Mogwasha Makhafola <daphneymakhafola@gmail.com>, Kabelo Edmond Ramohlola <kabelo.ramohlola@ul.ac.za>, Arjun Maity <maitya@csir.co.za>, Thabiso Carol Maponya <2209thabiso@gmail.com>

Dear Prof. Hato,

Thank you very much for submitting your full chapter for the book Polyaniline - From Synthesis to Practical Applications.

Current Step: Full chapter review

Next Step: Notification of Acceptance/Rejection

Expected Review Results: Within 30 days from the date of your full chapter submission

Upcoming Promotion!

I would also like to take this opportunity to inform you of an upcoming promotion. If your full chapter is accepted for publication you can pre-order your book and get one print copy for free on the first order you place. All contributing authors can benefit from this exclusive promotion available only through your Author Panel.

If you have any additional questions or concerns, I am at your disposal.

Cordially,

Ms. Sara Debeuc  
Author Service Manager

---

IntechOpen

The Shard, 32 London Bridge Street, London SE1 9SG, United Kingdom

+442080895700

[www.intechopen.com](http://www.intechopen.com)

# APPENDIX 5

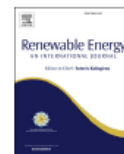
Renewable Energy 119 (2018) 62–72



Contents lists available at ScienceDirect

Renewable Energy

journal homepage: [www.elsevier.com/locate/renene](http://www.elsevier.com/locate/renene)



## Palladium deposition on copper(II) phthalocyanine/metal organic framework composite and electrocatalytic activity of the modified electrode towards the hydrogen evolution reaction



Gobeng R. Monama<sup>a</sup>, Siyabonga B. Mdluli<sup>b</sup>, Gloria Mashao<sup>a</sup>, Mogwasha D. Makhafola<sup>a</sup>, Kabelo E. Ramohlola<sup>a</sup>, Kerileng M. Molapo<sup>a</sup>, Mpitloane J. Hato<sup>a,\*</sup>, Katlego Makgopa<sup>c</sup>, Emmanuel I. Iwuoha<sup>b</sup>, Kwena D. Modibane<sup>a,\*\*</sup>

<sup>a</sup> Department of Chemistry, School of Physical and Mineral Sciences, University of Limpopo (Turfloop), Polokwane, Sovenga 0727, South Africa

<sup>b</sup> SensorLab, Chemistry Department, University of the Western Cape, Bellville 7535, Cape Town, South Africa

<sup>c</sup> Department of Chemistry, Faculty of Science, Tshwane University of Technology (Acadia Campus), Pretoria 0001, South Africa

### ARTICLE INFO

#### Article history:

Received 13 August 2017

Received in revised form

8 November 2017

Accepted 29 November 2017

Available online 30 November 2017

#### Keywords:

Metal-organic frameworks

Phthalocyanine

Palladium

Hydrogen evolution reaction

Hydrogen spillover

### ABSTRACT

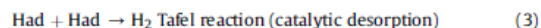
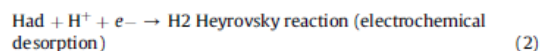
Pd-supported copper phthalocyanine/metal organic frameworks (Pd@CuPc/MOF) composite was synthesized by the reaction between CuPc and MOF followed by electroless Pd plating. The structural properties of MOF, Pd/MOF and Pd@CuPc/MOF composite were characterized using X-ray diffraction (XRD), Fourier transform infrared (FTIR), simultaneous thermal analysis (STA), ultraviolet–visible spectroscopy (UV–vis), scanning electron microscopy (SEM/EDS) and Brunauer–Emmett–Teller (BET). The XRD, UV–vis and FTIR analyses showed that Pd was coated on CuPc/MOF composite. SEM and EDS results revealed that Pd nanoparticles were well-dispersed and anchored tightly on the composite. The thermal stability of MOF increased upon addition of Pd and CuPc. The electrochemical hydrogen evolution reaction (HER) performance of the synthesized materials was studied by cyclic voltammetry (CV) and Tafel analysis. The Tafel slope of the composite was 176.9 mV/dec and the transfer coefficient of 0.67 which is close to 0.5. The HER results revealed that the Pd@CuPc/MOF composite has better catalytic characteristic such as high catalytic activity and lowest onset potential compared to MOF. More importantly, the significant enhancement of HER performance at ambient temperature for the composite with Pd content can be ascribed to the hydrogen spillover mechanism in such system.

© 2017 Elsevier Ltd. All rights reserved.

### 1. Introduction

The growing concern of energy crisis and environmental pollution promotes the development of an effective clean energy technology. Hydrogen gas has a potential to be an alternative energy carrier because it offers clean, efficient and renewable energy characteristics [1]. In addition, H<sub>2</sub> gas yields more energy, which is about 2.75 times greater as compared to traditional gasoline based energy resources [2]. However, the problem for practical usage of H<sub>2</sub> gas as an energy carrier lies in the production and storage technology [2,3]. Electrochemical water splitting (H<sub>2</sub>O → H<sub>2</sub> + ½

O<sub>2</sub>) consists of two half reactions known as oxygen reduction reaction (ORR) and hydrogen evolution reaction (HER) [3]. The ORR and HER normally take place on the anode and the cathode, respectively. The reaction mechanism of HER (2H<sup>+</sup> + e<sup>-</sup> → H<sub>2</sub>) in aqueous acid or alkaline solutions proceeds in a series of three elementary reaction steps which comprise of two electrochemical reactions and one chemical reaction [4]. In acidic medium, the HER could proceed via three main steps given in Eqs. (1)–(3) [5]:



\* Corresponding author.

\*\* Corresponding author.

E-mail addresses: [mpitloane.hato@ul.ac.za](mailto:mpitloane.hato@ul.ac.za) (M.J. Hato), [kwena.modibane@ul.ac.za](mailto:kwena.modibane@ul.ac.za) (K.D. Modibane).

<https://doi.org/10.1016/j.renene.2017.11.084>

0960-1481/© 2017 Elsevier Ltd. All rights reserved.